Modeling the Time to Corrosion Initiation

for Concretes with Mineral Admixtures and/or Corrosion Inhibitors

in Chloride-Laden Environments

Jerzy Żemajtis

Dissertation submitted to the Faculty of the
Virginia Polytechnic Institute and State University
in partial fulfillment of the requirements for the degree of

Doctor of Philosophy
in
Civil Engineering

Richard E. Weyers, Chair
Thomas E. Cousins
John G. Dillard
Richard D. Walker
James P. Wightman

January 19, 1998
Blacksburg, Virginia

Keywords: concrete, corrosion, permeability, reinforcing steel

Modeling the Time to Corrosion Initiation
for Concretes with Mineral Admixtures and/or Corrosion Inhibitors
in Chloride-Laden Environments

Jerzy Żemajtis

(ABSTRACT)

The application of a mineral admixture, or a corrosion inhibitor, or a combination of both are methods used for the corrosion protection for reinforced concrete bridges. The results of a study on evaluation of corrosion inhibitors from three different manufacturers and of concretes with fly ash, slag cement, and silica fume and a concrete with silica fume and a corrosion inhibitor are presented. The specimens were built to simulate four exposure conditions typical for concrete bridges located in the coastal region or inland where deicing salts are used. The exposure conditions were horizontal, vertical, tidal, and immersed zones. The specimens were kept inside the laboratory and were exposed to weekly ponding cycles of 6% (w/w) sodium chloride solution. In addition, cover depth measurements from 21 bridge decks and chloride data from 3 bridge decks were used, together with laboratory data, in modeling the service lives of the investigated corrosion protection methods.

The methods used to assess the condition of the specimens included chloride concentration measurements, corrosion potentials, and corrosion rates (3LP). Additionally, visual observations were performed for identification of rust stains and cracking on concrete surfaces.

Modeling the time as a function of probability of the end of functional service life (EFSL) is presented. It has been shown that the distributions of surface chloride concentration, C_0, and diffusion coefficient, D_c, are key elements in the model. Model predictions show that the concretes with mineral admixtures provide much better level of protection against moisture and chlorides than the ordinary portland cement concrete alone. Application of a corrosion inhibitor causes an elevation of the chloride threshold resulting in an additional increase in time to EFSL.

More field studies are needed to better estimate distributions of surface chloride concentration and diffusion coefficient of Virginia bridge decks, and to confirm predicted times to EFSL for low permeable (LP) concretes.

ACKNOWLEDGMENTS

I would like to express my sincere gratitude to Dr. Richard E. Weyers for his guidance, encouragement, and support during this research and my studies at Virginia Tech.

The research study presented herein was sponsored by the Virginia Transportation Research Council (VTRC). The support is gratefully acknowledged. A special thank you is extended to Michael Sprinkel of VTRC for his assistance in the laboratory specimens testing and field surveys. Also, appreciation is extended to Chelik, Richard Steele and the district bridge and maintenance personnel for support and assistance in the field studies, as well as to Michael Burton for his help with the rapid permeability testing.

I am also grateful to the other committee members: Dr. Thomas E. Cousins, Dr. John G. Dillard Dr. Richard D. Walker, and Dr. James P. Wightman for their valuable comments on my research and dissertation.

Thanks are also due to Brett Farmer and Dennis Huffman for their assistance with laboratory work.

I am deeply grateful to my fiends and colleagues for their help and friendliness, especially John Haramis, David Mokarem, Casie Permenter, Youping Liu, Rick Drumm, Brian Prowell, Michael Fitch, Erin Larsen, and Eric Petersson.

Sincere gratitude goes to my parents, Jadwiga and Henryk, and my brother, Grzegorz, for their love and encouragement. Their pride in my accomplishments guided me throughout the best and the worst moments of my work.

Finally, I must thank my wife, Agata, for her love, belief in me, and constant support. Her guidance, patience and understanding helped me to finalize this project.

Table of Contents

List of Tables:

List of Figures:

1.0 INTRODUCTION

1.1 Background

The history of civil engineering materials, other than stones, goes back as far as Egyptian times. Gypsum was the primary source for producing mortars for construction purposes. The application of lime as a cementitious material did not occur until the Greek and Roman eras. Mortars of these days lacked the strength and durability of the primary material for construction - stones. The first documented approach to develop a new cement that would provide mortar of better durability was made by John Smeaton in 1756, when he was engaged in a project to rebuild the Eddystone Lighthouse off the coast of Cornwall [1].

> "Smeaton realized that, for a durable masonry construction, the ordinary lime mortars of the day would not resist the dissolved effects of the sea. He then undertook an investigation of the various kinds of limestones which he could obtain and the performance of the limes they produced. In the end, Smeaton says: '...I did not doubt but to make a cement that would equal the best merchantable Portland stone in solidity and durability.' It appears that this comparison to Portland stone may also be the origin of the name portland cement. Smeaton's structure stood for 123 years before being replaced."

Nowadays, since a majority of concrete structures includes embedded reinforcing steel, durability issues must include both concrete and steel. The durability problem is especially apparent with highway structures, for which 50 maintenance-free years is considered a success. At the beginning of 1980s, the total number of bridges in the United States was estimated at 578,218 [2]. According to the U.S. Department of Transportation about 40 percent of these bridges were either "structurally deficient or

functionally obsolete" [3]. More than 276,000 bridges in the U.S. are on the federal-aid system with 28 percent that have been classified as deficient [2]. Deficient bridges are those bridges that are closed or restricted to reduced traffic loads.

During the 1960s, states with winter climates introduced a "bare road policy" which resulted in a significant increase in deicer salt applications [4]. The amount of salt applied on highways in 1970 was approximately four times more than in 1960. After 1970, about 10 million tons of salts were being applied annually [5]. Because of the winter maintenance activities, a large number of concrete bridge decks is contaminated with chlorides which initiate the corrosion of the reinforcing steel. Poor preventative maintenance may also lead to a faster rate of deterioration, which in turn may decrease the time to rehabilitation. Deterioration caused by the corrosion of reinforcing steel is not limited to concrete bridge decks only. It can also affect other concrete bridge members such as piles, walls, diaphragms, girders, abutments, piers, and pier caps [6]. One of the I-81 Interstate bridges serves as an example of pier cap deterioration due to corrosion of the reinforcing steel, see Figures 1 and 2.

Presently, the extent of the rapid deterioration of reinforced concrete bridges from chloride ion induced corrosion is well known. During the early recognition stages of the cause, process and severity of the concrete bridge deterioration problem in the United States, a multitude of corrosion abatement techniques were developed for existing and newly constructed bridges. Epoxy-coated reinforcing steel (ECR) and corrosion inhibiting admixtures are two techniques developed to extend the service life of newly constructed concrete bridge components. ECR, presently, is the most used corrosion protection method for concrete bridges in the United States. Corrosion inhibitors have been used for over 20 years but significantly less frequent than ECR and in Virginia primarily in precast-prestressed members. Also, mineral admixtures

FIGURE 1. Typical Bridge, I-81 Interstate, Virginia – Pier Cap Deterioration

FIGURE 2. Typical Bridge, I-81 Interstate, Virginia – Close-up of Pier Cap Deterioration.

have not been used frequently.

Until 1986 when Florida reported that the Long Key Bridge showed signs of corrosion only six years after construction, the corrosion protection effectiveness of ECR remained unquestioned. Since the Florida reported findings, 12 field studies have been conducted on the corrosion protection effectiveness of ECR [7]. Conclusions have been mixed, from satisfactory corrosion protection performance to date for bridge decks to poor performance in substructures, with predictions that ECR will not provide long-term (50 years) corrosion protection performance for substructures or decks [7]. The reason for the mixed conclusions of the performance of ECR include limited or inappropriate evaluation methods, a lack of knowledge of the cause(s) of failure, and subjectively defined failure criteria. From studies where care and appropriate evaluation methods and failure criteria have been employed, the conclusions are that ECR will not provide 50 years of corrosion free protection for steel in concrete bridge components [8, 9]. More recent studies, including one in Virginia, support the earlier conclusions that ECR will not provide long term corrosion protection performance [10, 11]. As a result of these recent findings on the limited effectiveness of ECR, more interest has been developed in the effectiveness of low permeable (LP) concretes and corrosion inhibiting admixtures.

1.2 Scope of the Study

The study on corrosion protection performance effectiveness for newly constructed concrete bridges was initiated by the Virginia Department of Transportation (VDOT). The laboratory study was limited to present VDOT mixture specification of a maximum water-to-cementitious material ratio (w/cm) of 0.45 and practices in the use of fly ash, slag cement, and silica fume mineral admixtures. As for the corrosion

inhibitors, the study was limited to a corrosion inhibitor presently used in prestressed members in Virginia, DCI-S (DCI), and two other commercial products, Armatec 2000 (A2000) and Rheocrete 222 (R222), being marketed as corrosion inhibitors for reinforced concrete at the time this study was initiated. The dual protection system included both silica fume and DCI-S corrosion inhibitor admixtures. A field study on concrete chloride permeability was also included. The field study bridges were three 17 year old bridge decks in Virginia's deicer salt environment.

The purpose of this study was twofold:

1. To evaluate the short term laboratory corrosion protection performance of low permeable concretes and three commercial corrosion inhibiting admixtures for concrete.

2. To develop a methodology for predicting the field corrosion protection effectiveness of concrete with mineral admixtures and/or corrosion inhibitors based on short term laboratory testing.

2.0 STATE OF THE PRACTICE

2.1 Mechanism of Corrosion

Corrosion, in general terms, means deterioration or destruction of a material due to a reaction with its environment [12]. Corrosion of a metal can be defined as a chemical reaction which returns the metal to compounds that are similar to the minerals from which it was extracted in the first place [13]. Some call metallic corrosion *"extractive metallurgy in reverse"* [12, 13]. Nearly all metallic corrosion processes are electrochemical in nature, they involve water that is in the liquid or vapor phases.

The chemical reaction of a corroding metal occurring at the metal-liquid interface can be written in a form of anodic and cathodic reactions. An anodic reaction, oxidation, produces electrons. The anodic site is the place where corrosion of metals occur [14]. The cathodic reaction, called reduction, consumes electrons. The anodic and cathodic reactions for a metal (M) are as follows [12, 13]:

anode: $M \rightarrow M^{n+} + ne^-$ (1)

cathode: $2H^+ + 2e^- \rightarrow H_2$ for pH < 7 (2)

$O_2 + 2H_2O + 4e^- \rightarrow 4OH^-$ for pH > 7 (3)

For corrosion to proceed both oxidation and reduction must occur simultaneously and at the same rate. Also, the electrolyte must allow for movement of cations from cathodic sites to the anodic ones and anions in the opposite direction. Finally, the anode and cathode must be electrically connected to allow current flow.

2.2 Corrosion of Steel in Concrete

Concrete

Portland cement concrete is the most widely used engineering material in the building industry. It is usually low cost, about $4/kg, and the most readily available material. Its elements can be easily formed into a variety of shapes and sizes. It has an excellent resistance to water and fire. Its production requires less energy input than other materials. The tensile strength of concrete is about one-tenth of its compressive strength. For these reasons, reinforcing steel is used to control cracking and provide tensile strength. Creep and shrinkage are two other factors that also need to be taken into account during the design process.

Hydraulic cement concrete is a composite material which consists primarily of a binding medium with aggregate embedded in it [15]. The term binding medium, or binder, in hydraulic cement concrete refers to a mixture of hydraulic cement and water. The most common hydraulic cement is portland cement, which primarily consists of hydraulic calcium silicates, aluminates, and ferroaluminates. The term aggregate refers to a granular material, such as sand, gravel, or crushed stone.

Hardened concrete consists of solid phases and voids [15]. Solid phases include hydrated cement paste (HCP), aggregate, and transition zone -- a layer between the aggregate and cement paste. The transition zone is about 20 μm thick and is characterized by a higher void content than the bulk paste. Among the solid constituents of concrete, it is the transition zone that has the greatest influence on concrete strength, elastic modulus, and permeability. At early ages, ettringite and calcium hydroxide form in the transition zone making this layer weak and porous. If

mineral admixtures are incorporated into concrete, calcium hydroxide further reacts with the supplementary materials and forms calcium silicate hydrate (C-S-H), which reduces zone thickness, makes it denser, and thus less permeable.

The void system in the HCP can be divided into entrapped air voids (1000 -- 5000 µm), entrained air voids (50 -- 1000 µm), capillary voids (0.01 -- 1 µm), and interparticle spaces (0.001 -- 0.003 µm).

The porosity of the HCP, or rather pore size distribution, determines the rate of penetration of deleterious substances such as carbon dioxide and chlorides. Pore size distribution depends primarily on the water to cement ratio and on the degree of cement hydration. It is generally known that small pores, less than 50 nm, influence drying shrinkage and creep. Large pores, greater than 50 nm, develop with increasing water to cement ratio and in turn, reduce concrete strength and increase permeability. It has been shown that for well-cured laboratory specimens, the permeability of concrete increases exponentially for mixtures with water to cement ratios greater than 0.5 [16]. For w/c > 0.7 pore system in concrete remains continuous regardless of the degree of hydration, and for the w/c = 0.6 pores become segmented after six months of curing.

Water in Concrete

Water may accumulate in concrete pores and capillaries. The amount of water depends on the pore size distribution and environmental humidity. This water, or rather pore water solution, can be classified into different types depending on how difficult it is to remove it from concrete. For the water in the hardened cement paste, it can exist in the following forms:

1. Capillary Water. The capillary water refers to water existing in capillaries 5 nm in diameter or larger. The water will be held by capillary tension if the capillary size is smaller than 50 nm. For large capillaries, diameter greater than 50 nm, water is considered as free water because its removal will not have any effect on concrete volume.
2. Adsorbed water. This type of water exists close to the solid surface and is held in place by attractive forces. Adsorbed water is lost when the paste is dried to about 30% relative humidity. Depending on the surface energy of the solid, water adsorption is not limited to a mono-layer, but follows a model of multi-layer adsorption.
3. Interlayer water. This is a monomolecular water layer that is held between the layers of calcium silicate hydrate, C-S-H (C-S-H is one of the solid phases in the HCP). This water is lost only on very strong drying, below 11% relative humidity.
4. Chemically combined water. This water exists in the cement hydration products in the form of hydrates and is not lost on drying.

Transport of Water and Chlorides in Concrete

The concrete pore system filled with air and pore water solution provides an excellent path for deleterious substances and an electrolyte. In mature concrete water movement is controlled by cracking and the HCP properties. Aggregate is usually less permeable than HCP; however, its inclusion in concrete creates low density transition zones and makes concrete more permeable. Furthermore, the movement of water in HCP depends on changes in pore structure due to continued hydration, as well as changing solubility of its constituents. The proposed mechanisms of mass transfer in concrete include adsorption, surface diffusion, vapor diffusion, ionic diffusion, and

bulk flow [17-20]. The analysis, even when only one mechanism is being considered, is very complicated because of the complexity of concrete pore structure, variation in mixture proportioning and curing, or continued hydration [20]. Discussion and comparison of different methods and theories dealing with water transport in concrete have been presented by Garboczi [21].

Permeability can be defined as the ease with which a gas or fluid can flow through a solid. It is obvious that the continuity of the pore system determines concrete permeability. Pressure induced gas flow through concrete follows Darcy's law [20]. The disadvantage of testing concrete permeability with gas is that the moisture condition of the sample must be known and carefully controlled. Also, the moisture level must be constant throughout the tested material. Relationships between gas and water permeabilities were studied by Klinkenberg and Bamforth [22, 23]. Gas permeability for low porosity concrete was always greater than the water permeability [22]. Water permeability can be tested by water-vapor diffusion, absorption and rate of absorption, water penetration, or saturate flow tests [20].

Chloride Migration

Chloride ions can migrate into concrete by capillary movement, through cracks, and by diffusion. Capillary movement is a fast method of transport; however, it is unlikely for water to migrate this way. First, mature concrete has a discontinuous pore system, and second, concrete holds water in the capillaries, so the driving potential -- capillary attraction -- is ceased [24]. Cracking provides an easy path way for chloride ions to penetrate concrete cover and reach the reinforcing steel. Structural cracks, however, are aligned perpendicular to the main reinforcement and thus limit access to the steel bars. Only subsidence cracking is dangerous with respect to chloride induced

corrosion. These cracks are positioned parallel and directly above the bars. Development of subsidence cracks depends on concrete cover, bar diameter, and the slump of concrete [25, 26]. Therefore, the primary modes of transport of chloride ions into the concrete are through diffusion in uncracked concrete and through cracks and by diffusion in cracked concrete [24].

Chloride ion migration into concrete is an ionic diffusion process following Fick's second law [20, 24, 27-35]. Fick's second law of diffusion represents non-steady state diffusion and is expressed in a form of a partial differential equation:

$$\frac{\partial C}{\partial t} = D_c \frac{\partial^2 C}{\partial x^2} \tag{4}$$

where: C = chloride ion concentration,
D_c = diffusion coefficient,
t = time, and
x = depth.

Equation 4 has many solutions depending on the boundary conditions. The most common solutions used in the analysis of chloride distribution in concrete are the ones with a boundary condition of surface chloride concentration, C_0, being either constant (Equation 5) or dependent on square root of time (Equation 6).

$$C_{(x,t)} = C_0 \left(1 - erf \frac{x}{2\sqrt{D_c t}}\right)] \tag{5}$$

where: $C_{(x, t)}$ = chloride ion concentration at depth x after time t,

C_0 = chloride surface concentration,

erf = error function.

or

$$C_{(x,t)} = k\sqrt{t}\ [e^{-x^2/4D_c t} - \frac{x\sqrt{\pi}}{2\sqrt{D_c t}}\ (1 - erf\frac{x}{2\sqrt{D_c t}})] \quad (6)$$

where: k = materials characteristics coefficient dependent on surface concentration ($C_0 = k\sqrt{t}$)

Reinforcing Steel Corrosion

In reinforced concrete structures steel bars that are embedded in concrete do not normally corrode. First, the concrete cover, if dense, intact and thick, forms a barrier which greatly reduces the penetration rate of exterior degradation agents. Second, concrete is highly alkaline in nature and causes embedded steel bars to be covered with a passivation layer, a thin and dense impermeable film of iron oxide [36]. This film is strongly adherent to the surface and does not allow the anodic reaction to occur, thus making steel passive to corrosion. As long as the passivation layer is intact; the anodic reaction cannot take place. Due to the high concentration of alkalies in the pore water and soluble calcium hydroxide in concrete, the pH is usually well above 12. The passivation layer on the steel surface is thermodynamically stable as long as the pH of concrete (pore water) remains above 11.5. The pH of concrete has a significant influence on the behavior of steel in concrete. It is generally believed that, the lower the pH of concrete, the higher the probability of corrosion [37]. For different values

of pH of concrete, the rate of corrosion occurrence changes in the following manner [37]:

- pH > 10 : no corrosion
- 4 < pH < 10 : corrosion rate is constant
- pH < 4 : corrosion rate is rapid

Carbonation reduces the pH of concrete [20]. The carbonation reaction involves carbon dioxide in the atmosphere and dissolved calcium hydroxide in the pore water. The carbonation reaction is a rather slow process and therefore, corrosion in reinforcement due to carbonation is normally observed only when the cover to the reinforcement is very thin, or when the concrete is of poor quality [31].

Another cause of passive film breakdown occurs when chloride ions are present at high concentrations on the bar surface [15]. Chloride ion induced corrosion of reinforcing steel in concrete elements is one of the main causes of concrete deterioration. Corrosion of steel in concrete structures is caused primarily by gradual intrusion of water and chloride ions from deicing salts, as well as from saltwater exposure in coastal regions, into the concrete [15, 20, 38-42]. Cracks are not necessary for chloride penetration [20]. Salts are capable of penetrating concrete together with water in which they are dissolved. The resulting presence of chlorides and the loss of the alkaline environment causes the embedded steel to loose its surface passivity. Corrosion follows as water and oxygen become available to the steel. Accumulated corrosion products, which occupy more volume than the reactants, cause cracking of the protective concrete cover. This allows for intrusion of chlorides and oxygen at a much faster rate, thus accelerating the corrosion process. Depending on the bar size, bar spacing, and cover depth, cracking can be in the form of either

delamination cracking or inclined cracking. Delamination cracking is characterized by horizontal cracks extending from one bar to another. Inclined cracking are those that propagate to the surface at an angle of about 45° and result in section loss and potholes, often seen in bridge decks. Figure 3 presents the two types of cracking. Steel corrosion is also intensified when the protective concrete cover of the embedded bars is inadequate, or other design or construction inadequacies occur [6].

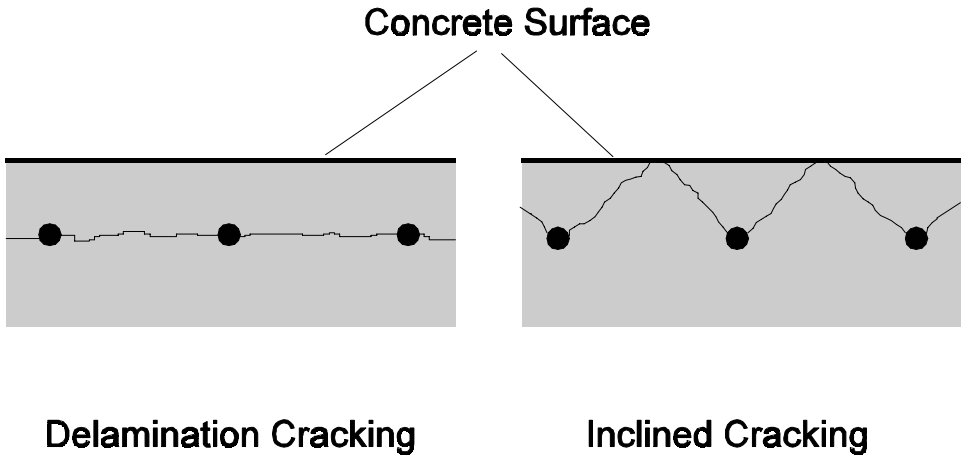

FIGURE 3. Corrosion Related Cracking in Concrete.

Steel corrosion in concrete is an electrochemical process where corrosion cells are generated due to differences in electrochemical potentials. Some areas of the bar become anodes, and some cathodes. The chemical half-cell reactions occurring at the anodic and the cathodic areas are as follows [15]:

anode: $Fe \rightarrow 2e^- + Fe^{2+}$ (7)

cathode: $\frac{1}{2} O_2 + H_2O + 2e^- \rightarrow 2(OH)^-$ (8)

The hydroxyl ions, OH^-, that arrive at the anodic area, electrically neutralize the Fe^{2+} ions dissolved in pore water and form a solution of ferrous hydroxide [38]:

anode: $Fe^{2+} + 2OH^- \rightarrow Fe(OH)_2$ (9)

The product further reacts with available oxygen and water and forms water insoluble red rust:

anode: $4Fe(OH)_2 + O_2 + 2H_2O \rightarrow 4Fe(OH)_3$ (10)

Red rust is not the only product of corrosion of steel in concrete. Compounds such as black rust, Fe_3O_4, green rust, $FeCl_2$, and other ferric and ferrous oxides, hydroxides, chlorides, and hydrates are also formed. Their composition depends on the availability of pore water, its pH and composition, and oxygen supply.

Corrosion products are very dangerous to concrete elements because their volume is much larger than the metallic iron [31]. The black rust volume is twice as large as that of steel, and red rust volume is four times as large [38]. The increase in volume causes tensile stresses in concrete which crack and spall the cover concrete.

As mentioned above, chloride ions accelerate corrosion of steel in concrete. The mechanism of action of the chloride ion is not entirely understood. The general opinion is that the chloride ion acts as a catalyst in corrosion reactions [13, 43-45].

When the concentration becomes large enough, ferrous corrosion products form an acid solution with chlorides which neutralizes the alkaline concrete environment and further enhances corrosion. Ferrous chlorides being more soluble than the oxides move away from the reinforcing steel and expose new areas to the corrosive environment.

Corrosion Types

Pitting and general corrosion are the two most common types of corrosion of steel reinforcement in concrete. Pitting corrosion occurs when only a small area of steel loses its passive layer, usually due to high concentrations of Cl^- ions. Pitting corrosion is characterized by a large cathode area and a small anode area resulting in accelerated corrosion. General corrosion occurs when the pits grow together and anode areas are large and the cathode areas are small. The corrosion rate is much slower when compared to pitting corrosion because of the lower cathode to anode ratio.

Another classification is based on relative position of anodic and cathodic sites. This relative position depends on a potential difference between the anodic and cathodic sites. The larger the potential difference, the further apart the anode and the cathode can be. If the two sites are in close proximity to each other, microcell corrosion occurs. Macrocell corrosion occurs when the anode and cathode sites are further apart and a large potential difference between the anode and cathode exists. Slater suggested that accelerated corrosion of bare steel reinforcement in the decks with bottom mat of coated steel is a result of macrocell corrosion [46]. In most cases however, since macrocell corrosion requires larger potential difference than the microcell corrosion does, it is more likely for the microcell to be a dominant type.

2.3 Corrosion Assessment Methods

2.3.1 Corrosion Potentials

Corrosion potentials non-destructively identify the probability of an active corrosion. A method uses a copper-copper sulfate half-cell electrode (CSE) that is placed on the concrete surface above reinforcing steel and is connected to the voltmeter and then to the reinforcing steel, see Figure 4.

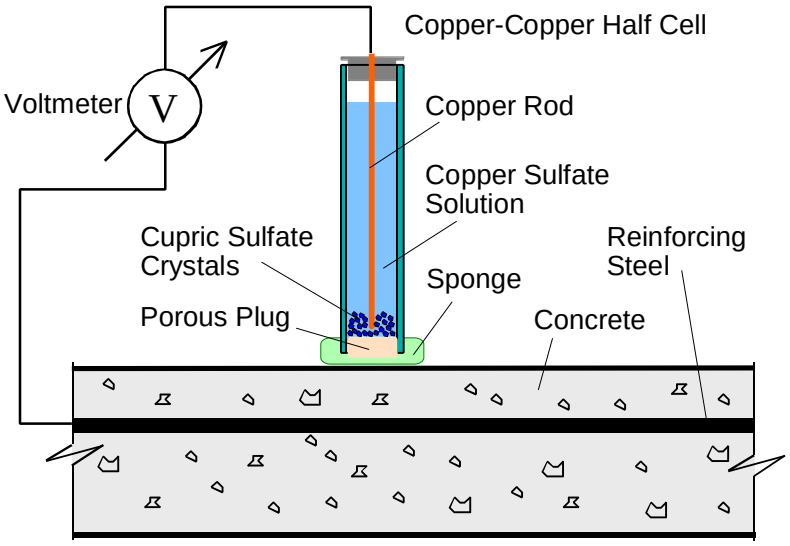

FIGURE 4. Potentials Test Setup – Schematic.

The potential of the reinforcing steel changes as the electrochemical reaction takes place. The voltmeter measures the difference in electrical potential between the electrode and reinforcing steel. The significance of potential readings and their relationship to the corrosion of the reinforcing steel in concrete is well documented [47, 48]. According to the standard test method ASTM C 876, Standard Test Method

for Half Cell Potentials of Reinforcing Steel in Concrete, the more negative the voltmeter reading, the greater the probability of active corrosion [49]. Table 1 presents the guidelines for the interpretation of the potential readings for bare reinforcing steel in concrete.

TABLE 1. Interpretation of Potential Readings.

Voltmeter Reading	Interpretation
greater than -200 mV	90% probability of no corrosion
from -200 mV to -350 mV	uncertain
less than -350 mV	90% probability of active corrosion

2.3.2 Corrosion Rates

The linear polarization technique is a non-destructive method for assessing the instantaneous corrosion current density. It has been widely used in monitoring corrosion of laboratory specimens, as well as field structures [50-53]. The name refers to the linear regions of the current vs. potential curve (polarization curve). Stern and Geary showed that for a few millivolts above and below the corrosion potential, the polarization curve may be considered linear [54]. Corrosion current density is directly proportional to the instantaneous rate of metal loss. Often the corrosion current density is referred to as the corrosion rate. Several devices, based on the linear polarization method, presently exist to determine the corrosion current density of steel in concrete. One of the most common is the 3LP device, see Figure 5 [55].

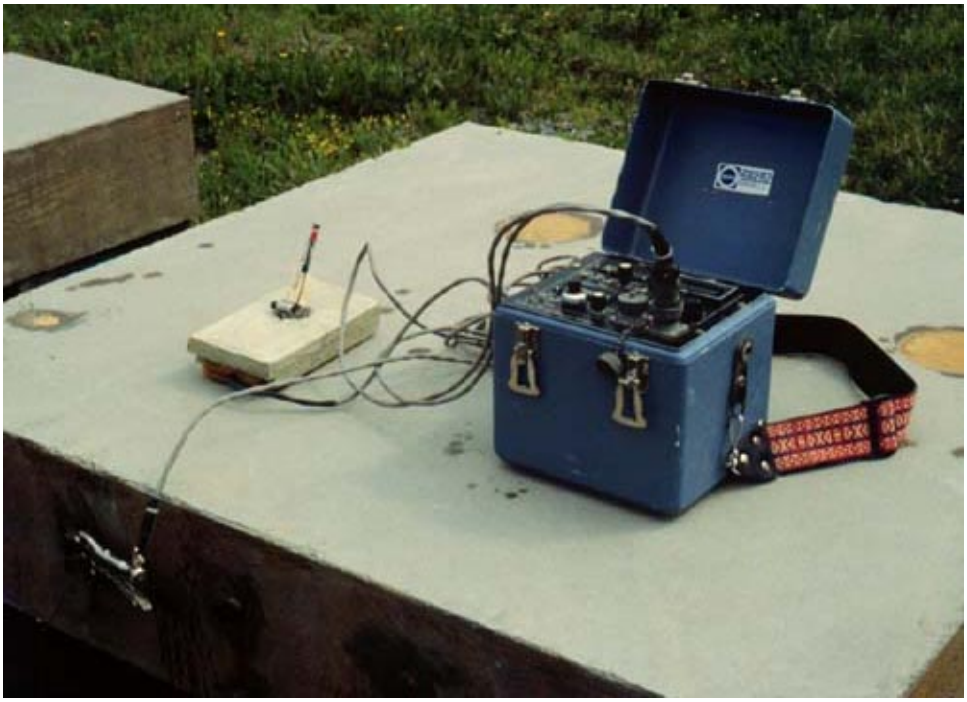

FIGURE 5. 3LP Device.

The name “3LP” stands for “three electrode linear polarization”. The three electrodes are as follows : counter, working, and reference electrodes. The counter electrode applies current to the steel reinforcement, which is the working electrode. The reference electrode measures the change in potential due to applied current. A corrosion current can be determined from the Stern-Geary relationship. Once the corrosion current is determined, corrosion current density or corrosion rate can be calculated by dividing the current by the area of steel that was polarized. Corrosion current density measurements are very susceptible to variable field conditions: concrete temperature, moisture, and oxygen content. The manufacturer’s interpretation of measured corrosion current density, corrosion rate, using the 3LP device is given in Table 2.

TABLE 2. Data interpretation for the 3LP Device.

i_{corr}	Interpretation
< 0.21 mA/cm^2	no damage expected
0.21 - 1.07 mA/cm^2	damage possible in 10-15 years
1.07 - 10.7 mA/cm^2	damage possible in 2-10 years
> 10.7 mA/cm^2	damage possible in less than 2 years

2.3.3 Chloride Ingress

Knowledge of the chloride content is a common measure to determine the possibility of corrosion activity. It is generally known that chlorides can be found in bound and/or unbound condition in either the aggregate or in the cement paste. The amount of unbound chloride, in the pore water, is considered significant relative to corrosion damage. Above the corrosion threshold level, the greater the chloride ion concentration, the greater the active corrosion [56]. Table 3 provides guidelines for interpretation of chloride content measurements [57].

TABLE 3. Recommended Action for Chloride Content Measurements.

Chloride Concentration	Recommendation
< 0.59 kg/m^3	leave intact
0.59 - 1.19 kg/m^3	questionable area
> 1.19 kg/m^3	remove concrete below bar level or replace entire section

Samples for chloride concentration are collected as pulverized concrete at several average depths. The collection apparatus uses an impact drill with 29 mm (1-1/8 in) hollow diameter bit, 2.3 times the maximum aggreeate size, connected to a vacuum collection unit [58]. Figure 6 shows such a setup with a portable power generator necessary for the vacuum and the drill operation.

FIGURE 6. Sampling for Chloride Concentrations – Collection Apparatus: Impact Drill with Hollow Drill Bit, Powder Concrete Collection Unit, and Vacuum.

The concrete powder is collected in the coffee filter, see Figure 7, which is then stored in a plastic container until chemical analysis. ASTM C 114 provides guidelines for determining chloride ion concentration in mortar and concrete [59]. A titration method is used to determine the quantity of acid soluble chlorides in the concrete digestion solution. A simple formula transfers the amount of milliliters of titration solution into chloride ion concentration expressed in kg/m^3 of concrete.

FIGURE 7. Powder Concrete Collection Unit.

Rapid Permeability

The determination of concrete diffusion characteristics based on chloride profile data requires a relatively long time period since the time for chlorides to reach greater depths is very long. For this reason the FHWA and Construction Technology Laboratories undertook a project whose goal was to develop a rapid test procedure for determining chloride permeability of field and laboratory concrete [20]. The developed test requires (artificial) high saturation of the concrete sample and an applied voltage, and is only a few hours in duration. That method, often referred to as "rapid permeability", provides rapid indication of concrete resistance to the

penetration of chloride ions. The method relies on the results from a test in which electrical current passes through a concrete sample during a six-hour exposure period [60]. The interpretation is that the larger the Coulomb number, or the charge transferred during the test, the greater the permeability of the sample. The method has shown good correlation with chloride tests [60].

2.3.4 Visual and Sounding Observations

A visual survey will identify rust stains on the surface, cracking and spalls. Rust stains appear on the surface due to migration of rust products. Cracking may be in the form of delamination cracking (not visible) or inclined cracking. Delamination cracking can easily be detected by sound methods. A chain drag and hammer are the tools that produce different sound vibrations over intact and delaminated concrete. Delaminations can also be detected by an ultrasonic reflective method [61].

2.4 Corrosion Protection Methods

Since corrosion of the reinforcing steel causes early deterioration of concrete bridges, it is necessary to develop methods which extend the service life of theses bridges. One method is to use high quality concrete with a low water/cement ratio, which makes concrete more dense and less permeable. A thicker concrete cover depth, of at least 75 mm, will also prolong the time to corrosion initiation; the distance for deleterious substances to reach the reinforcing steel will be greater. ACI 201 recommends low water-cement ratios and good concrete cover to be employed when chloride exposure conditions are moderate and severe [62]. Tougher and even more crack resistant concrete can be made by addition of stainless steel, glass, and polypropylene fibers [63]. Fiber concrete is mostly used for protection of bridge decks in the form of

overlays [64]. In recent years there has been a rapid development of various materials and methods which can be used for increasing the service life of concrete structures subjected to chloride attack [63]. They include mineral admixtures, corrosion resistant reinforcement, corrosion inhibitors, cathodic protection, and surface treatments. This study concentrates on concrete with mineral admixtures and corrosion inhibitors.

2.4.1 Reduction of Diffusion Rate

2.4.1.1 Pozzolans

Pozzolans are materials that have little or no hydraulic activity of their own; however, they act as a hydraulic cement when mixed with water in the presence of calcium hydroxide. Pozzolans contain high quantities of silicon dioxide and may also contain significant amounts of aluminum oxide and iron oxide. Hydration of a pozzolan, when compared with hydration of silicates in portland cement, is a slow reaction and is characterized by low heat of hydration and slow strength gain. Hydration of silicates in portland cement results in the formation of C-S-H and calcium hydroxide (CH). In pozzolanic reactions, pozzolan reacts with CH from the portland cement hydration, and water, and forms C-S-H. The C-S-H produced in the pozzolanic reaction has lower density than from the portland cement hydration. However, since the reaction is much slower, the products of the pozzolanic reaction fill the already existent capillary spaces in the cement paste. It improves strength properties and reduces permeability. Bentz and Garboczi stressed that the pozzolanic mineral admixtures do not eliminate the capillary porosity, but reduce it by significantly lowering the volume fraction of CH and at the same time increasing the total amount of C-S-H [65]. Mineral admixtures with very fine particle sizes are known to increase the water requirement in almost direct proportion to their amount present, so if the normal consistency of the mixture

is desired at an unchanged w/c ratio, a water reducing admixture may be required [66].

Pozzolans used in concrete include both natural and by-product materials. Natural materials include volcanic glasses and tuffs, and calcined clays or shales. Natural pozzolans require processing such as crushing, grinding, and size separation. The process may also involve thermal activation. The major sources of by-products are power plants and metallurgical furnaces producing cast iron, ferrosilicon alloys and silicon metal. The benefit of using industrial by-products is that they may not require any processing before being used in concrete, thus result in cost and energy savings.

2.4.1.1.1 Fly Ash

Fly ashes are by-products manufactured during combustion of powdered coal in power plants. A summary of the properties and chemical composition of different fly ashes was presented by Helmuth [67]. In general, depending on the chemical composition, fly ash can be classified as Class F or Class C. Class C fly ash has higher amount of CaO so it possesses more cementing characteristics and is less pozzolanic than Class F. ASTM 618 states that Class F fly ash is "normally produced from burning anthracite or bituminous coal" while Class C fly ash is "normally produced from lignite and subbituminous coal" [68]. Class F fly ash is mostly composed of silicate glass containing aluminum, iron, and alkalies. The particles are in the form of solid spheres with sizes ranging from less than 1 µm to 100 µm, and an average diameter of 20 µm [15]. At least 70% of the chemical composition is made up of SiO_2, Al_2O_3, and Fe_2O_3 [20].

The benefits for using fly ash in concrete include the following characteristics [20]:

- improved workability,

- lower heat of hydration,
- lower cost concrete,
- improved resistance to sulfate attack,
- improved resistance to alkali-silica reaction,
- higher long-term strength,
- opportunity for higher strength concrete,
- equal or increased freeze thaw durability,
- lower shrinkage characteristics, and
- lower porosity and improved impermeability.

2.4.1.1.2 Silica Fume

Silica fume is also knows as microsilica, volatilized silica, or condensed silica fume. It is a by-product from silicon metal and ferrosilicon alloy production. The material is a very fine powder with spherical particles about 100 times smaller in size than portland cement or fly ash. The diameters range from 0.02 to 0.5 µm with an average of 0.1 µm. Silica fume contains 85 to 95% noncrystalline silicon dioxide.

The first application of silica fume in the United States was conducted in Kentucky in 1982 [20]. The use of silica fume will make concrete with the following properties [20]:

- low heat of hydration,
- retarded alkali-aggregate reaction,
- reduced freeze-thaw effects and water erosion,
- high strength,
- increased sulfate resistance,
- reduced permeability.

Silica fume is also known for creating problems in handling and cracking related to its small particle sizes and increased water requirement.

2.4.1.2 Slag Cement

Slag is a by-product from the production of steel. During production liquid slag is rapidly quenched from a high temperature by immersion in water [15]. The slag is a glassy, granular, non-metallic product that consists "essentially of silicates and aluminosilicates of calcium and other bases" [20]. It is also known as granulated blast-furnace slag (GBFS). Slag, in addition to pozzolanic properties, and unlike Class F fly ash and silica fume, also has cementitious properties. With regard to strength, there are three grades of slag: Grade 80, Grade 100, and Grade 120. Each number corresponds to a minimum 28-day compressive strength ratio of a mortar cube made with only portland cement and a mortar cube made with 50% portland cement and 50% slag. Because of cementitious properties, particles smaller than 10 µm contribute to early strength, while particles larger than 10 µm and smaller than 45 µm contribute to later strength. Since particles greater than 45 µm are difficult to hydrate, slag is mostly pulverized to particles with diameter less than 45 µm [15].

When used in concrete, slag provides the following benefits [69]:

- high ultimate strength with low early strength,
- high ratio of flexural to compressive strength,
- resistant to sulfates and seawater,
- improved alkali-silica reaction resistance,
- low heat of hydration,
- decreased porosity and permeability, and
- better finish and lighter color.

Slag is also known for improved workability and lower water requirement [70]. Slag hydration is significantly influenced by temperature: hydration is accelerated at higher temperatures and retarded at lower ones, when compared to portland cement hydration. This may lead to differences between the strength of concrete in the field and the laboratory specimens [15].

2.4.2 Corrosion Inhibitors

Corrosion inhibitor admixtures are widely used to delay or retard corrosion of reinforcing steel in concrete. The theory of mutual dependance of anodic and cathodic reactions was carefully examined when developing corrosion inhibitors. The theory states that corrosion rate can be reduced by reducing the rate of only one of the half-cell reactions. Fontana defined a corrosion inhibitor as "a substance that when added in small amounts to a corrosive reduces its corrosivity. Corrosion inhibitors function by interfering with either the anodic or cathodic reactions or both. Many of these inhibitors are organic compounds; they function by forming an impervious film on the metal surface or by interfering with either the anodic or cathodic reactions [12]."

General types of inhibitors are as follows: anodic, cathodic, and mixed. Anodic inhibitors react with the corrosion products of the reinforcement and form a protective film on the surface. Gradually all surface of steel is covered and the corrosion process ceases. Sufficient quantities of the inhibitor must be present to provide effective inhibition. Anodic inhibitors are said to be "dangerous" because when used in too small quantities, they may cause the corrosion rate to increase. According to Trethewey and Chamberlain two types of anodic corrosion inhibitors are important for steel. The first type includes oxidizing agents such as nitrates, nitrites, and chromates. The second type includes silicates, phosphates, molybdates, and borates. These

materials require dissolved oxygen to be effective [71].

Cathodic inhibitors affect the cathodic reaction by reacting with the hydroxyl ions to precipitate insoluble compounds on the cathode site and prevent access of oxygen. Examples are salts of zinc and magnesium, or calcium. Materials such as arsenic, bismuth, antimony and some organic compounds also affect the cathodic reaction by forming a layer of adsorbed hydrogen on the cathode surface [71]. Cathodic inhibitors are said to be "safe" because the active cathode area is reduced regardless of the amount of inhibitor used.

The corrosion inhibiting reaction is influenced by many factors, such as solubility, precipitation, dispersion, chloride to inhibitor ratio (anodic inhibitors only), chemical composition of cement, curing conditions, molecular structure, temperature, and the pH of pore solution [66].

From the two corrosion inhibitor groups, anodic inhibitors were found to be more efficient than cathodic corrosion inhibitors. Presently, mixed corrosion inhibitors, chromate / polyphosphate / zinc, are being used to provide the best corrosion protection [71].

Inhibitors can also be grouped as barrier layer formers, neutralizers, scavengers, and miscellaneous [72, 73].

2.4.3 Dual Systems: Reduction of Diffusion Rate and Corrosion Inhibition

Dual systems include reduced concrete permeability and a corrosion inhibitor. An example is a mineral admixture which provides reduced permeability of the cover

concrete, while the corrosion inhibitor elevates corrosion threshold level. The net result is that corrosive elements not only arrive at the bar depth later, but also must be present at higher concentrations for corrosion to start.

2.5 Service Life Predictions

Corrosion Threshold Concentration

As mentioned in previous sections, chloride induced corrosion of reinforcing steel is the main cause for deterioration of concrete in bridge decks and marine structures. The use of deicing chemicals and the influence of the coastal region environment were found to be the primary sources of chlorides necessary for the corrosion process to take place.

Reinforcing steel in concrete is normally protected by an oxide layer that forms on the steel surface and the high alkalinity of concrete. The corrosion process will take place when the passive oxide layer is destroyed. Chloride ions migrating through concrete will cause depassivation of steel after they reach the threshold concentration at the steel-concrete interface. The value of the threshold concentration is of primary importance. It varies for different concrete types. The results of previous studies on threshold chloride ion concentration determination are presented in Table 4 [74]. A level of 0.71 to 0.89 kg/m^3 is usually considered a threshold level for bare steel in regular reinforced concrete bridge decks. According to AASHTO, concentration less than 1.42 kg/m^3 are acceptable for bridge decks; however, deck replacement should occur when the level of chlorides reaches 2.8 kg/m^3 [75].

TABLE 4. Threshold Chloride Ion Concentration.

Researcher(s)	Year	kg/m^3 of concrete
Lewis	1962	0.7
Hausmann	1967	0.2 - 2.8
Berman	1972	0.77
Clear and Hay	1973	0.6 - 0.9
Clear	1974	0.66
Stratfull, Jaukovich, and Spellman	1975	0.66
Cady	1978	0.6 - 1.3
Browne	1982	1.33
Pfeifer, Landgren, and Zoob	1986	0.5 - 0.9

A second theory states that the threshold should not be based on chloride ions only, but rather on a ratio of chloride to hydroxyl ions [76]. According to Hausmann, ratios above 0.6 indicate high probability of active corrosion, while ratios below 0.6 not [77]. It can easily be deducted that not only an increase in chloride ion concentration will cause the ratio to increase, but a decrease in hydroxyl ion concentration as well. However, accurate determination of hydroxyl ion concentration is difficult, especially at high concrete pH levels.

Selected Case Studies

Locoge and coworkers studied the influence of microcracks on transport of chloride ions by diffusion and relationship between cracking specific area and flow rate of chloride ions [78]. The effects of cracking and self healing on chloride migration on a w/c = 0.4 concrete were investigated by Jacobsen et al [79]. The internal cracking was achieved by exposing specimens to freeze-thaw cycles and self healing was

simulated by immersing specimens in lime saturated water. A reduction of 28 to 30% in chloride migration was observed in the self-healed concretes when compared to newly cracked concrete.

Fick's second law of diffusion and Danckwert's solution was used by Tumidajski to model chloride diffusion [80]. He obtained a good fit of the solution to experimental data from Page and co-workers with the diffusion coefficients of 125 and 49 mm^2/yr. Berke and Hicks reported that Dc for the quality concrete is about 63 mm^2/yr, but may be an order of magnitude lower or higher depending whether a pozzolan additive is added or a low-quality concrete is used, respectively [81].

In another study, Tumidajski and Chan found the chloride diffusion coefficient being dependent on both time and chloride concentration / depth [82, 83]. The authors suggested the chloride diffusion coefficient to be a linear function of "Boltzman variable, $x/\sqrt{t}$." The authors also observed a significant decrease of chloride diffusion coefficients; however their analysis was based on a solution with surface concentration being time independent -- constant. On the other hand, Frey and coworkers found the diffusion coefficient to be dependent on porosity and the composition of the HCP, but not on chloride concentration [35]. Mangat and Malloy [84] study of the chloride diffusion coefficient found it to be strongly dependent on time of exposure to chloride environment. The proposed relationship is in the following form:

$$D_c = D_i\, t^{-m} \qquad (11)$$

where D_i = diffusion coefficient at time t = 1 second, and m is an empirical coefficient that is dependent on w/c ratio. Their predictions were made based on Fick's 2nd law

of diffusion and a solution with constant surface concentration and modified diffusion coefficient. Chloride concentration profiles in a concrete cylinder were modeled by Arora and coworkers [85]. The authors showed that a model with constant surface concentration and a constant diffusion coefficient can be successfully used to predict the chloride concentration profiles, but found it applicable only for short periods of time. Uji and coworkers suggested that the surface chloride concentration should be dependent on the square root of time, rather than being constant [34].

Zhang and Gjorv reported the transport of chloride ions in concrete is "a more complex and complicated transport process than what can be described by Fick's law of diffusion" [86,87]. The authors emphasized the importance of the effects of ionic interaction, lagging motion of cations, formation of electrical double layer on concrete solid surfaces, as well as the chemical binding. Also, Chatterji reported that the Fick's second law is not suitable for modeling chloride migration through concrete [88].

In another experiment Zhang and Gjorv used AASHTO T 277 electrochemical test method, rapid permeability, for chloride ion migration determination and found the concentration of chloride source solution has a significant influence on the results and a correction factor needs to be introduced [89]. Feldman and coworkers investigated influence of changing parameters on the rapid permeability results [90]. The factors included temperature, AC impedance, initial DC current, charge passed. In addition chloride ion profiles were monitored during polarization. The major conclusion was that the test induces change in the concrete pore structure and its resistivity. The authors suggested a simple measurement of initial current or resistivity as a replacement for the rapid permeability test when concrete with Type I cement is used. Arup and coworkers found good correlation between rapid permeability and resistivity measurements [91]. Andrade and Sanjuan [92] studied the rapid permeability test

using a modified test with a 12 V applied voltage, different sample sizes and solutions. However, their conclusions may apply to the rapid permeability test as well. The authors reported that highly concentrated solutions are not recommended because the chloride activity decreases, but also excessively diluted solutions may not provide adequate driving force and result in inaccurate results. The authors also found that the resistivity of concrete is a promising parameter for mass transport characterization.

In spite of the controversy in the method of water and chloride transport in concrete, rapid permeability and diffusion according to Fick's 2nd law are used by many for comparison and service life predictions.

Influence of Mineral Admixtures

Many studies have been performed on mineral admixtures and their influence on chloride permeability and diffusion characteristics. Studies varied in type of mineral admixture used, percent cement replacement, curing and exposure conditions, and others. In general concrete with mineral admixtures exhibit reduced permeability and diffusion coefficients are lower that for the ordinary Portland cement concrete [35, 93-97].

Naik and coworkers studied the influence of fly ash percentage replacement on water permeability and found that for up to 50% cement replacement, chloride permeability was reduced, but this was not the case for higher percentages of cement replacement [94].

Zhang and Gjorv reported that for silica fume replacement, in the amount of 10 %,

chloride diffusivity reduces to such an extent that the w/c ratio is of a lesser importance [95].

Torii and Kawamura investigated concrete with various percentages of silica fume [96]. From the results of AASHTO-T-277, same as ASTM C 1202, the authors reported that chloride ion permeability into mortar containing 10 and 15% SF drastically decreased with the distance from the sample surface, but this was not the case with the OPC samples. The authors concluded that AASHTO T 277 underestimates the "real chloride ion permeability" in concrete samples containing silica fume or fly ash. However, they did not comment on eventual influence of the shrinkage related surface micro-cracking in the SF samples. This might have explained the relatively high concentrations at the shallow depth (0 -- 10 mm) and very low or zero concentrations at higher depths (50 mm). Such a comment was made by Frey and coworkers [35]. Based on the results of their study on the reduction of the diffusion rates of chloride ions in concrete with addition of granulated blast furnace slag or fly ash, the authors said that micro-cracks may be present due to shrinkage.

An extensive study on concrete with slag cement and silica fume was performed by Ozyildirim [97]. The rapid permeability results indicate much better performance of specimens with slag / silica fume / Type II cement than with slag / silica fume / Type III cement, and the corresponding 28-day Coulomb values were from 471 to 824 and from 791 to 1195, respectively.

Service Life Models

The average service life of bridges in the United States, including rehabilitation and the

component replacement, was estimated to be 70 years. Major rehabilitation of a bridge takes place when the structure is about 35 years old [98]. The design life for buildings and other structures in Europe is 50 years, while bridges are expected to last 120 years [28]. Under these conditions predicting the service life of concrete structures which includes present knowledge of their deteriorated condition became an important subject in making the most cost-effective decisions concerning future management of these structures.

Cady-Weyers Deterioration Model

A corrosion deterioration model for bridge structures was proposed by Cady and Weyers, see Figure 8 [99]. This general representation of deterioration versus time relationship can be divided into three stages: diffusion, corrosion, and deterioration. The diffusion period is the time when chloride ions penetrate the concrete cover until their concentration, at a rebar level, reaches the corrosion threshold level. The second period in this model is called the corrosion period. In this stage the corrosion of the reinforcing steel initiates and progresses until first cracking occurs. Factors such as bar size, its spacing, and concrete cover above the steel determine whether incline or delamination cracking occurs [38]. The last period in the Cady-Weyers deterioration model is the deterioration phase. In this period, the bridge deck continues to deteriorate until the time when repair or rehabilitation is required. Factors such as delaminations, spalling, patches, and cracking influence decisions regarding the time of repair or rehabilitation. Based on a Strategic Highway Research Program (SHRP) report, the end of service life is determined when the damage of the worst traffic lane reaches 9.3 -- 13.6% of the area [100].

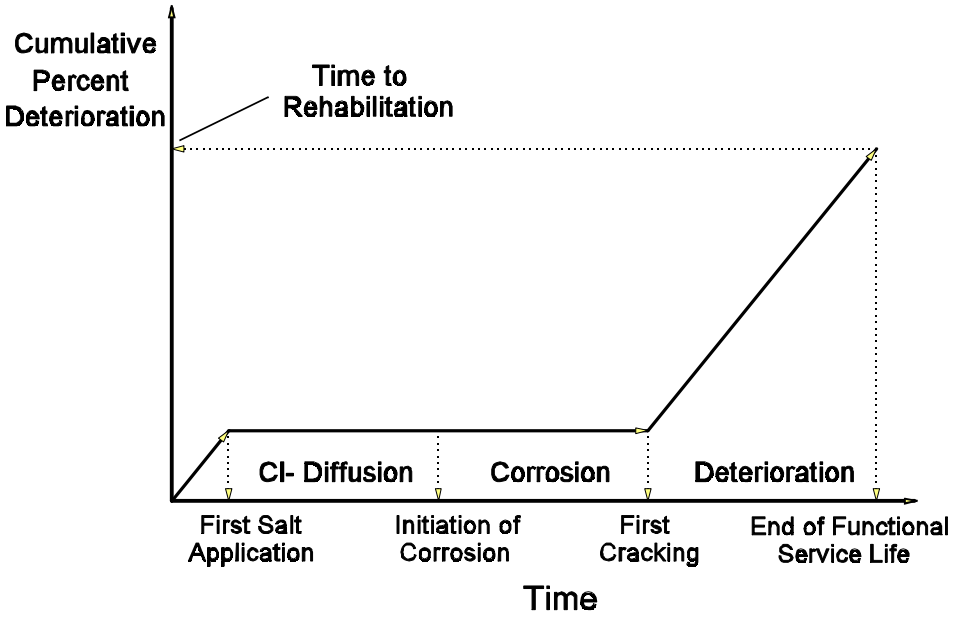

FIGURE 8. Cady-Weyers Deterioration Model.

Other Models

In 1982 Browne [28] proposed a basis for design, repair and inspection procedures by predicting the time of corrosion onset using the diffusion rate for chlorides to reach the reinforcing steel, t_1, and the time from the activation of corrosion of steel to the presence of damage in the concrete structure, t_2. Accordingly, corrosion of steel causing damage, d, in the existing concrete structure should be described using the following equation:

$$d = t_1 + t_2 \qquad (12)$$

A series of chloride distribution curves were obtained by testing samples drilled from different concrete structures at different depths. Fick's second law of diffusion was applied, see Equations 4 and 5. The series of curves were drawn based on obtained diffusion coefficients, D_c, and determined surface chloride concentrations, C_0, for different exposures times, allowing to predict the design life for the steel at different cover depths. Browne suggested that t_1 should be considered the design life with the assumption of chloride level remaining below the threshold limit at reinforcing steel depth for the life of the structure, since the time to structure damage, t_2, is more difficult to predict. Time t_2 was found to be influenced by many factors including the rate of oxygen diffusion through the concrete, concrete moisture content and its quality, as well as reinforcing steel cover depth, steel size and concentration, and the shape of the structure. Values of t_2 obtained from real concrete structures ranged from 6 months to 5 years.

Fick's diffusion law was also used by Funahashi [74] to calculate the time for the chloride concentration level to exceed the threshold limit and initiate corrosion for prestressed strands in a deck system of a parking garage. He developed a prediction method for the chloride concentration movement in time using a computerized finite difference method, which could be used to evaluate the condition of concrete structures exposed to chloride laden environments. He used the relationship between the normal distribution function and the error function in a solution to Fick's equation. The data comply with Fick's diffusion equation if, after plotting, they appear as the straight line.

A combined effect of diffusion and subsidence cracking was modeled by Cady and Weyers in 1983 [24]. The proposed relationship is presented in Equation 13.

$$At = Ac + [1 - (Ac / 100)] Ad \quad (13)$$

where

At = the percent of the deck area having rebars in critically chloride contaminated concrete at time t,

Ac = the percent of the deck area having subsidence cracking, and

Ad = the percent of the deck area having bars in critically chloride contaminated concrete at time t resulting from diffusion.

The authors found that cover depths showed the greatest influence on the relative contributions of subsidence cracking and diffusion to chloride concentration. Concrete slump and the size of the reinforcing steel had relatively little effect in comparison with cover depth. Also, application of Equation 5 for bridge decks in early years was found not appropriate because the time is too short to establish "the steady-state diffusion process." The authors pointed out, however, that the "early deterioration resulting from reinforcement corrosion is virtually the result of subsidence cracking through shallow cover," and not ionic diffusion.

Diffusion characteristics and corrosion rates were the basis for a 1992 model for the prediction of service life for concrete bridge decks subjected to chloride reinforcing steel corrosion proposed and validated by Cady and Weyers [98]. They suggested that chlorides can reach reinforcement and start the corrosion process within a few months to a few years after construction due to presence of subsidence cracking. If the concrete surface is uncracked, chloride transfer occurs by diffusion, which can be expressed using Fick's second law, see Equation 4. Based on Fick's second law and typical exposure conditions for concrete bridge decks the following relationship was

proposed:

$$t = 0.4918 (L - 2.0)^2 \quad (14)$$

where: t = time to reinforcement corrosion initiation due to diffusion of chloride ions, years

L = mean reinforcement cover, cm.

It was determined that the diffusion coefficient, D_c, varies with the concrete water to cement ratio and temperature. For the adopted model the following values were assumed: a w/c ratio equal to 0.45, an average ambient temperature of 15 °C, and D_c equal to 95 mm^2/year. Based on research performed on bridge decks located in Pennsylvania, Virginia and Wisconsin, a new average value of D_c of 47 mm^2/year was found and the range was from 16 mm^2/year to 120 mm^2/year. The correct calculation of D_c appears to be critical for the determination of the time to corrosion initiation. Time to corrosion initiation varies inversely and linearly with the diffusion constant, D_c, for known cover depth, chloride surface concentration and corrosion threshold chloride concentration. Based on a variation in one order of magnitude in D_c values obtained for typical bridge deck samples, the authors suggested that D_c should be calculated for each bridge deck for which service life is being determined. Another characteristic that should be included in the service life determination is corrosion rate. Cady and Weyers [98] incorporated a corrosion rate of 1.2×10^{-3} g/cm^2/yr into the model. This value was later found to be equal to 5.9×10^{-3} g/cm^2/yr based on the mean corrosion current obtained from six bridge decks located in Pennsylvania, Virginia and Florida. The average corrosion rate was further developed and modeled by Liu [101].

For the proper life-cycle cost analysis two things should be determined: the maintenance free period, T_m, and the deck age at rehabilitation, T_r. They are influenced by the concrete cover depth, L, chloride diffusion constant, D_c, and corrosion rate, J_r. Cady and Weyers [98] determined that major rehabilitation took place when about 40% of the deck surface experienced spalls, delaminations, and patching. Under these conditions and including all the characteristics influencing service life determination, the time-to-corrosion, T_m, for a mean typical cover depth of 40 to 60 mm was found to be between 3 and 20 years, and about 4 to 16 years for mean D_c and J_r values. The mean bridge deck life to rehabilitation, T_r, was determined to be in the range from 16 to 39 years with a mean of 29.

This study concentrates on a diffusion period of the Cady-Weyers deterioration model, which also is the maintenance free period in their last model [98, 99]. Based on Figure 8, it is clear that one method to extend time to rehabilitation is to extend the time to corrosion initiation. It can be achieved by reducing the diffusion rate or by increasing the chloride threshold level. Reduction of the diffusion rate can be accomplished by mineral admixtures, while chloride threshold level can be elevated with corrosion inhibitors. The proposed model uses both laboratory and field data, and estimates field performance of "new low permeable" concrete mixtures. Another feature that makes the proposed model different is the fact that rather than using fixed numbers of the diffusion coefficient and surface chloride concentration, the model incorporates probability distributions of these variables. These distributions will allow making predictions not only for a particular structure, as provided by other models, but for a population of bridges.

3.0 EXPERIMENTAL DESIGN

3.1 Specimen Design

To assess the corrosion performance of the reinforcing steel in concrete with mineral admixtures and/or corrosion inhibitors, specimens with fly ash, slag cement, silica fume, DCI-S corrosion inhibitor, Rheocrete 222 corrosion inhibitor, Armatec 2000 corrosion inhibitor, and silica fume with DCI-S corrosion inhibitor, as well as two control specimens with neither mineral admixture nor corrosion inhibitor, were cast. The constant design parameters for these specimens were a 0.45 water to cementitious material ratio, slump, and air content. All specimens had 25 mm reinforcing cover depth and had been exposed to a 6%, by weight, sodium chloride wetting solution. Each specimen, as shown in Figure 9, was 1.72 m (68 in.) high, had horizontal dimensions of 1.12 m by 1.12 m, (44 in. by 44 in.) and was designed to simulate four exposure conditions: wetted deck surface (horizontal zone), wetted vertical surfaces of bridge members (vertical zone), tidal zone, and immersed zone. The immersed zone covered an area from the bottom of specimens' legs to the height of 305 mm. The tidal zone was 305 mm to 610 mm from the bottom of specimens' legs. A vertical surface area above 610 mm from the bottom of a specimen corresponded to the vertical zone, and the horizontal zone was the top surface area of the specimen.

The specimens differed by the following parameters (see Table 5):

- configuration of the reinforcing steel (RS) in specimen’s legs:

  type I - RS electrically disconnected in both legs,

  type II - RS electrically connected in both legs (same bars for vertical, tidal, and immersed zones),

type III - RS electrically disconnected in the right leg and RS electrically connected in the left leg (same bars for vertical, tidal, and immersed zones)

- concrete type:
  - Virginia Department of Transportation (A4) concrete - control specimens, CTL1 and CTL2,
  - A4 concrete with fly ash (removal of 15% portland cement and replacement with 20% fly ash by weight) - FA specimen,
  - A4 concrete with slag cement (40% portland cement replacement with slag cement by weight) - SC specimen,
  - A4 concrete with silica fume (7% portland cement replacement with silica fume by weight) - SF specimen,
  - A4 concrete with DCI-S corrosion inhibitor and silica fume (7% portland cement replacement with silica fume by weight) - SFD specimen,
  - A4 concrete with DCI-S corrosion inhibitor - DCI specimen,
  - A4 concrete with Rheocrete 222 corrosion inhibitor - R222 specimen, and
  - A4 concrete with Armatec 2000 corrosion inhibitor - A2000 specimen.

Discontinuity of the bars was achieved by employing fiberglass-epoxy rods that were used in place of regular steel reinforcement in the transition areas between selected exposure zones as well as between the two mats of deck reinforcement. These bars were connected to the steel reinforcement with plastic ties to ensure that the steel bars were isolated from each other. Also, steel hooks used for lifting the specimens were protected with an electrochemical tape to prevent continuity between bottom and top mats of reinforcing steel, see Figure 10.

TABLE 5. Specimen Configuration.

Specimen Legs' Reinforcing Steel	Control Specimens A4 Concrete	LP Concrete Specimens Concrete with Mineral Admixtures: Fly Ash	Slag Cement	Silica Fume	Silica Fume & DCI-S	CI Concrete Specimens Concrete with Corrosion Inhibitors: DCI-S	Rheocrete 222	Armatec 2000
Type I	CTL-1							
Type II	CTL-2							
Type III		FA	SC	SF	SFD	DCI	R222	A2000

Specimens were cast in steel forms, which were carefully cleaned and oiled with a form release agent before each concrete placement. While placing concrete, a concrete vibrator was used to achieve good consolidation especially in the specimens' legs. Placing and vibrating concrete is presented in Figure 11.

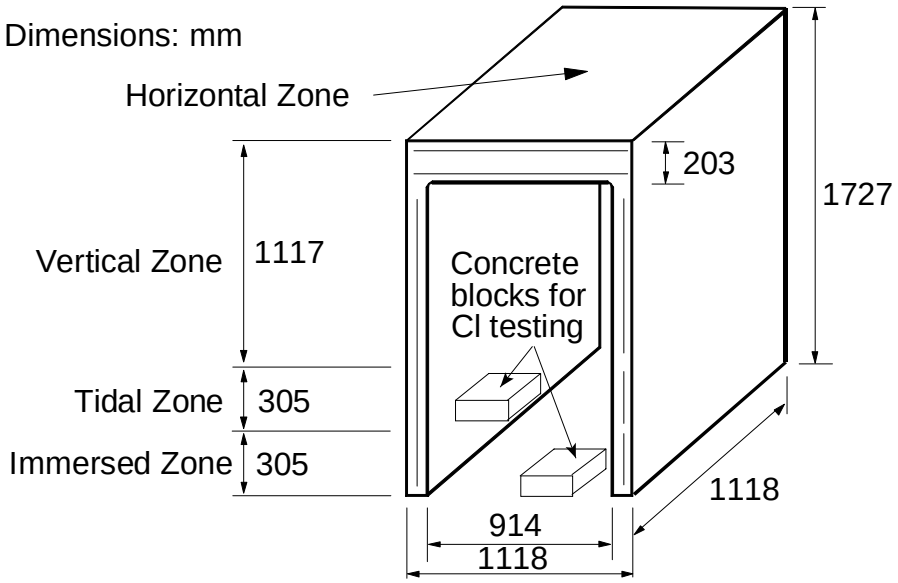

FIGURE 9. Typical specimen.

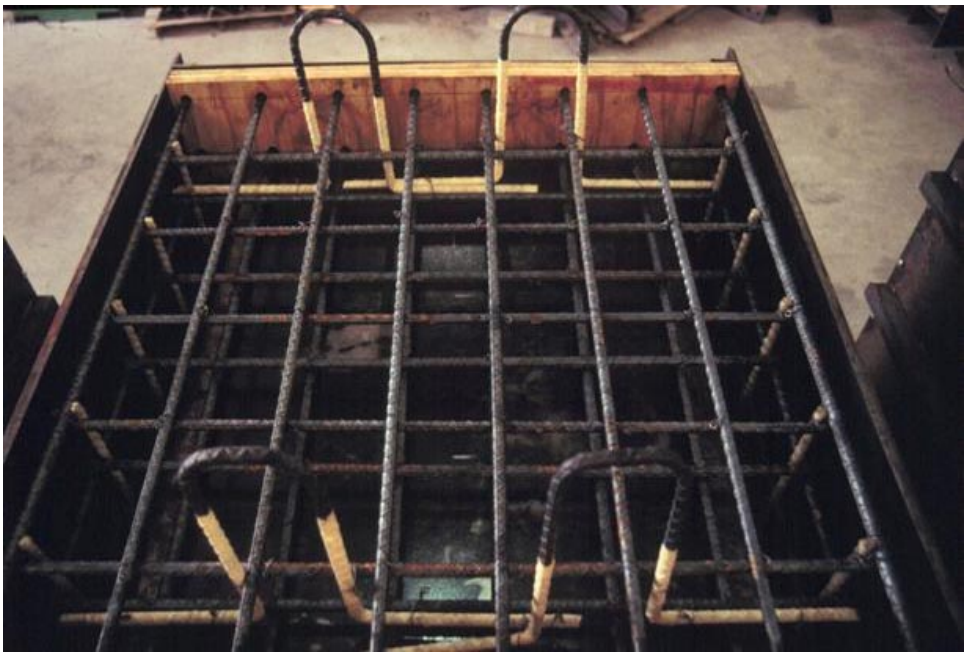

FIGURE 10. Reinforcing Steel in the Forms Prior to Concrete Placement – Typical Specimen.

FIGURE 11. Concrete Placement and Vibration – Typical Specimen.

Specimens were wet cured in the forms for seven days. After removing the specimens from the forms the specimens were wrapped with wet burlap and covered with plastic for additional 21 days of wet curing. Concrete specimen, after being removed from the steel forms, is presented in Figure 12. After 28 days of wet curing, specimens were air-dried in the laboratory for a minimum of 30 days. During that time the specimens were prepared for wet-dry cycles. All bar ends protruding from specimen legs in the lower part of the legs (0.61 m from the bottom) were protected with plastic

tubing, stoppers, and silicone rubber against contact with wetting solution. Then plexiglass dikes were assembled on the specimen's top surface so that the NaCl solution would wet the horizontal zone and uniformly wet the legs. Each specimen was placed into a 0.71 m deep high-density polyethylene (HDPE) tank and exposed to wet-dry cycles.

FIGURE 12. Typical specimen after Removal from the Steel Forms.

During the specimens' removal from the steel forms, one or two structural cracks developed at the interface of the legs and deck sections on some specimens. Before exposure to the sodium chloride solution, all structural cracks were filled with silicone rubber and a duct tape was applied over the crack to minimize the influence of these cracks on corrosion development.

3.2 Exposure Conditions

Specimens were kept indoors and were exposed to wet-dry ponding cycles. Each cycle was one week in duration and was divided into two stages. In the first stage the wetting solution was at high tide level (610 mm from the bottom of a specimen), thus the tidal zone and the immersed zone areas were covered with NaCl solution, and the horizontal and vertical zones of the specimen were allowed to air dry. In the second stage the wetting solution, while at low tide level (water level at 305 mm from the bottom of a specimen), was pumped to the top of a specimen, thus wetting specimen surfaces in the horizontal and vertical zones. At the same time surfaces in the tidal zone were allowed to air dry. Horizontal, vertical, and tidal zones were subjected to wetting for an average of 3.5 days a week and to air drying also for an average of 3.5 days a week. The immersed zone was constantly submersed in the NaCl solution. The wetting solution used in the study was 6% sodium chloride by weight. Photographs showing specimens exposed to wet-dry cycles and a close-up of plexiglass dike in the horizontal zone are presented in Figures 13 and 14, respectively.

After approximately 1.5 years of wet-dry cycles, the specimens were removed from the tanks and moved outdoors.

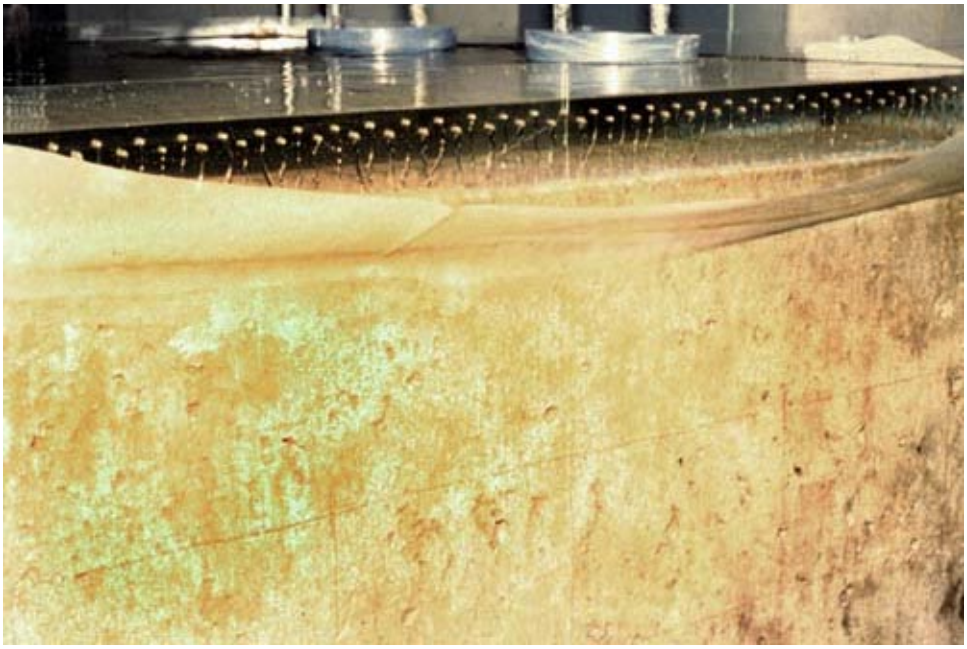

FIGURE 13. Plexiglass Dike: Horizontal / Vertical Exposure Zones.

FIGURE 14. Experiment in Progress – Exposure to Wet / Dry Cycles.

3.3 Materials

3.3.1 Reinforcing Steel

Bare reinforcing steel was used for fabrication of all tested specimens including controls. All bare steel was #5 (D = 16 mm) bars, Grade 60, and came from one heat. Physical and chemical properties of bare steel, based on mill certificates, are presented in Table 6. Bare reinforcing steel was manufactured by Resco Steel, located in Roanoke, Virginia.

TABLE 6. Physical and Chemical Properties of Bare Steel.

Physical Properties:		**Chemical Properties:**	
Yield Point [MPa]	425 - 473	C [%]	0.38 - 0.43
Tensile Strength [MPa]	645 - 703	Mn [%]	0.83 - 1.00
% Elongation [200 mm]	10	P [%]	0.01
		S [%]	0.03 - 0.05

Fiberglass-epoxy rods were used in the transition areas between exposure zones when discontinuity of the reinforcing steel was desired. The fiberglass-epoxy bars were manufactured by International Grating, located in Houston, Texas.

3.3.2 Concrete

Concrete, designated as Virginia Department of Transportation A4, was used for all

specimens. The quantities of cement, admixtures, and aggregate used are presented in Table 7.

TABLE 7. Concrete Mixture Proportions.

Specimen Type	CTL1	CTL2	FA	SC	SF	SFD	DCI	R222	A2000
Ingredients [kg/m^3 of concrete]									
Cement	377	377	320	226	351	351	377	377	377
Fly Ash	-	-	75	-	-	-	-	-	-
Slag Cement	-	-	-	151	-	-	-	-	-
Silica Fume	-	-	-	-	26	26	-	-	-
#78 Coarse Aggregate	867	867	867	867	867	867	867	867	867
Fine Aggregate	864	864	825	854	856	848	856	864	864
Water	170	170	170	170	170	153	153	170	170
Corrosion Inhibitor [l/m^3 of concrete]:									
DCI-S	-	-	-	-	-	20	20	-	-
Rheocrete 222	-	-	-	-	-	-	-	5.0	-
Armatec 2000	-	-	-	-	-	-	-	-	2.5
Admixtures [ml/100 kg of cement]:									
HRWR: WRDA-19	1215	914	847	682	1063	1605	782	-	-
HRWR: Rheobuild 1000	-	-	-	-	-	-	-	780	792
AEA: Daravair-M	72	69	78	70	69	87	69	69	52
AEA: MB-VR	-	-	-	-	-	-	-	69	-

Type I/II cement was used for all concrete mixtures. Its density was 3.15 g/cm^3 and was certified to meet ASTM C-150-92, AASHO M-85-88, and Federal SS-C-1960 Specifications. Chemical and physical test data are provided in Table 8.

Coarse aggregate used for the concrete mixes was #78 stone with unit weight of 96.7. Its density was 2.75 g/cm^3 and absorption was measured to be 0.66%. Natural sand, with fineness modulus (FM) of 2.7, 2.66 g/cm^3 density, and 0.84% absorption, was used as fine aggregate. Daravair-M air entraining admixture (1 fl. oz/100 lbs) was used for all mixtures. In addition to Daravair-M, MB-VR air entraining admixture was used in the concrete for the R222 specimen. Water reducing admixture was necessary to keep the water to cementitious material ratio constant and to provide adequate workability during placing of the concrete. The high range water reducer WRDA-19 was used with controls and concretes with mineral admixtures and with DCI-S corrosion inhibitor, while the Rheobuild 1000 was used for concrete with the Rheocrete 222 and Armatec 2000 corrosion inhibitors. The concrete was batched in 2.4 cubic meter batches at a local ready mix concrete plant, mixed and transported to the laboratory. About 0.78 m^3 of concrete was used in the casting of a specimen. Manufacturers' representatives for the R222 and A2000 corrosion inhibiting admixtures assisted in adjusting batch weights, verified batch weights and approved the concrete batching, mixing, transporting and placing procedures. Manufacturers' representatives for the DCI-S admixture were not present during any of the specimen fabrication procedures.

TABLE 8. Cement Properties (as Provided by the Manufacturer).

Chemical Test Data		**Physical Test Data**	
SiO_2	22.1	Fineness - Blaine	3760
Al_2O_3	4.29	Fineness - Wagner	2212
Fe_2O_3	2.83	Autoclave Expansion	0.05
CaO	63.4	Initial Set (H:min.)	2:25
MgO	2.86	Final Set (H:min.)	3:35
SO_3	2.23	Vicat (min.)	95
Total Alkalies	0.62	Air Content (Mortar)	6.6
Insoluble Residue	---	**Compressive Strength [MPa]**	
Ignition Loss	1.1	1 day	15.0
C_3S	51.3	3 day	27.4
C_3A	6.58	7 day	35.5

3.4 Evaluation Methods

The objective of the specimen testing was to investigate concrete with various mineral admixtures, three commercial corrosion inhibitors, and one mineral admixture with a corrosion inhibitor as corrosion protection systems and evaluate their performance in reference to bare steel. Methods used to assess specimen performance included the rate of chloride ingress, rapid chloride permeability, corrosion potentials, and corrosion rate measurements. Additionally, visual observations were performed for identification of rust stains and cracking on concrete surfaces.

3.4.1 Chlorides

Chloride ingress was monitored by collecting concrete powder samples at three depths: 13 mm, 25 mm, and 38 mm after 33 weeks, one year, and 1.5 years of ponding. In order not to significantly damage specimens, samples collected at 33 weeks and 1 year, were obtained from small concrete blocks, 300 mm by 300 mm by 130 mm, placed in the tidal and immersed zones. These blocks were cast from the same batch of concrete as the test specimens, cured under the same conditions, and placed into the HDPE tanks at the same time as the test specimens. After 1.5 years of ponding, chloride samples were collected from all four exposure zones of the test specimens. In addition to the chloride samples from the three above mentioned depths, a chloride sample from the depth of 51 mm was collected in the horizontal zone.

The depths of 13, 25, 38, and 51 mm are the average depths of collected samples. A 13 mm depth sample was obtained by drilling between the depths of 6 and 19 mm., 25 mm depth sample - between 19 and 32 mm, 38 mm depth sample - between 32 and 44 mm, and 51 mm depth sample - between 44 and 57 mm. Because of high variability of chloride content close to the surface, powdered concrete samples from the top 6 mm were discarded.

All chloride content measurements include additional chlorides that are present in concrete from mixing ingredients and admixtures. These chlorides are further referred to as background chlorides. To compensate for non-diffused chlorides, background chloride content measurements were performed by sampling concrete cylinders that were made with the compressive strength cylinders.

3.4.2 Rapid Concrete Chloride Permeability

Rapid concrete chloride permeability was tested at the Virginia Transportation Research Council (VTRC), Charlottesville, VA. The rapid permeability was measured on cylinders of all concrete types according to ASTM C-1202 [60]. The measurements were taken after 28 days and 1 year of moist curing.

3.4.3 Corrosion Potentials

Corrosion potential measurements in the horizontal zone were taken on a monthly basis and were recorded at 12 locations: 3 locations each of 4 tested bars. For vertical, tidal, and immersed zones, corrosion potentials were recorded at 9 locations: 3 bars, 3 locations each, for each zone and for each leg of the specimen. Total number of corrosion potential measurement locations was 66: horizontal zone - 12, vertical zone left leg - 9, tidal zone left leg - 9, immersed zone left leg - 9, vertical zone right leg - 9, tidal zone right leg - 9, and immersed zone right leg - 9. The locations for potential measurements are shown in Figure 15.

3.4.4 Corrosion Rates

Corrosion rates were measured at three locations for each exposure zone and each leg, for a total of 21 different locations per specimen. See Figure 15 for a measurement location plan for the horizontal zone and vertical, tidal, and immersed zones on the specimen's right leg. Measurement locations on the specimen's left leg were the same as on the right leg.

3.4.5 Cover Depths - Field Study

Concrete cover depths were measured in the field structures with a rebar locator device, see Figure 16. The device used in the study was Profometer III.

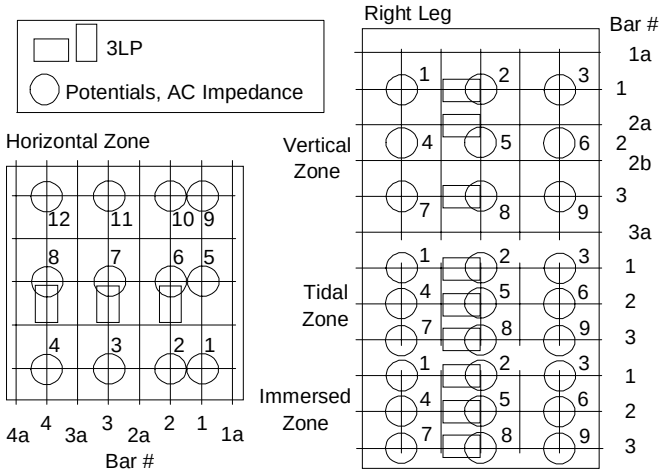

FIGURE 15. Typical specimen – Measurement Locations.

FIGURE 16. Cover Depth Measurement – Profometer III Device.

4.0 RESULTS AND DISCUSSION

4.1 Concrete Properties

4.1.1 Fresh Concrete Properties

Slump, air content, concrete temperature, and concrete density (unit weight) were recorded before concrete placement. Results of these tests and the actual w/cm ratios are presented in Table 9.

TABLE 9. Fresh Concrete Properties.

Specimen	Water/Cement Ratio	Slump [mm]	Air [%]	Temperature [°C]	Density [g/cm^3]
BS-1	0.46	191	6.2	25	2.34
BS-2	0.44	203	5.5	26	2.34
FA	0.42	203	3.1	27	2.41
SC	0.44	165	8.5	24	2.24
SF	0.44	178	5.7	23	2.32
SFD	0.45	64	4.5	29	2.36
DCI	0.45	152	5.4	26	2.33
R222	0.44	178	4.7	22	2.36
A2000	0.44	152	5.2	25	2.33

4.1.2 Compressive Strength

While placing concrete, several 100 by 200 mm (4 by 8 in.) cylinders were made for compressive strength measurements. Compressive strength was tested after 3, 7, 28, 56 days and 1 year of moist curing. The compressive strengths are presented in Table 10. The results show that even the lowest values were well above 28 MPa, the required minimum strength for A-4 concrete at 28 days.

TABLE 10. Compressive Strengths.

Specimen	Average Compressive Strength (MPa)				
	3 days	7 days	28 days	56 days	1 year
BS-1	39	48	58	62	72
BS-2	35	40	48	54	63
FA	28	36	48	58	68
SC	18	29	42	44	52
SF	31	39	54	53	63
SFD	28	42	62	61	73
DCI	31	36	49	52	60
R222	29	36	41	44	54
A2000	29	34	45	47	58

4.1.3 Rapid Concrete Chloride Permeability

Cylinders for rapid chloride permeability tests were made together with cylinders for the compressive strength tests and their dimensions were also 100 by 200 mm. The cylinders were sent to the Virginia Transportation Research Council (VTRC),

Charlottesville, VA for testing. The tests were performed on finished surface of the cylinders of all concrete types according to ASTM C 1202 at 28 days and 1 year of wet curing. Based on numerical values, presented in Table 11, rapid permeability of the A4 concrete after 28 days and 1 year of wet curing averaged 3085 and 1932 Coulombs, respectively. Rapid permeability values for all LP specimens were significantly lower than for the controls. The explanation is in the pozzolanic reaction of mineral admixtures resulting in denser concrete matrix. The rapid permeability for the DCI specimen was about two times that of controls after 28 days of wet curing and about 50% more than the controls after 1 year. The explanation may be the accelerating action of this product on cement hydration. The rapid hydration of the cement causes larger crystals to be developed and permeability is increased. The rapid permeability results for the two other corrosion inhibitors were also higher than the controls but to a lesser degree than the DCI specimen, see Table 11.

TABLE 11. Rapid Indication of Concrete Resistance to the Penetration of Chloride Ions.

Specimen	Water/Cement Ratio	Rapid Permeability [Coulomb]	
		28 days	1 year
BS-1	0.46	3049	1816
BS-2	0.44	3120	2048
FA	0.45	1653	332
SC	0.44	1700	708
SF	0.44	815	584
SFD	0.46	1130	814
DCI	0.45	6413	3002
R222	0.44	3595	2384
A2000	0.44	3236	2516

Based on the chloride permeability test results, a relationship between 28-day and one-year values was established and is presented in Figure 17 and in Equation 15.

$$Perm1y = 0.57\ (Perm28d) \qquad (15)$$

where Perm1y is the rapid permeability in Coulombs after 1 year of curing and Perm28d is the rapid permeability in Coulombs after 28 days. The performed regression analysis was based on the results from all specimens plus three additional concrete samples: A4 concrete and two Portland cement concrete specimens with high water-to-cement ratio of 0.71 and 0.74. The correlation coefficient, R^2, was 0.95.

4.2 Corrosion Assessment Measurements

4.2.1 Corrosion Potentials

Specimens were monitored with the half-cell potential measurements in the horizontal and vertical zones throughout the experiment period. The last two readings were taken after the ponding was discontinued and the specimens were moved outdoors. The potential data collected in the horizontal zone are presented in Figures 18a-18i, for specimens CTL1, CTL2, FA, SC, SF, SFD, DCI, R222, and A2000, respectively. Data for the vertical zone are presented separately for the left and right legs in Figures 19a-19r.

Immediately after the ponding was discontinued, half-cell potential measurements were taken in the immersed and tidal zones on both legs of each control specimen. Then, the specimens were moved outdoors and additional two sets of potential readings, in a

two-month interval, were taken from all exposure zones. These three sets of readings, for horizontal and vertical zones, are included in the graphs presented in Figures 18 and 19, and for the tidal and immersed zones are presented in Figures 20 and 21.

Note: each curve or bar in Figures 18-21 represents an average of three readings taken from one reinforcing steel bar.

Corrosion potentials were monitored on the control specimens, CTL1 and CTL2, from the 18th and 19th week of ponding till the 105th and 106th week of total exposure time, respectively. Corrosion potentials on the FA, SC, SF, and SFD specimens were monitored from the 18th, 10th, 19th, and 8th week of ponding till the 105th, 97th, 106th, and 95th week of total exposure time, respectively. Corrosion potentials on the DCI, R222, and A2000 specimens were monitored from the 10th, 9th, and 8th week of ponding till the 96th, 96th, and 95th week of total exposure time, respectively.

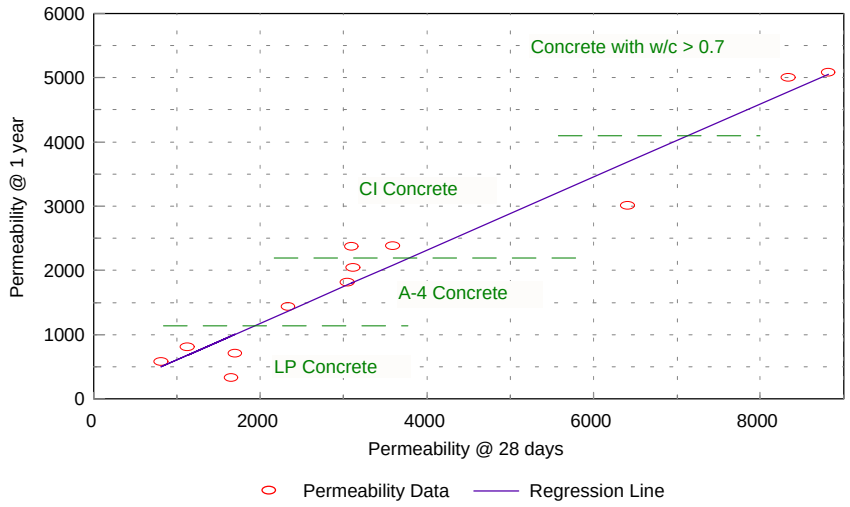

FIGURE 17. Relationship between Rapid Permeability Results at 28 Days and One Year.

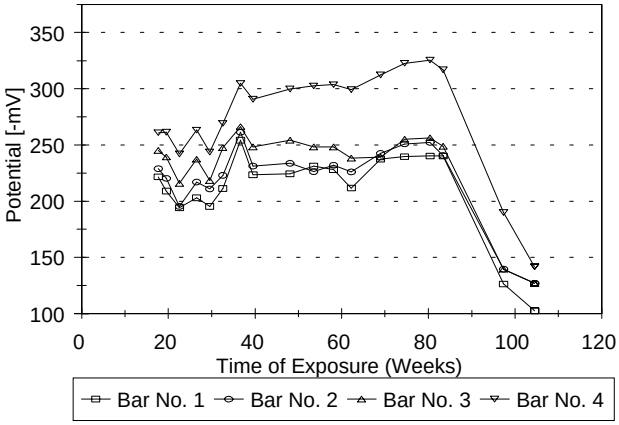

a. CTL1 Specimen.

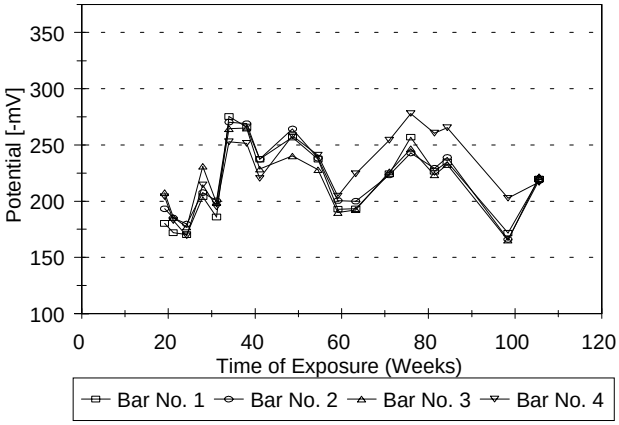

b. CTL2 Specimen.

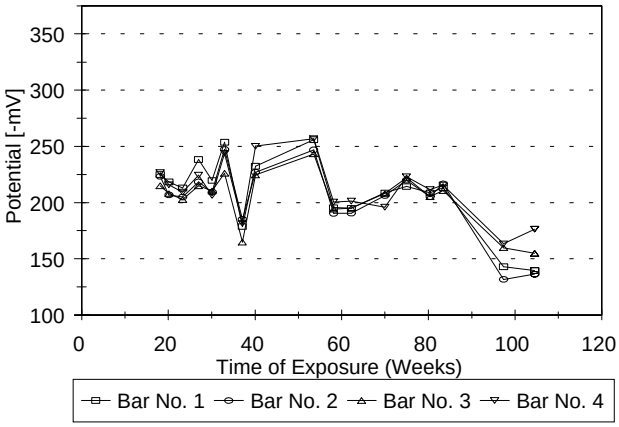

c. FA Specimen.

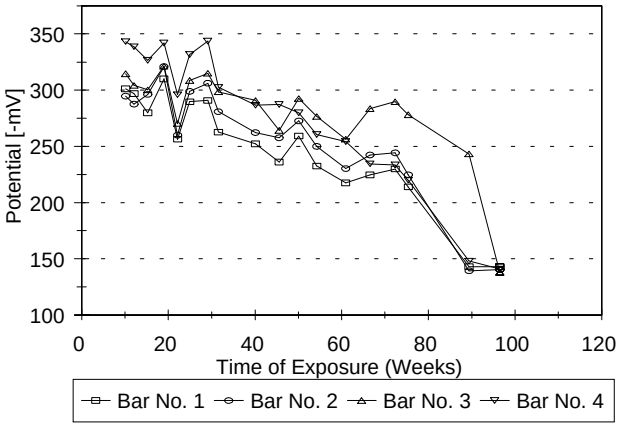

d. SC Specimen.

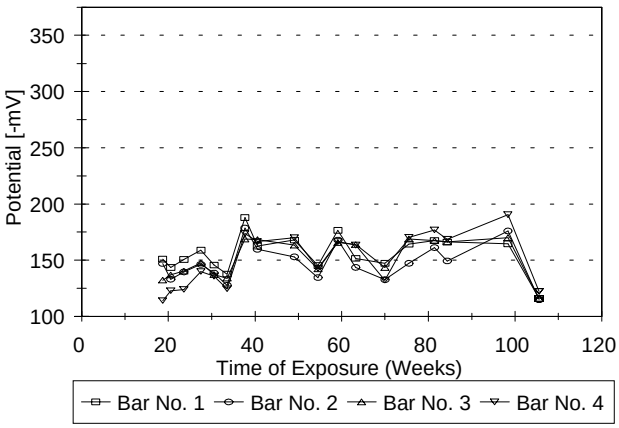

e. SF Specimen.

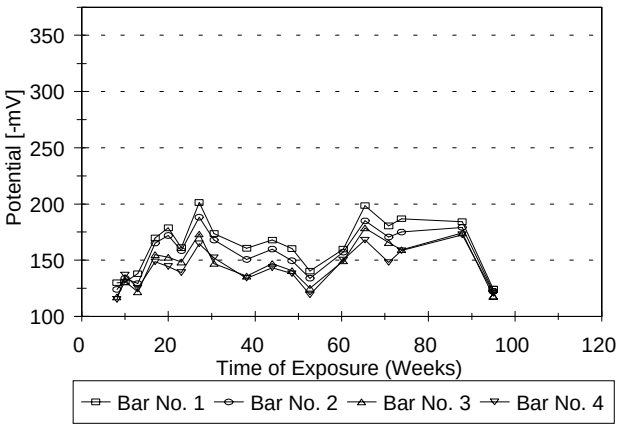

f. SFD Specimen.

FIGURE 18 a-f. Corrosion Potentials in the Horizontal Exposure Zone.

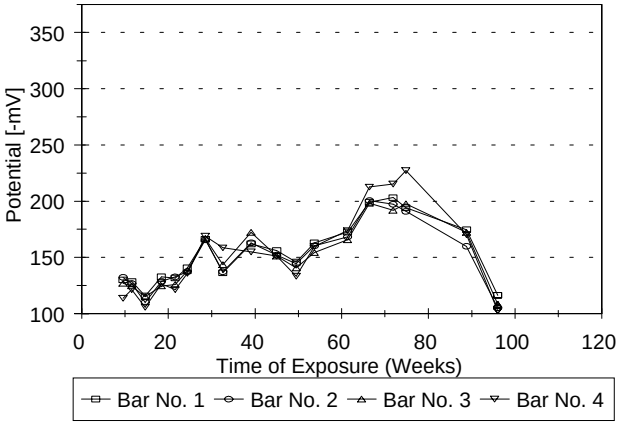

g. DCI Specimen.

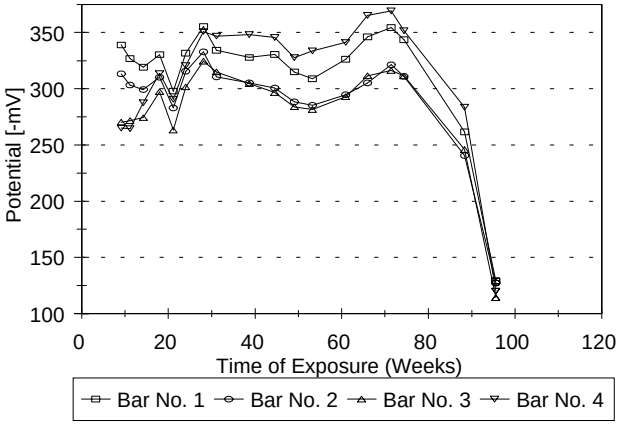

h. R222 Specimen.

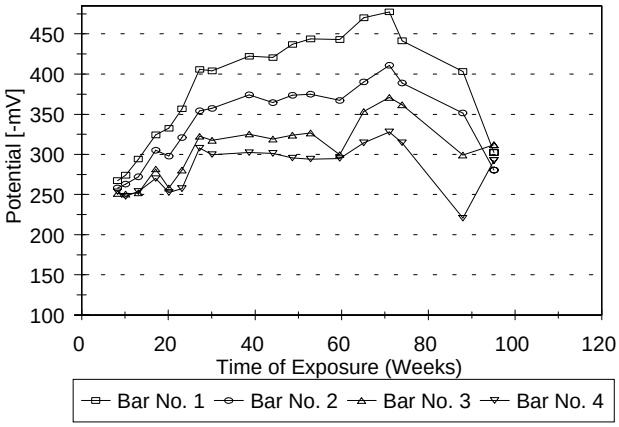

i. A2000 Specimen.

FIGURE 18 g-i. Corrosion Potentials in the Horizontal Exposure Zone.

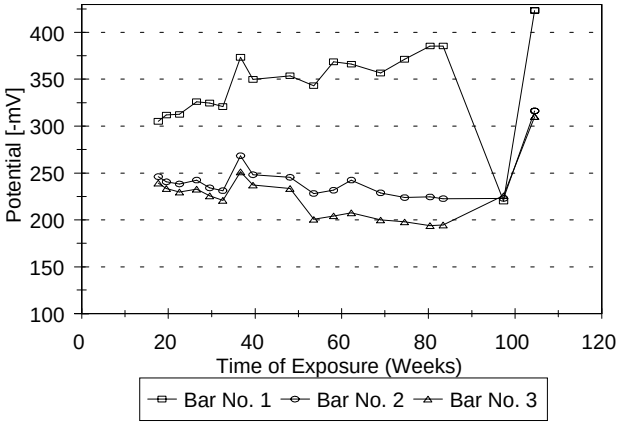

a. CTL1 Specimen - Left Leg (Reinforcing Steel Electrically Disconnected).

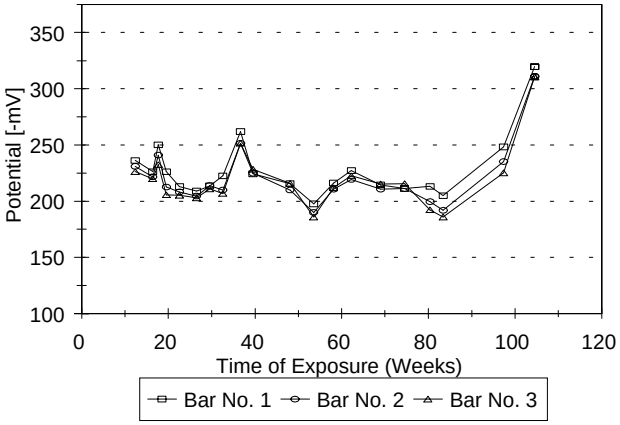

b. CTL1 Specimen - Right Leg (Reinforcing Steel Electrically Disconnected).

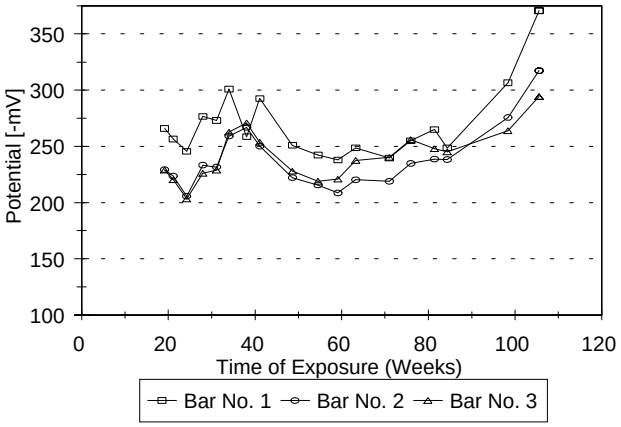

c. CTL2 Specimen - Left Leg (Reinforcing Steel Electrically Connected).

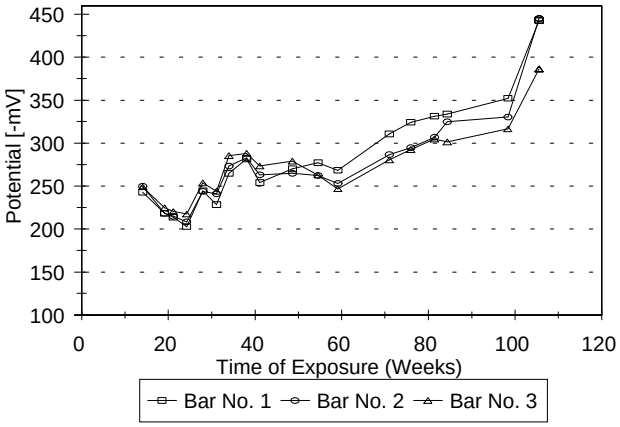

d. CTL2 Specimen - Right Leg (Reinforcing Steel Electrically Connected).

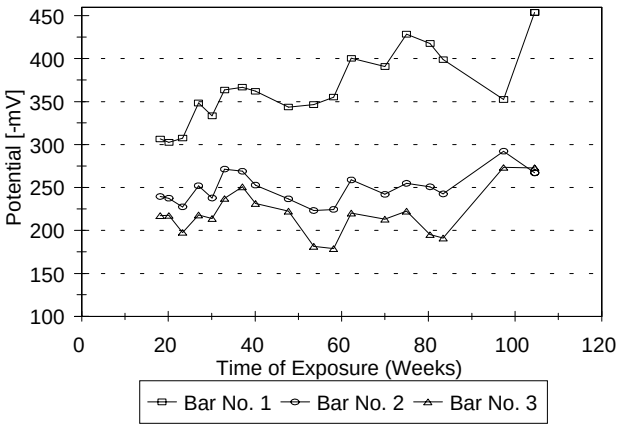

e. FA Specimen - Left Leg (Reinforcing Steel Electrically Connected).

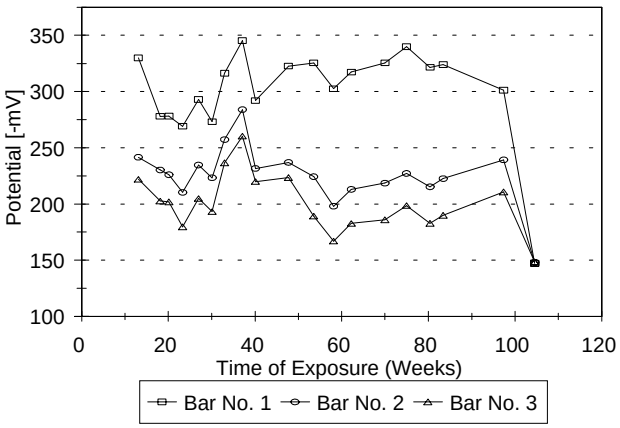

f. FA Specimen - Right Leg (Reinforcing Steel Electrically Disconnected).

FIGURE 19 a-f. Corrosion Potentials in the Vertical Exposure Zone.

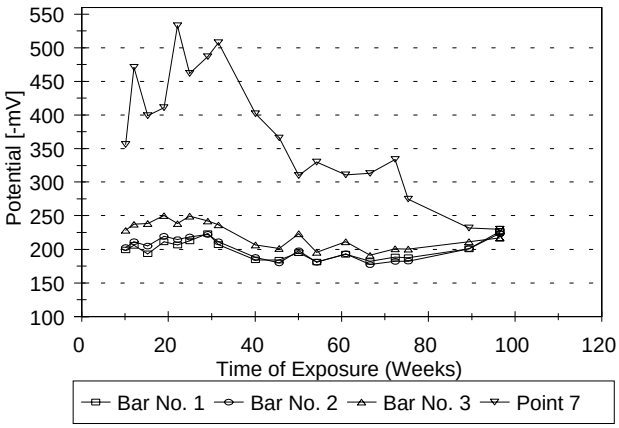

g. SC Specimen - Left Leg (Reinforcing Steel Electrically Connected).

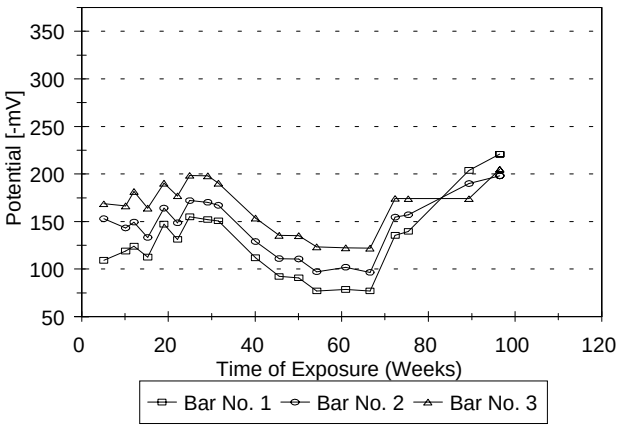

h. SC Specimen - Right Leg (Reinforcing Steel Electrically Disconnected).

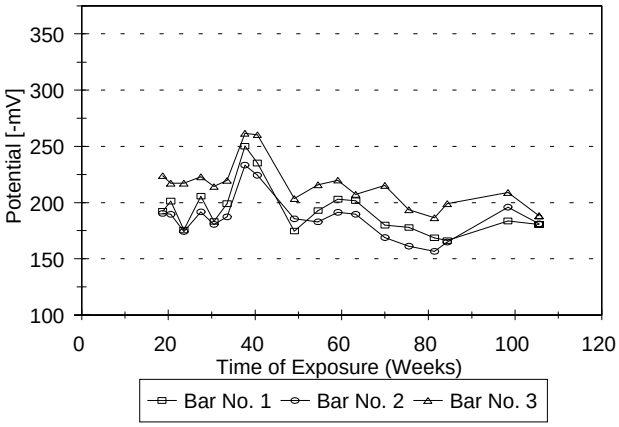

i. SF Specimen - Left Leg (Reinforcing Steel Electrically Connected).

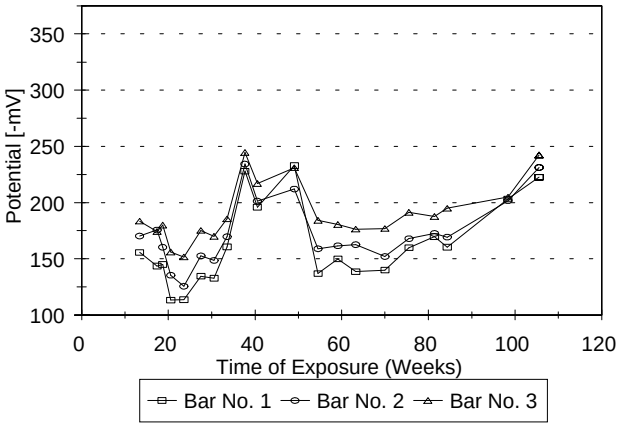

j. SF Specimen - Right Leg (Reinforcing Steel Electrically Disconnected).

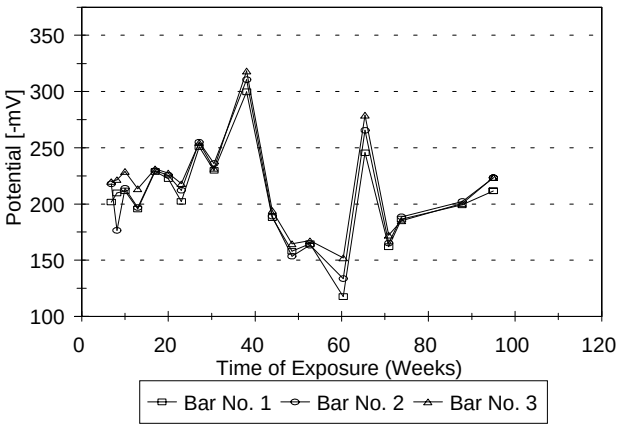

k. SFD Specimen - Left Leg (Reinforcing Steel Electrically Connected).

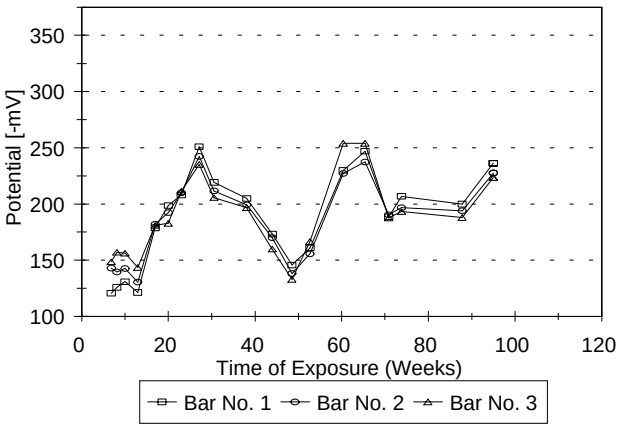

l. SFD Specimen - Right Leg (Reinforcing Steel Electrically Disconnected).

FIGURE 19 g-l. Corrosion Potentials in the Vertical Exposure Zone.

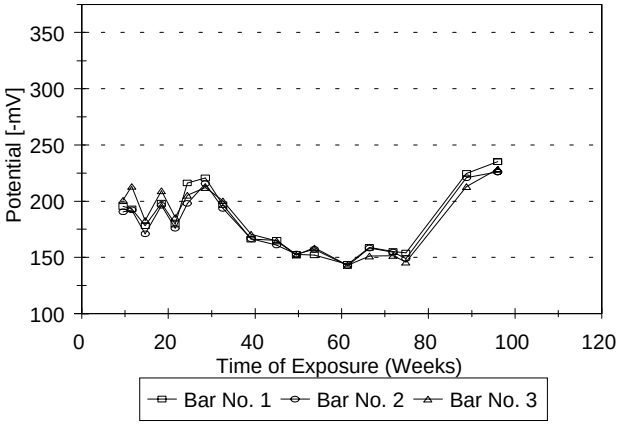

m. DCI Specimen - Left Leg (Reinforcing Steel Electrically Connected).

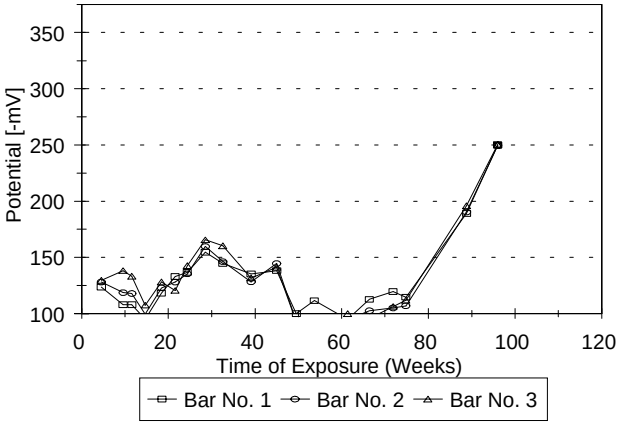

n. DCI Specimen - Right Leg (Reinforcing Steel Electrically Disconnected).

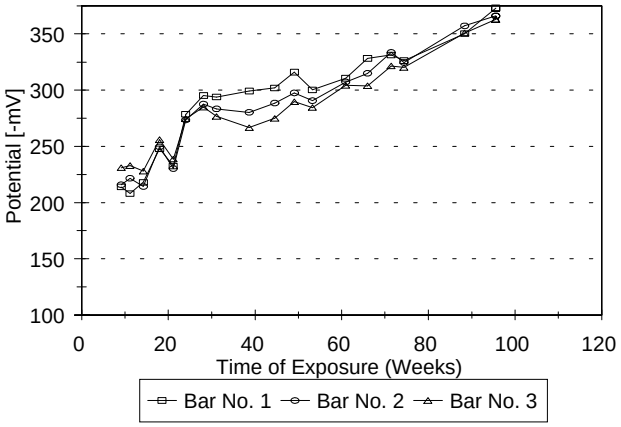

o. R222 Specimen - Left Leg (Reinforcing Steel Electrically Connected).

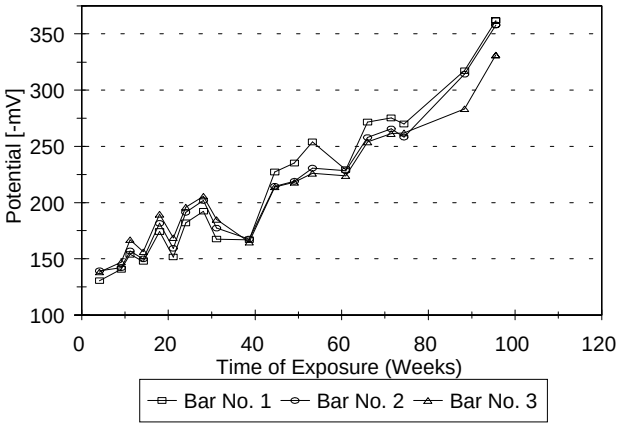

p. R222 Specimen - Right Leg (Reinforcing Steel Electrically Disconnected).

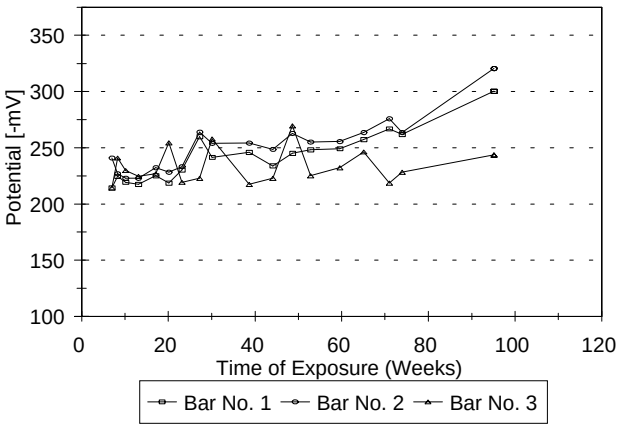

q. A2000 Specimen - Left Leg (Reinforcing Steel Electrically Connected).

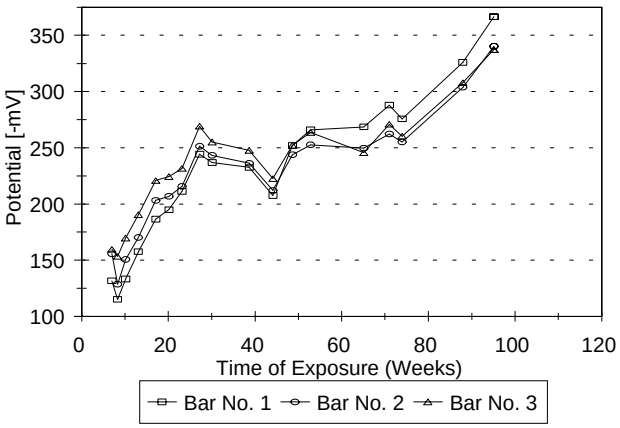

r. A2000 Specimen - Right Leg (Reinforcing Steel Electrically Disconnected).

FIGURE 19 m-r. Corrosion Potentials in the Vertical Exposure Zone.

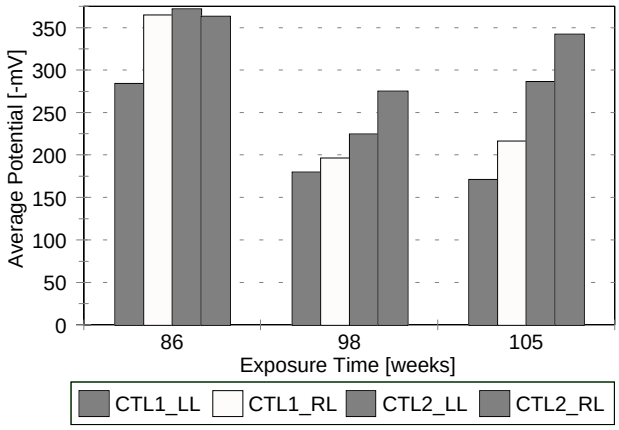

a. CTL1 and CTL2 Specimens.

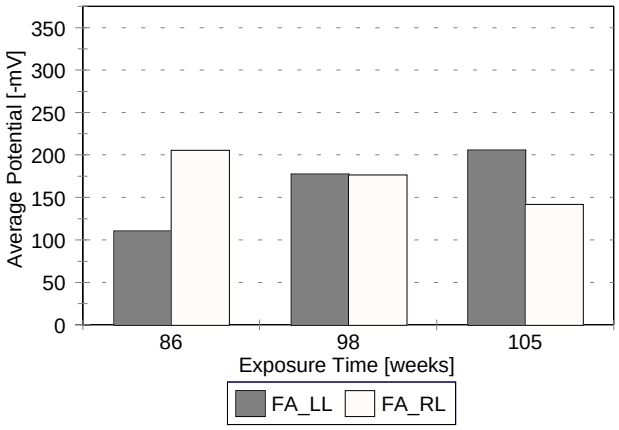

b. FA Specimen.

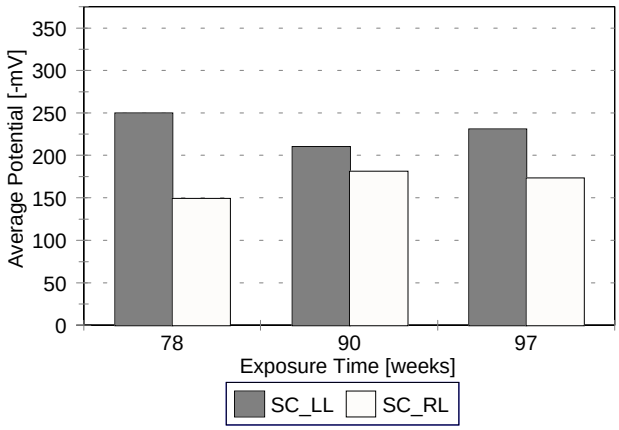

c. SC Specimen.

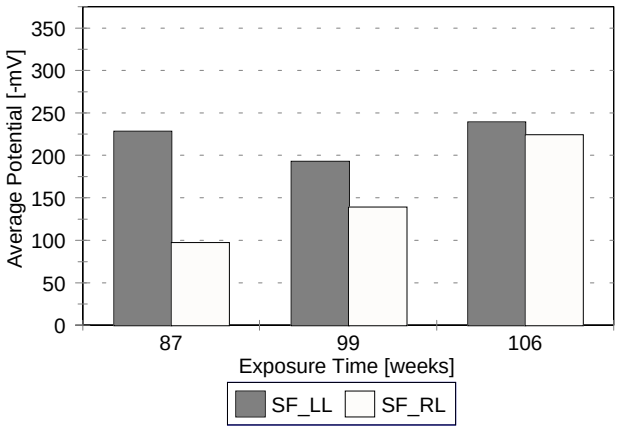

d. SF Specimen.

FIGURE 20 a-d. Corrosion Potentials in the Tidal Exposure Zone.
(LL = Left Leg, RL = Right Leg).

e. SFD Specimen.

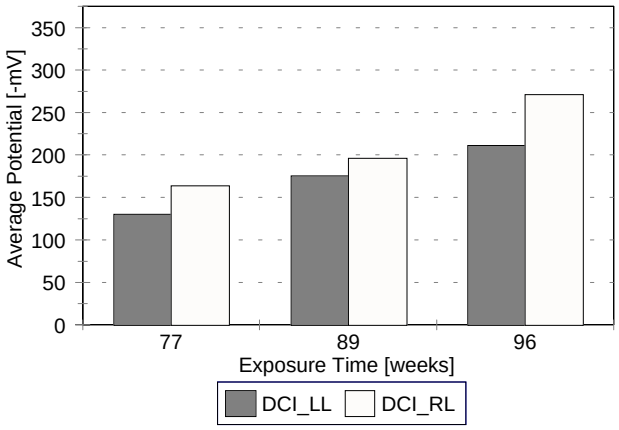

f. DCI Specimen.

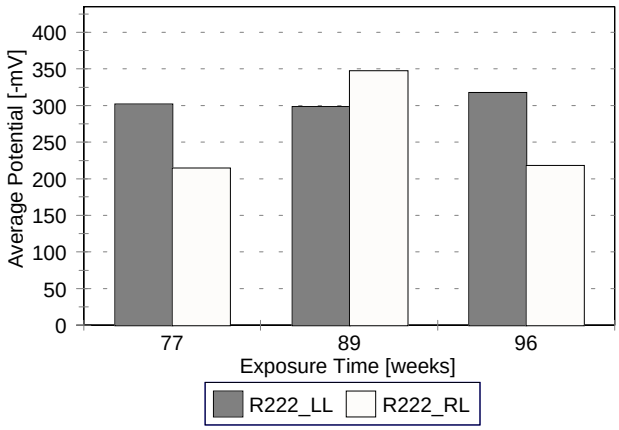

g. R222 Specimen.

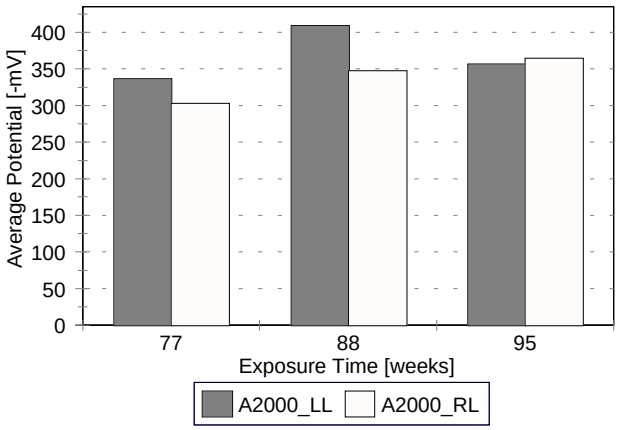

h. A2000 Specimen.

FIGURE 20 e-h. Corrosion Potentials in the Tidal Exposure Zone.
(LL = Left Leg, RL = Right Leg).

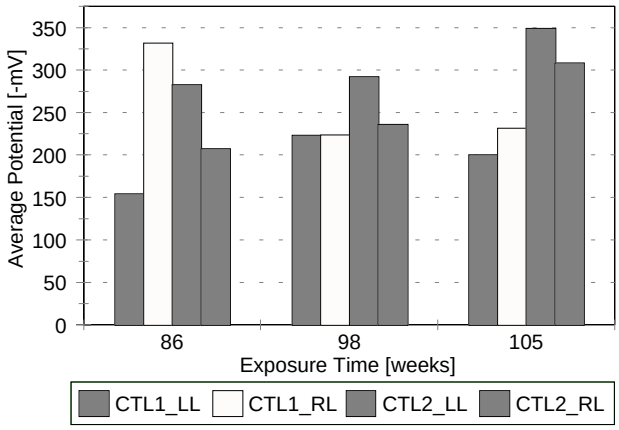

a. CTL1 and CTL2 Specimens.

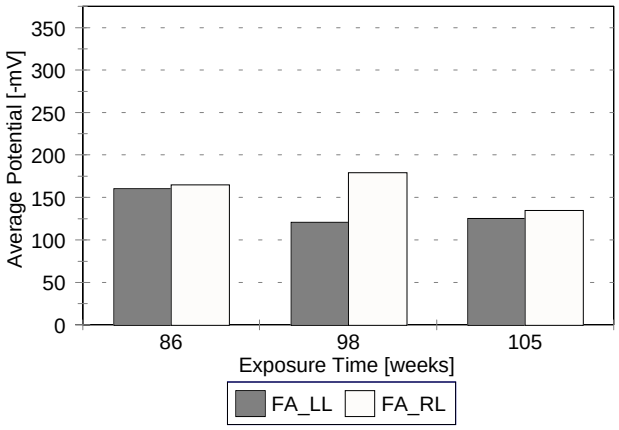

b. FA Specimen.

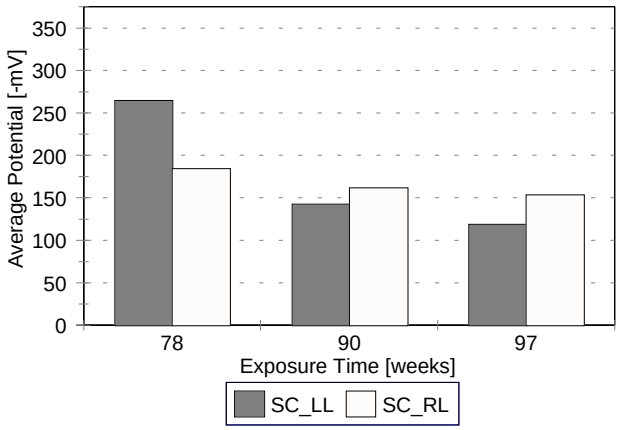

c. SC Specimen.

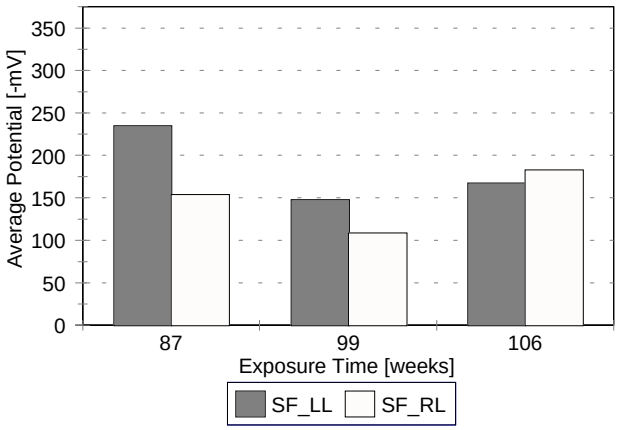

d. SF Specimen.

FIGURE 21 a-d. Corrosion Potentials in the Immersed Exposure Zone.
(LL = Left Leg, RL = Right Leg).

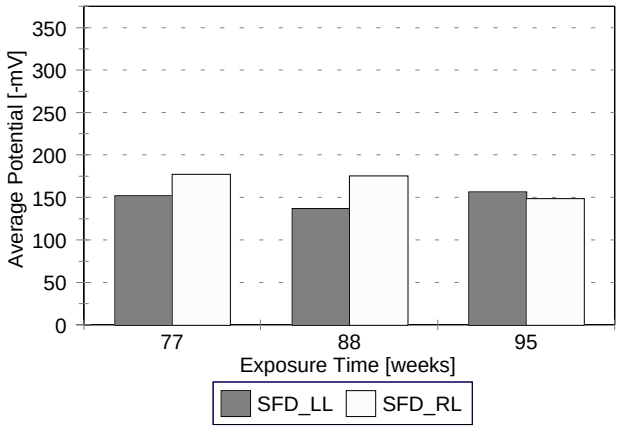

e. SFD Specimen.

f. DCI Specimen.

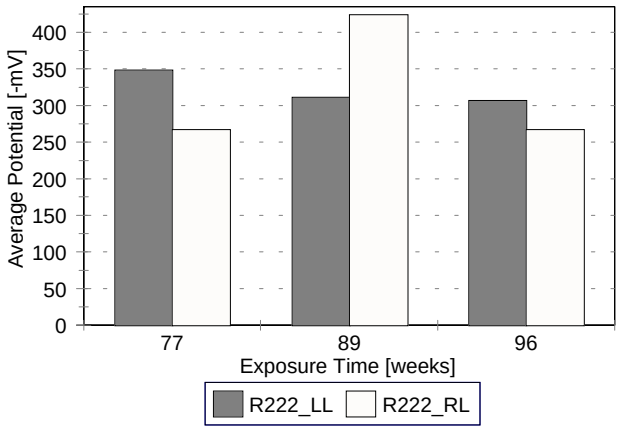

g. R222 Specimen.

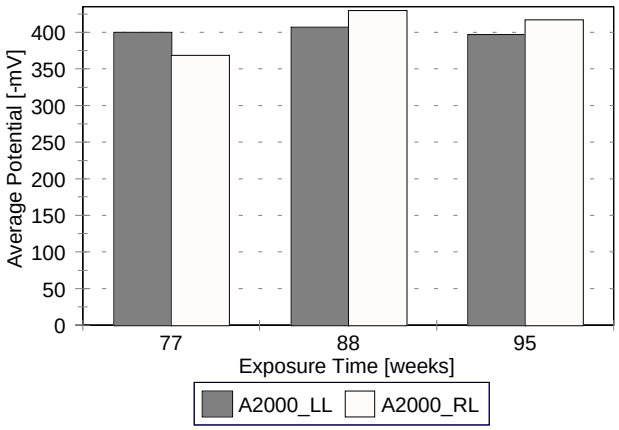

h. A2000 Specimen.

FIGURE 21 e-h. Corrosion Potentials in the Immersed Exposure Zone.
(LL = Left Leg, RL = Right Leg).

Horizontal Zone

Corrosion potentials observed in the horizontal zone of the CTL1 and CTL2 specimens suggest the possibility of an active corrosion process development during indoor exposure. As seen in Figures 18a and 18b a shift towards more negative potentials was observed after about 33 weeks of ponding for all bars of both control specimens. It is also apparent that the bar No. 4, CTL1 specimen, has a higher potential for active corrosion, with the highest measured potential of -326 mV after 80 weeks of ponding, than any other bar. Corrosion potentials for all other bars of the two control specimens ranged from -170 to -278 mV, except the two sets of readings that were taken after the specimens were moved outdoors. After a few weeks of outdoor exposure the potential values decreased significantly, especially for all bars in the CTL1 specimen, and their average values after 105 and 106 weeks of exposure were -125 and -219 mV for the CTL1 and CTL2 specimens, respectively. A possible explanation of the low measured potentials is the fact that the specimens have dried out and the possible active corrosion process taking place has been reduced. It was confirmed by impedance measurements of the cover concrete before and after the specimens were moved outdoors. An average indoor and outdoor impedance from 24 readings, 12 readings on each control specimen, were 983 and 2005 ohms, respectively. It is expected that once the moisture content of the concrete decks rises to a certain level, potentials will become more negative again and corrosion process will accelerate.

As seen in Figures 18c-18f, indoor measurements of corrosion potentials for the FA, SC, SF, and SFD specimens varied from -182 to -256 mV, -147 to -343 mV, -114 to -188 mV, and -115 to -201 mV, respectively. Corrosion potentials observed on the FA specimen were in the uncertain region of corrosion activity and were similar to the

controls in the first 54 weeks of ponding, and then, the potentials decreased and were slightly less negative than the controls, see Figure 18c. Potentials recorded on the SC specimen were significantly more negative than on any other specimen with mineral admixtures. SC potentials were even more negative than the controls in the beginning of ponding, and similar to the controls at the end of indoor exposure, see Figure 18d. During the indoor exposure period SC potentials started from the average of -314 mV, stayed in the uncertain region of corrosion activity, and increased to an average of -233 mV at the end of indoor exposure. No corrosion indication was found on the SF and SFD specimens. Indoor and outdoor readings on these specimens were less negative than -200 mV, see Figures 18e and 18f.

As for the CI concrete, only the DCI specimen had corrosion potentials significantly less negative than the controls, see Figure 18g, indicating no corrosion activity. Two other specimens with corrosion inhibitors, R222 and A2000, however, had more negative potentials than the control specimens, see Figure 18h and 18i. It suggests a high probability of an active stage of corrosion for these two specimens. Besides, the potential data for the A2000 specimen is more variable than it is for the R222 specimen indicating various stages of corrosion on different bars.

Another phenomenon was observed while measuring potentials after few weeks of outdoor exposure. The potential values in the horizontal zone of all specimens increased significantly, especially for all bars in the CTL1 and R222 specimens, see Figures 18a-18i. A possible explanation is the fact that the specimens, after being moved outdoors, have dried out and a possible corrosion process taking place has been reduced. It is expected that once the moisture content of the concrete decks rises to a certain level, potentials will become more negative again and corrosion process will accelerate.

Vertical Zone - Control Specimens

Potentials measured on the left and right legs in the vertical zone of the CTL1 specimen stayed in an uncertain region of the corrosion process with the exception of bar No.1 in the left leg, see Figures 19a and 19b. For the bar No. 1 observed potentials were always more negative than -300 mV. After 37 weeks of exposure potentials entered the region of higher probability of active corrosion and reached -386 mV after 84 weeks of exposure. After moving specimens outdoors, measured potentials on the bar No. 1 in the left leg of the CTL1 specimen decreased at first, but then increased significantly reaching -424 mV after 105 weeks of total exposure, see Figure 19a. Potentials, for all other bars in both legs, also increased significantly, see Figures 19a and 19b. Potentials measured on the left leg of the CTL2 specimen were in an uncertain region of corrosion throughout the indoor exposure period, see Figures 19c and 19d. Only bar No. 1 in the left leg had more negative potentials than others, but not negative enough to suggest an active corrosion occurring on this bar, see Figure 19c. Potentials measured on the right leg were more negative than on the left leg, indicating an active corrosion stage, see Figure 19d. After the specimens were moved outdoors a significant shift towards negative potentials was observed, especially for the right leg where the potentials were the most negative of all readings collected on the CTL1 and CTL2 specimens.

Vertical Zone - Specimens with Low Permeable Concretes

Potential data recorded in the vertical zone for the left and right legs of the FA, SC, SF, and SFD specimens are presented in Figures 19e-19f, 19g-19h, 19i-19j, and 19k-19l, respectively.

Potentials measured on the FA specimen were very similar to the potentials in the control specimens, see Figures 19e and 19f. Bar No.1 in the left leg had significantly lower potentials than two other bars, with the most negative potential of -429 mV after 75 weeks of ponding. The average potentials observed in the left leg were always more negative than -300 mV. Also in the right leg, potentials collected on the bar No.1 were more negative than two other bars, but not as negative as in the left leg, see Figure 19f. The most negative potential, -345 mV, was observed after 37 weeks of ponding. After moving the specimen outdoors measured potentials on the left leg increased while potentials on the right leg decreased, see Figures 19e and 19f.

Potentials measured on both legs of the SC specimen were less negative than the controls, with the most negative potential of -250 mV in the left leg and -199 mV in the right leg, see Figures 19g and 19h. After 97 weeks of total exposure time, potentials were in the uncertain region with the most negative potentials equal to -227 and -221 mV on the left and right legs, respectively. As shown in Figure 19g, potentials at point No. 7, bar No. 3, were significantly more negative than at any other bar. The potential values at that point were as negative as -533 mV after 22 weeks of ponding, but after 97 weeks of total exposure potential measured at this point was very close to the average potentials measured on other bars.

Corrosion potentials on the SF specimen were in the uncertain region and the region of 90% probability of no corrosion during the experiment duration, see Figures 19i and 19j.

Corrosion potentials on the SFD specimen were, as on the SF specimen, in the uncertain region and the region of 90% probability of no corrosion during the experiment duration, see Figures 19k and 19l.

Vertical Zone, Specimens with Corrosion Inhibitors

Potential data recorded in the vertical zone for the left and right legs of the DCI, R222, and A2000 specimens are presented in Figures 19m-19n, 19o-19p, and 19q-19r, respectively.

Potentials measured on both legs of the DCI specimen indicate no corrosion activity while the specimens were kept indoors. The most negative potential was recorded once the specimen was removed outdoors and was equal to -251 mV, see Figures 19m and 19n.

Corrosion potentials in the vertical zone of the R222 and A2000 specimens were very similar, see Figures 19o-19r. For the left legs potentials were in the uncertain region for the duration of the indoor exposure. For the right legs potentials started in the 90% of no corrosion region and entered the uncertain region after 39 and 17 weeks of ponding for the R222 and A2000 specimens, respectively. After the specimens were moved outdoors, potentials entered the region of 90% probability of active corrosion. The most negative potentials recorded indoors for the R222 specimen were -326 mV on the left leg and -270 mV on the right leg, outdoor values were -373 and -362 mV, respectively. The most negative potentials recorded indoors for the A2000 specimen were -278 mV on the left leg and -276 mV on the right leg, outdoor values were -334 and -367 mV, respectively.

Immersed and Tidal Zones

The potential readings in the immersed and tidal zones were collected three times.

The first set of readings was collected after the ponding was discontinued and two other ones, after the specimens were moved outdoors. Figures 20a and 21a present potential data for the control specimens, Figures 20b and 21b for the FA specimen, Figures 20c and 21c for the SC specimen, Figures 20d and 21d for the SF specimen, Figures 20e and 21e for the SFD specimen, Figures 20f and 21f present potential data for the DCI specimen, Figures 20g and 21g for the R222 specimen, and Figures 20h and 21h for the A2000 specimen, in the tidal and immersed zones, respectively.

As for the tidal zone, potential data presented in Figure 20a demonstrate no significant difference between specimens CTL1 and CTL2 during the first set of readings. The last two readings, however, show more negative potentials on the CTL2 specimen than on the CTL1 specimen, indicating influence of macrocell corrosion. Similar behavior can be observed in the immersed zone, see Figure 21a. In this case, potential data demonstrate no significant difference between the CTL1 and CTL2 specimens during the first two sets of readings. The last reading, however, indicates macrocell action on the CTL2 specimen since potential values on both legs are more negative than the potentials on the CTL1 specimen.

As shown in Figures 20b and 21b, potential readings in the tidal and immersed zones of the FA specimen indicate high probability of no active corrosion in the specimen with fly ash. Only two readings were more negative than -200 mV: -206 mV and -205 mV, both in the tidal zone, after 86 and 105 weeks of total exposure time, respectively. The most negative potential in the immersed zone was -178 mV, after 98 weeks of exposure.

Potentials in the tidal and immersed zones of the SC specimen were more negative on the left leg than on the right leg, indicating some macrocell activity, see Figures 20c

and 21c. However, the potentials were not very negative. In the tidal zone potentials were in the uncertain region with the most negative reading of -250 mV on the left leg after 78 weeks of ponding. In the immersed zone only the first reading on the left leg was -265 mV, all other readings, on both legs, were less negative than -200 mV.

Potentials measured on the left and right legs of the SF specimen in the tidal zone were in the range from -98 to -224 mV and from -193 to -239 mV, respectively, see Figure 20d. Potentials in the immersed zone were less negative than -200 mV on both legs, except -235 mV reading on the left leg after 87 weeks of ponding, see Figure 21d.

Potentials recorded on both legs in the tidal and immersed zones of the SFD specimen were less negative than -220 and -180 mV, respectively, see Figures 20e and 21e.

Potentials for the DCI specimen in the tidal and immersed exposure zones were less negative than -200 mV, except for the -211 mV on the left leg and -271 mV on the right leg in the tidal zone, and -242 mV reading on the right leg in the immersed zone, after 96 weeks of total exposure time, see Figures 20f and 21f. These readings indicate good corrosion inhibition by the DCI-S corrosion inhibitor.

Poor or even no corrosion inhibition was provided by the Rheocrete 222 and Armatec 2000 corrosion inhibitors. As seen in Figures 20g and 21g all potential readings collected in the tidal and immersed zones of the R222 specimen were more negative than -200 mV and -250 mV, respectively. As seen in Figures 20h and 21h potentials recorded on the A2000 specimen were more negative then -300 mV in the tidal zone and -350 mV in the immersed zone.

4.2.2 Corrosion Rates

Corrosion rates for the two control specimens, CTL1 and CTL2, in the horizontal zone were collected after 74, 80, 83, 97, and 105 weeks of exposure, in the vertical zone were collected after 74, 80, 83, and 105 weeks of exposure, in the immersed and tidal zones were collected after 83, 97, and 105 weeks of exposure. A relationship of corrosion rates (i_{corr}) versus time for the control specimens with bare steel bars is presented in Figures 22a-22b for the horizontal zone, Figures 23a-23d for the vertical zone, Figures 24a-24d for the tidal zone, and Figures 25a-25d for the immersed zone. Readings collected after 74 and 80 weeks of exposure were made while the specimens were still indoors and the ponding was in progress. Readings after 83 weeks of exposure were made indoors immediately after the ponding was discontinued. Readings at 97th week of exposure and later were taken after the specimens were moved outdoors.

Corrosion rates in the horizontal zone for the specimens with low permeable concretes were collected after 74, 80, 83, 97, and 105 weeks of exposure for the FA specimen, 66, 72, 75, 89, and 97 exposure weeks for the SC specimen, 75, 81, 84, 98, and 106 exposure weeks for the SF specimen, and 65, 71, 74, 88, and 95 exposure weeks for the SFD specimen. Corrosion rates in the vertical zone were collected at the same time as the first three readings and the last reading in the horizontal zone. Corrosion rates in the tidal and immersed zones were collected at the same time as the last three readings in the horizontal zone. Corrosion rate data for these specimens is presented in Figures 22c-22f for the horizontal zone, Figures 23e-23l for the vertical zone, Figures 24e-24l for the tidal zone, and Figures 25e-25l for the immersed zone.

Corrosion rates in the horizontal zone for the specimens with corrosion inhibitors,

DCI, R222, and A2000, were collected after 65, 71, 74, 88, and 95 exposure weeks, in the vertical zone after 65, 71, 74, and 95 exposure weeks, and in the immersed and tidal zones after 74, 88, and 95 weeks of exposure. Corrosion rate data for these specimens are presented in Figures 22g-22i for the horizontal zone, Figures 23m-23r for the vertical zone, Figures 24m-24r for the immersed zone, and Figures 25m-25r for the tidal zone.

The first two sets of readings in the horizontal and vertical zones, for all specimens, were collected while the specimens were still indoors and the ponding was in progress. The third set of readings in the horizontal and vertical zones, and the first set of readings in the tidal and immersed zones were collected indoors immediately after the ponding was discontinued. The remaining readings were taken after the specimens were moved outdoors.

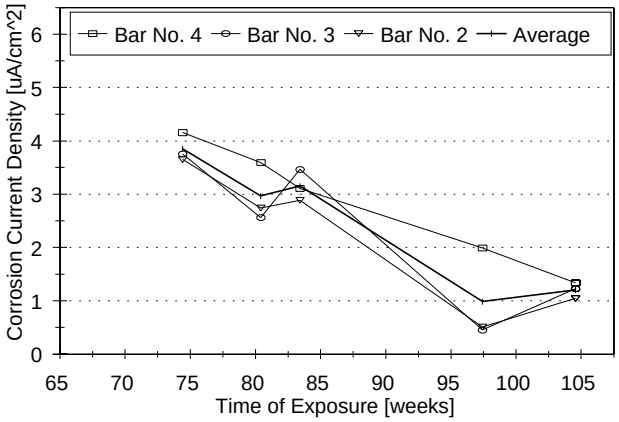

a. CTL1 Specimen.

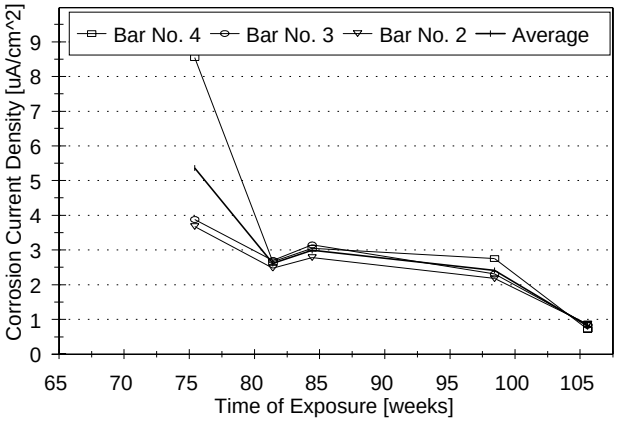

b. CTL2 Specimen.

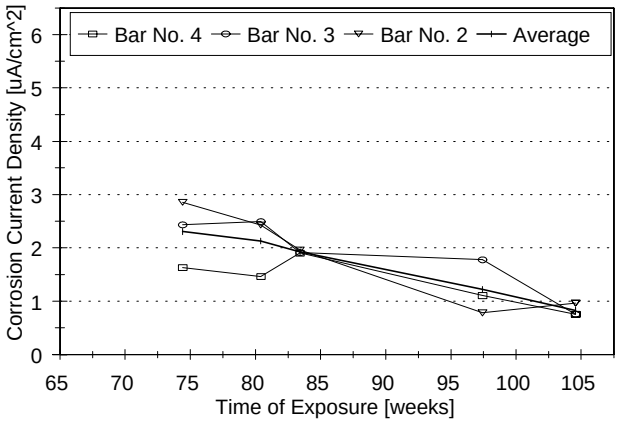

c. FA Specimen.

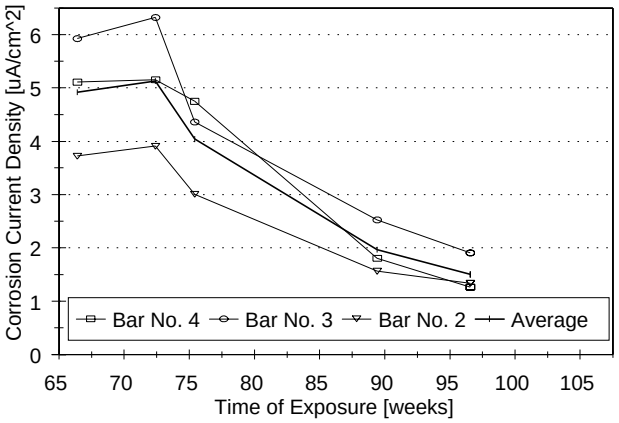

d. SC Specimen.

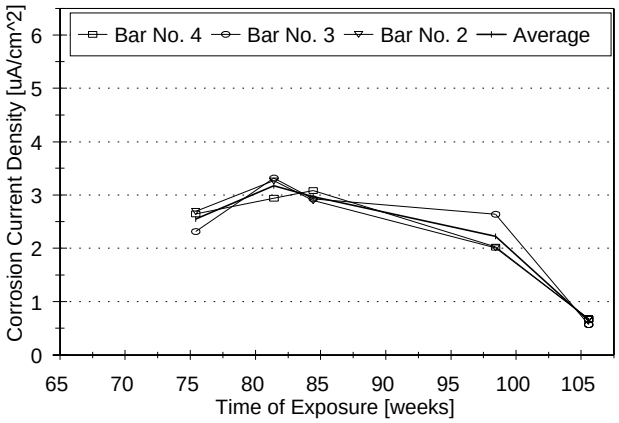

e. SF Specimen.

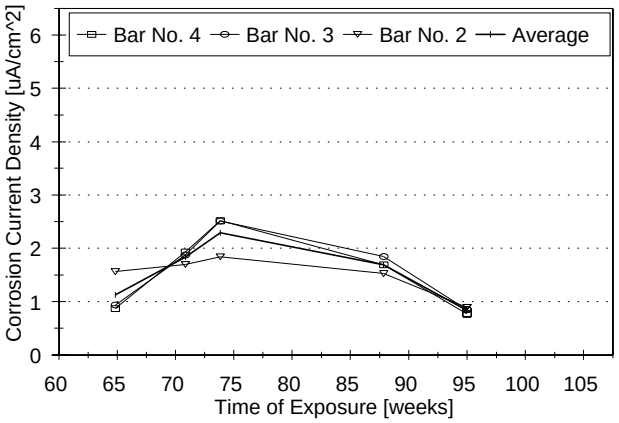

f. SFD Specimen.

FIGURE 22 a-f. Corrosion Rates in the Horizontal Exposure Zone.

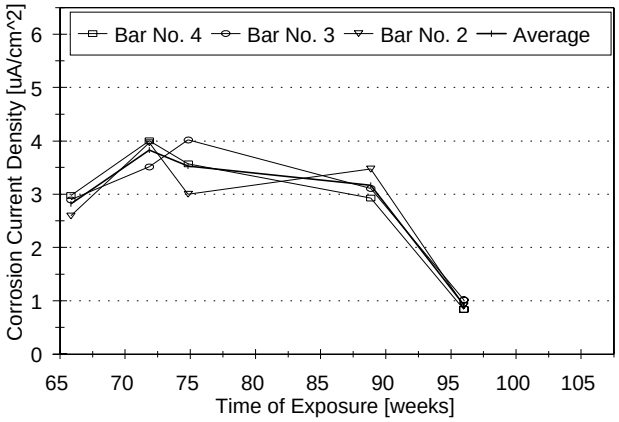

g. DCI Specimen.

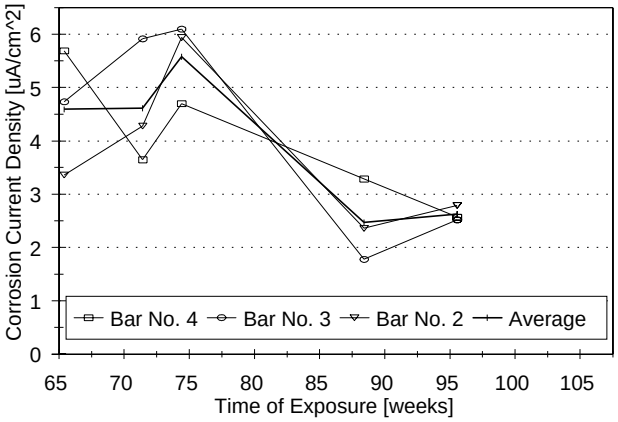

h. R222 Specimen.

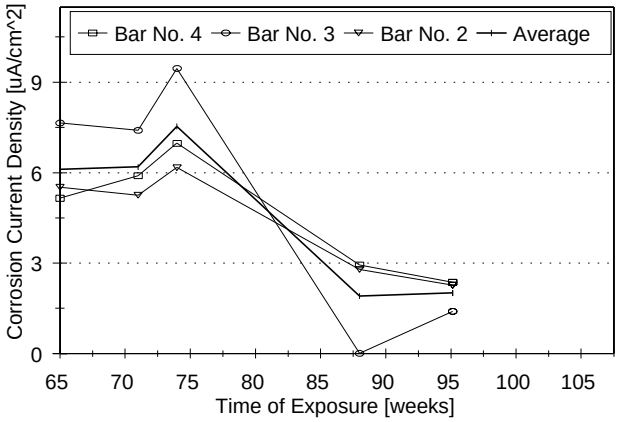

i. A2000 Specimen.

FIGURE 22 g-i. Corrosion Rates in the Horizontal Exposure Zone.

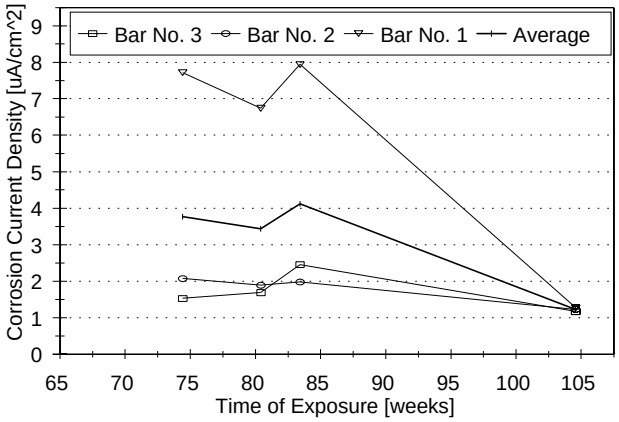

a. CTL1 Specimen - Left Leg (Reinforcing Steel Electrically Disconnected).

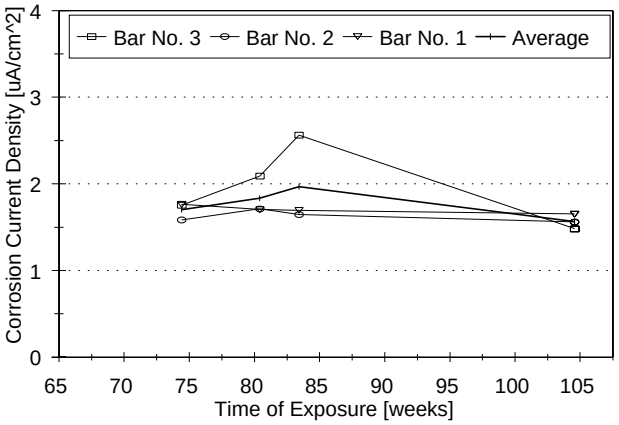

b. CTL1 Specimen - Right Leg (Reinforcing Steel Electrically Disconnected).

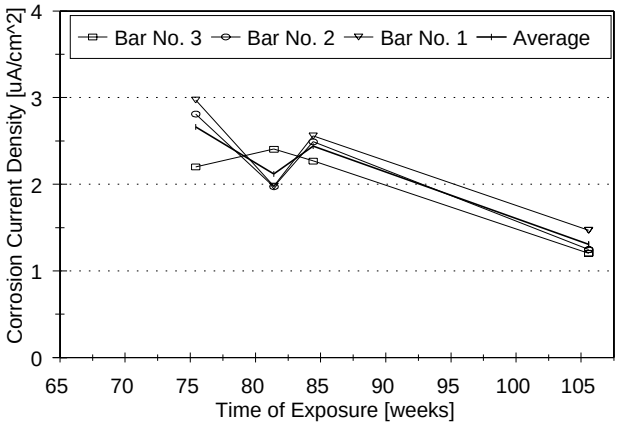

c. CTL2 Specimen - Left Leg (Reinforcing Steel Electrically Connected).

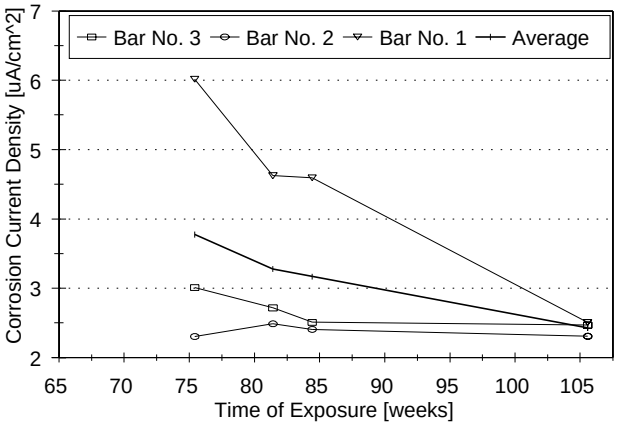

d. CTL2 Specimen - Right Leg (Reinforcing Steel Electrically Connected).

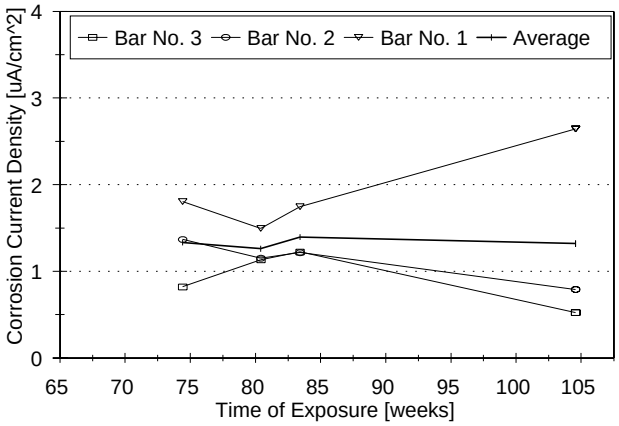

e. FA Specimen - Left Leg (Reinforcing Steel Electrically Connected).

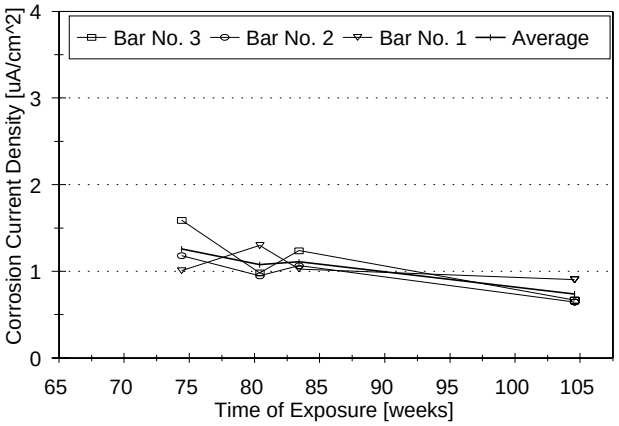

f. FA Specimen - Right Leg (Reinforcing Steel Electrically Disconnected).

FIGURE 23 a-f. Corrosion Rates in the Vertical Exposure Zone.

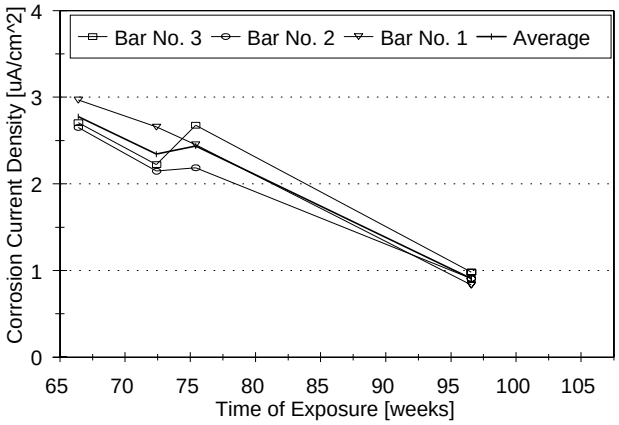

g. SC Specimen - Left Leg (Reinforcing Steel Electrically Connected).

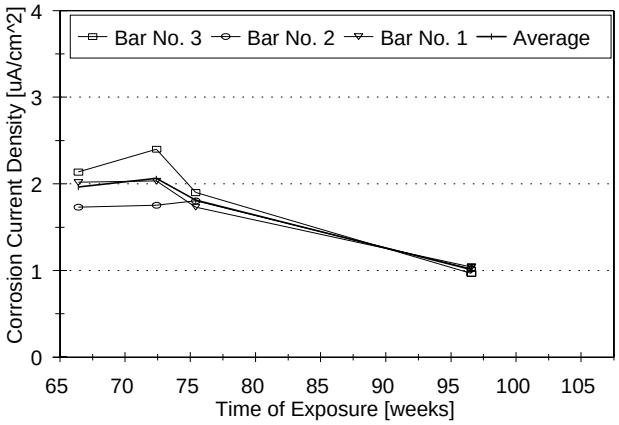

h. SC Specimen - Right Leg (Reinforcing Steel Electrically Disconnected).

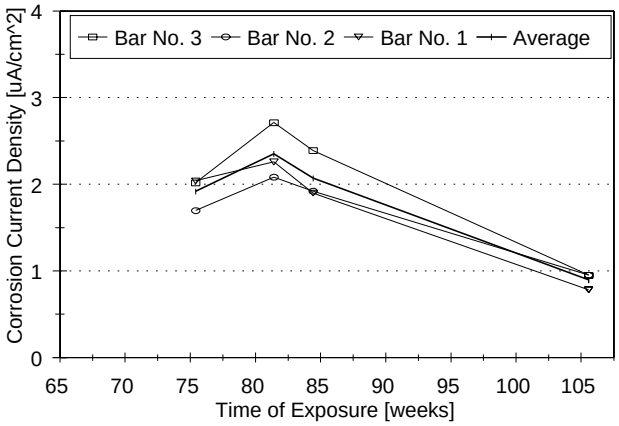

i. SF Specimen - Left Leg (Reinforcing Steel Electrically Connected).

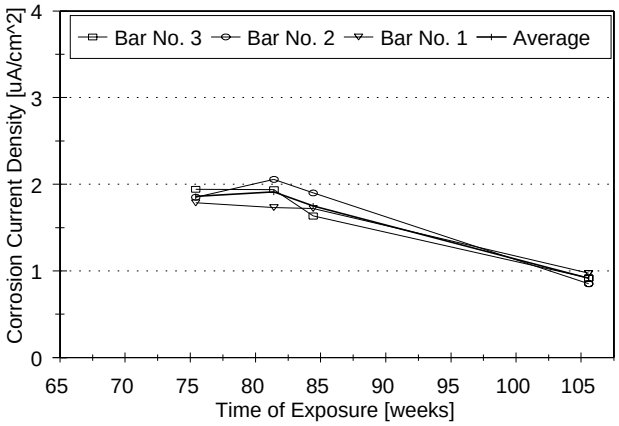

j. SF Specimen - Right Leg (Reinforcing Steel Electrically Disconnected).

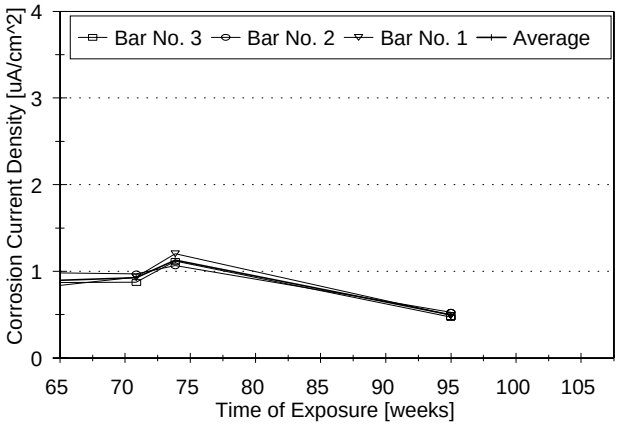

k. SFD Specimen - Left Leg (Reinforcing Steel Electrically Connected).

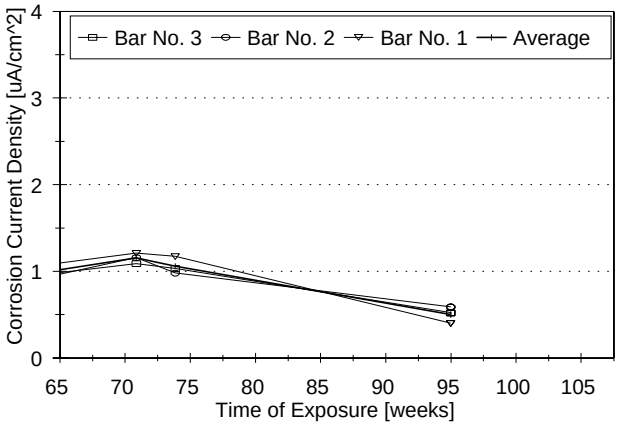

l. SFD Specimen - Right Leg (Reinforcing Steel Electrically Disconnected).

FIGURE 23 g-l. Corrosion Rates in the Vertical Exposure Zone.

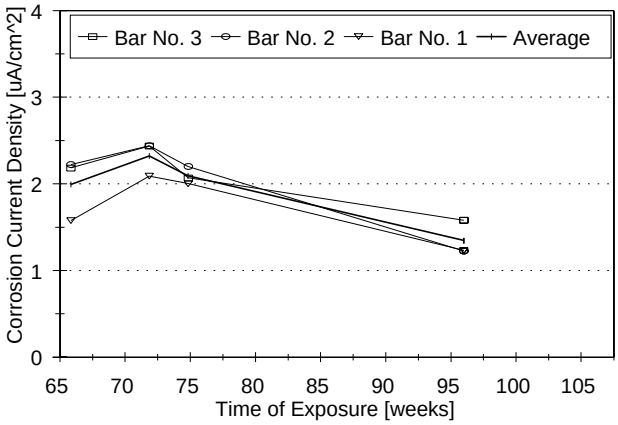

m. DCI Specimen - Left Leg (Reinforcing Steel Electrically Connected).

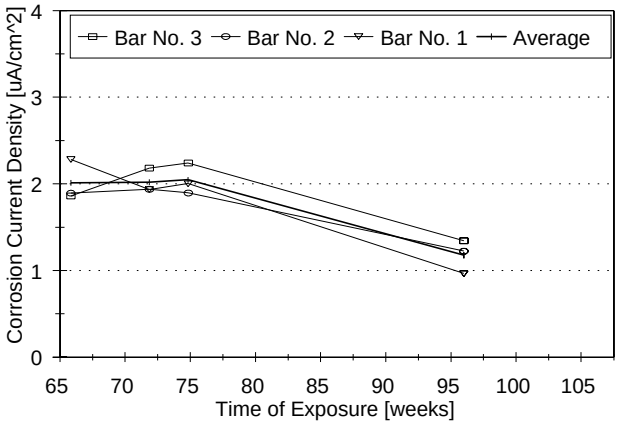

n. DCI Specimen - Right Leg (Reinforcing Steel Electrically Disconnected).

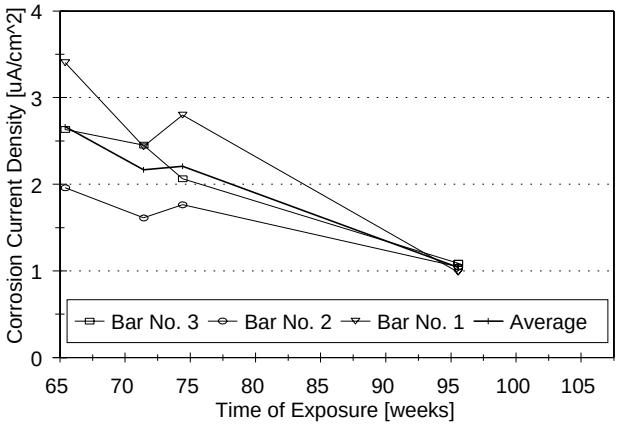

o. R222 Specimen - Left Leg (Reinforcing Steel Electrically Connected).

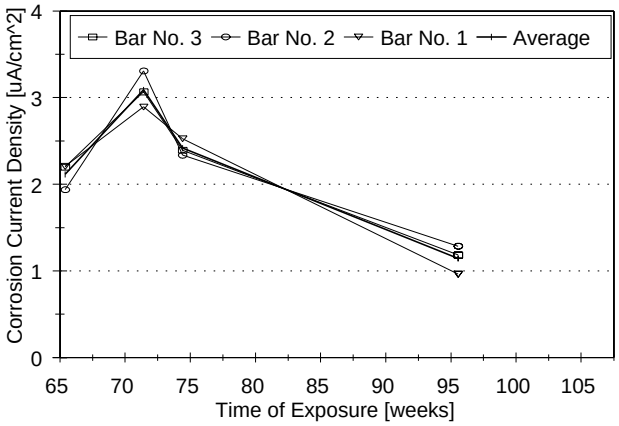

p. R222 Specimen - Right Leg (Reinforcing Steel Electrically Disconnected).

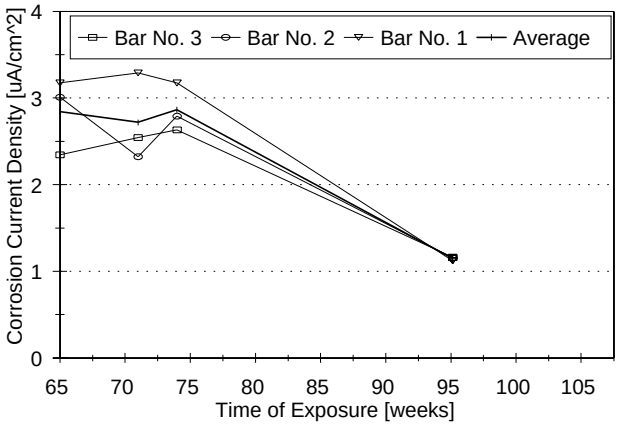

q. A2000 Specimen - Left Leg (Reinforcing Steel Electrically Connected).

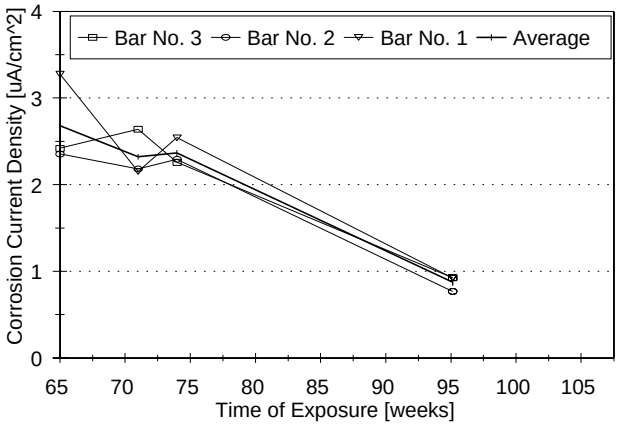

r. A2000 Specimen - Right Leg (Reinforcing Steel Electrically Disconnected).

FIGURE 23 m-r. Corrosion Rates in the Vertical Exposure Zone.

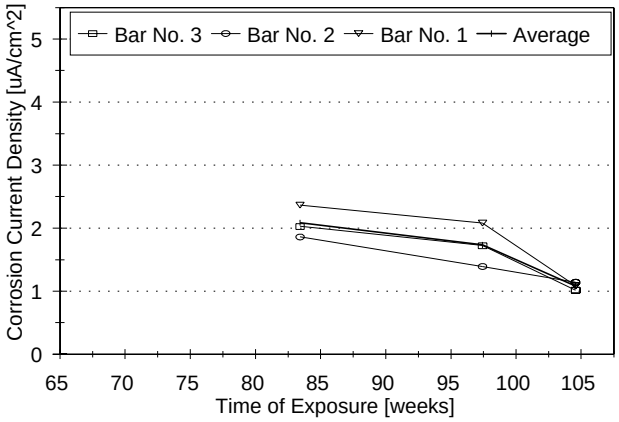

a. CTL1 Specimen - Left Leg (Reinforcing Steel Electrically Disconnected).

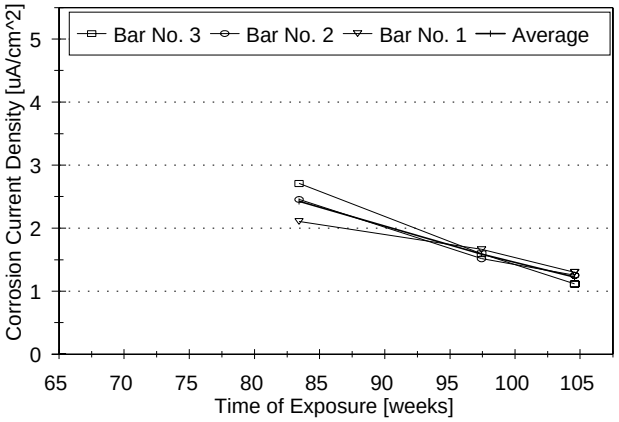

b. CTL1 Specimen - Right Leg (Reinforcing Steel Electrically Disconnected).

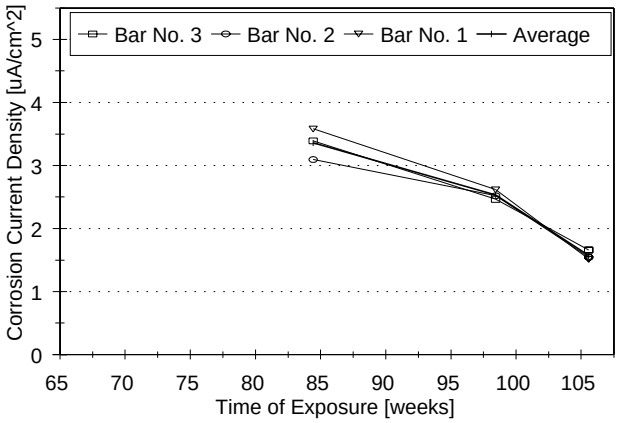

c. CTL2 Specimen - Left Leg (Reinforcing Steel Electrically Connected).

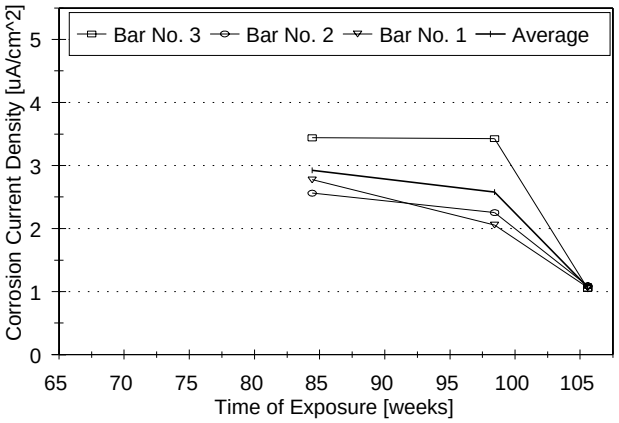

d. CTL2 Specimen - Right Leg (Reinforcing Steel Electrically Connected).

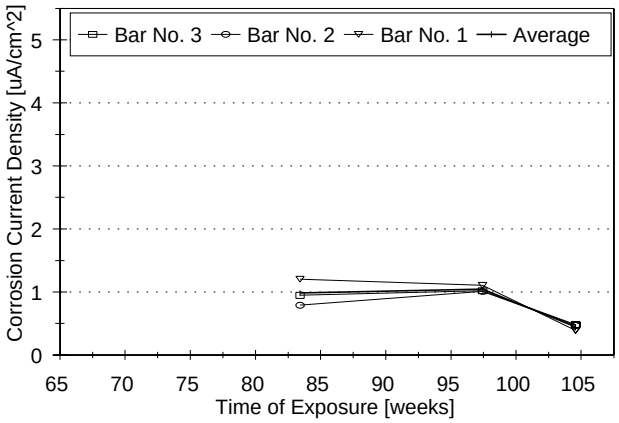

e. FA Specimen - Left Leg (Reinforcing Steel Electrically Connected).

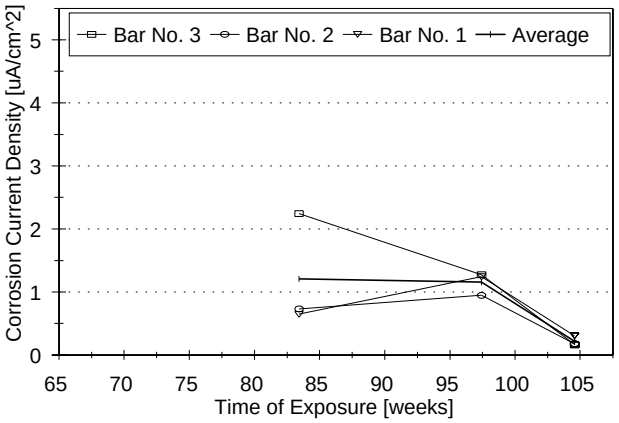

f. FA Specimen - Right Leg (Reinforcing Steel Electrically Disconnected).

FIGURE 24 a-f. Corrosion Rates in the Tidal Exposure Zone.

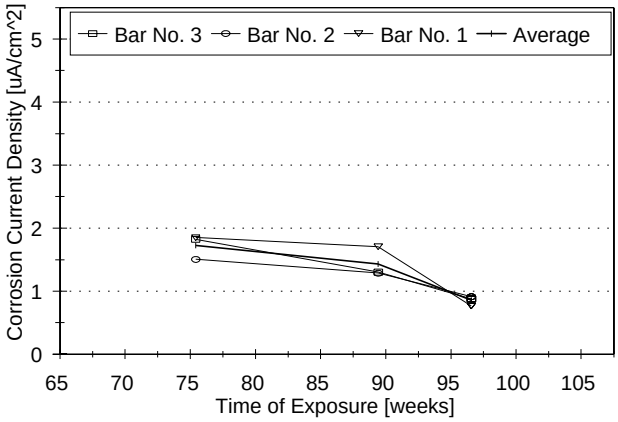

g. SC Specimen - Left Leg (Reinforcing Steel Electrically Connected).

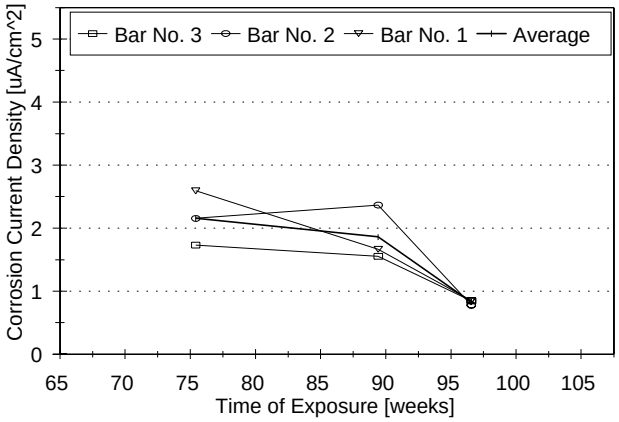

h. SC Specimen - Right Leg (Reinforcing Steel Electrically Disconnected).

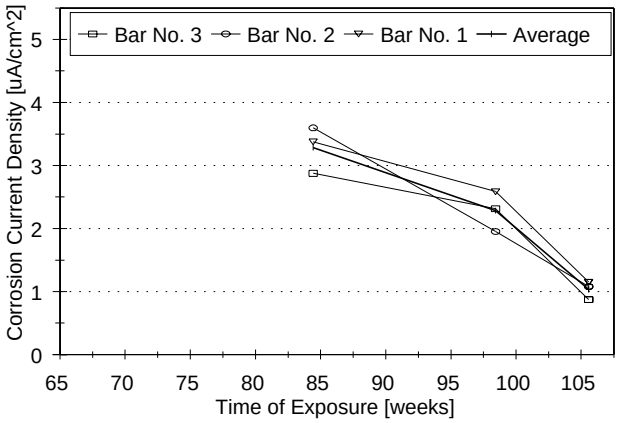

i. SF Specimen - Left Leg (Reinforcing Steel Electrically Connected).

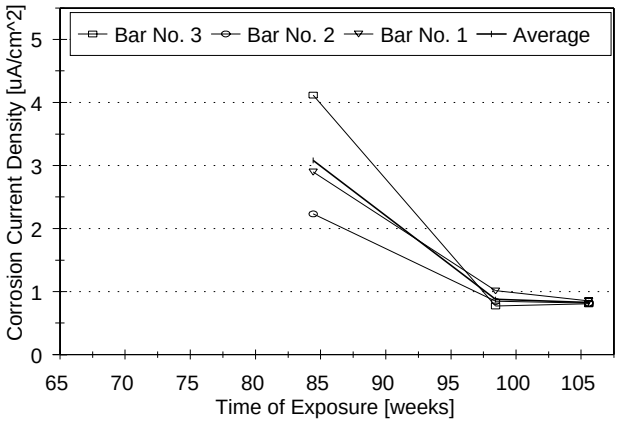

j. SF Specimen - Right Leg (Reinforcing Steel Electrically Disconnected).

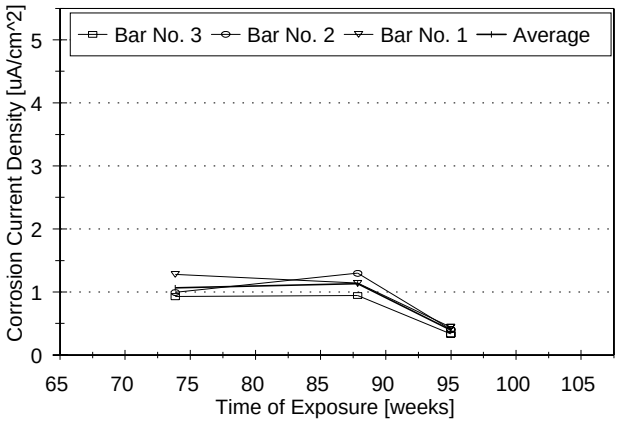

k. SFD Specimen - Left Leg (Reinforcing Steel Electrically Connected).

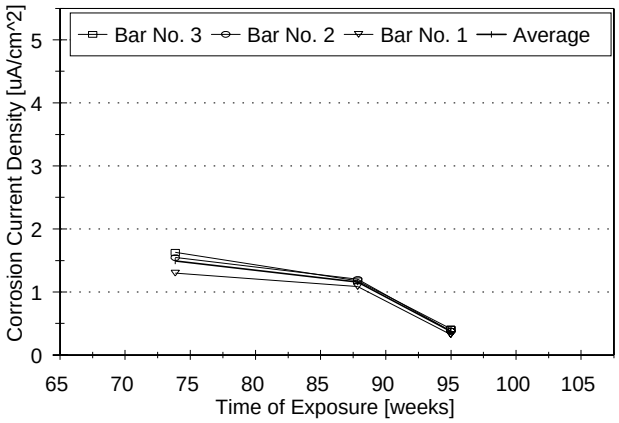

l. SFD Specimen - Right Leg (Reinforcing Steel Electrically Disconnected).

FIGURE 24 g-l. Corrosion Rates in the Tidal Exposure Zone.

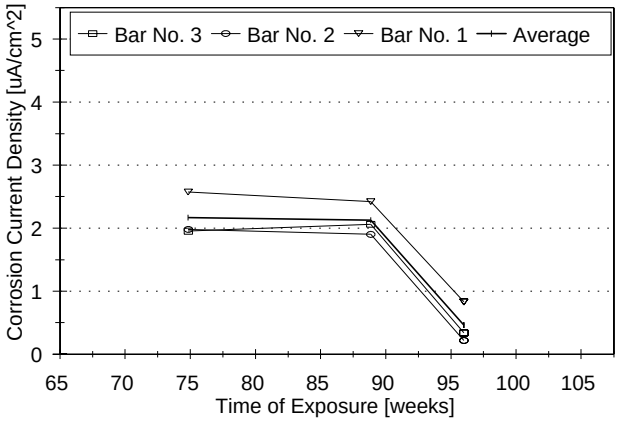

m. DCI Specimen - Left Leg (Reinforcing Steel Electrically Connected).

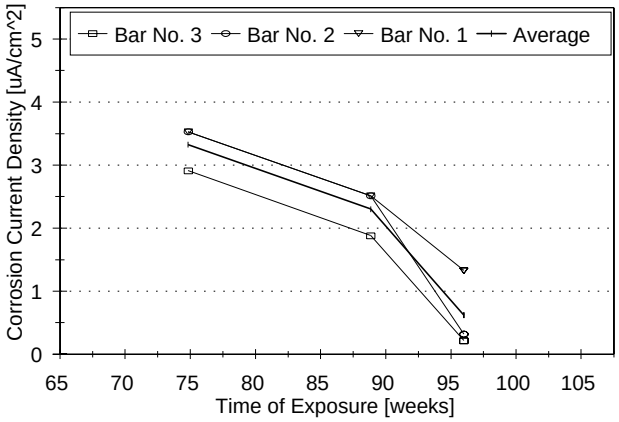

n. DCI Specimen - Right Leg (Reinforcing Steel Electrically Disconnected).

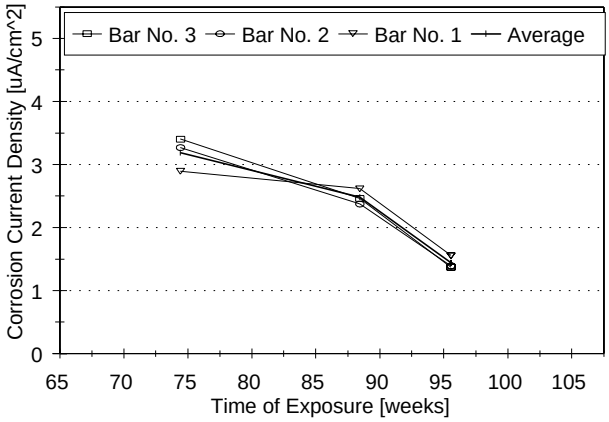

o. R222 Specimen - Left Leg (Reinforcing Steel Electrically Connected).

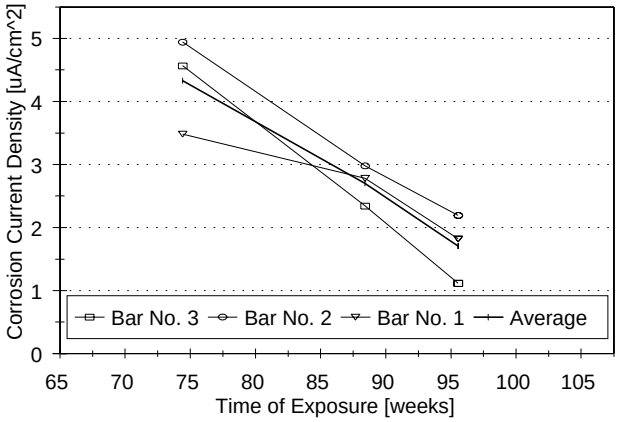

p. R222 Specimen - Right Leg (Reinforcing Steel Electrically Disconnected).

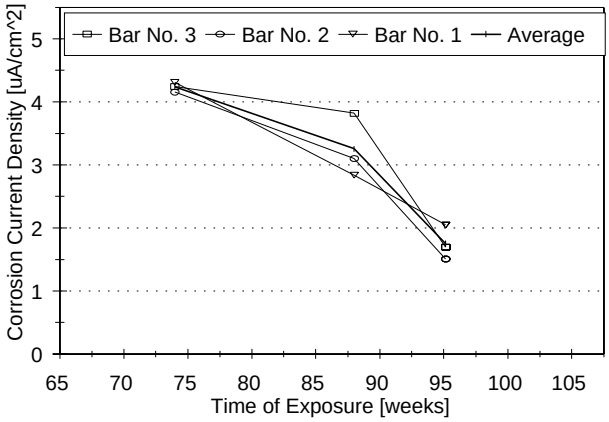

q. A2000 Specimen - Left Leg (Reinforcing Steel Electrically Connected).

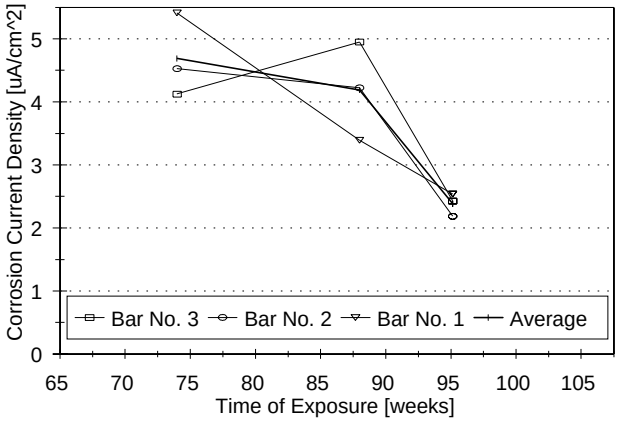

r. A2000 Specimen - Right Leg (Reinforcing Steel Electrically Disconnected).

FIGURE 24 m-r. Corrosion Rates in the Tidal Exposure Zone.

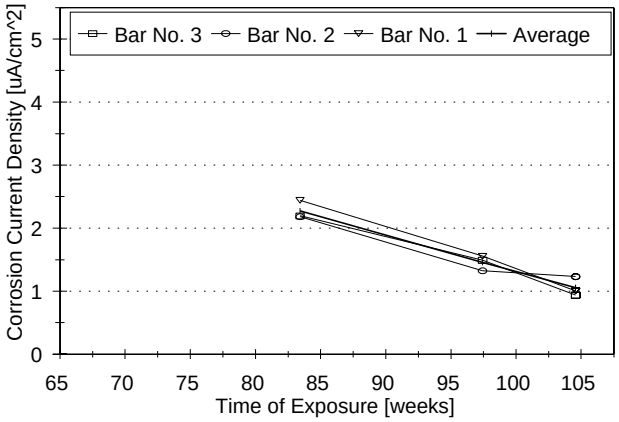

a. CTL1 Specimen - Left Leg (Reinforcing Steel Electrically Disconnected).

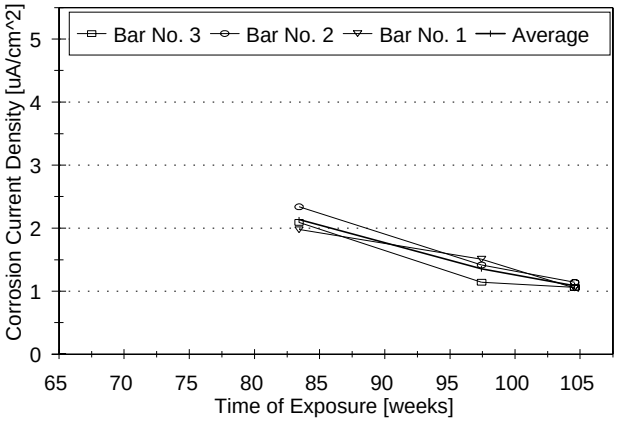

b. CTL1 Specimen - Right Leg (Reinforcing Steel Electrically Disconnected).

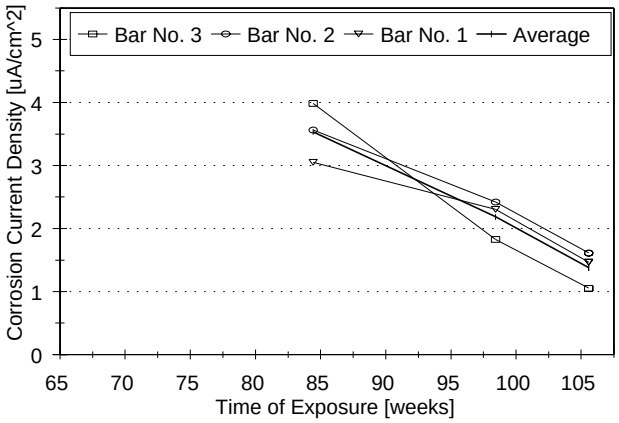

c. CTL2 Specimen - Left Leg (Reinforcing Steel Electrically Connected).

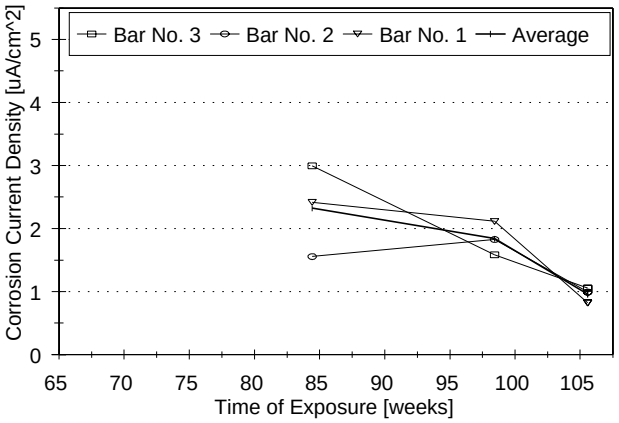

d. CTL2 Specimen - Right Leg (Reinforcing Steel Electrically Connected).

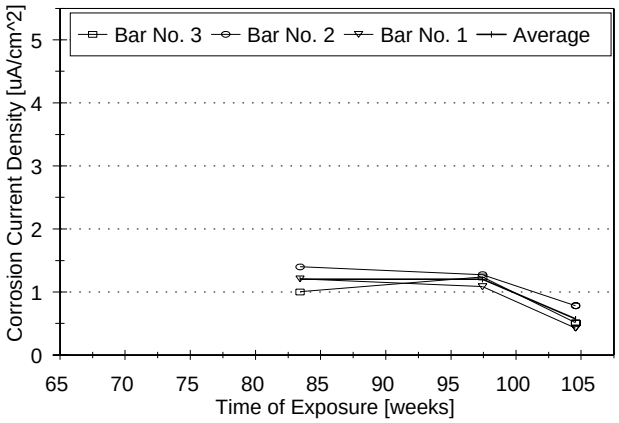

e. FA Specimen - Left Leg (Reinforcing Steel Electrically Connected).

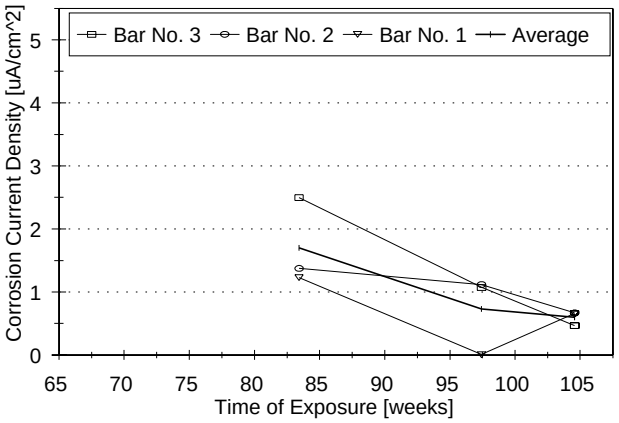

f. FA Specimen - Right Leg (Reinforcing Steel Electrically Disconnected).

FIGURE 25 a-f. Corrosion Rates in the Immersed Exposure Zone.

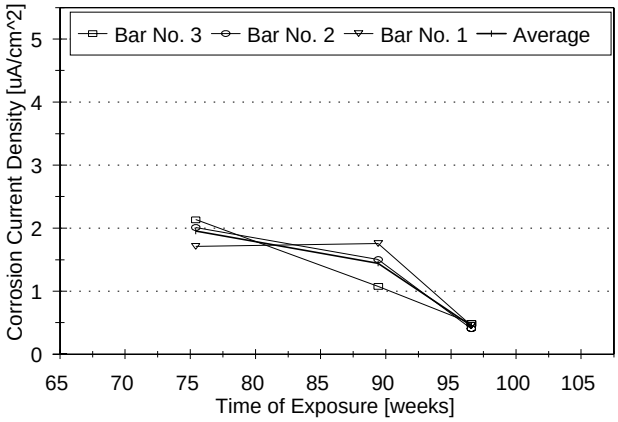

g. SC Specimen - Left Leg (Reinforcing Steel Electrically Connected).

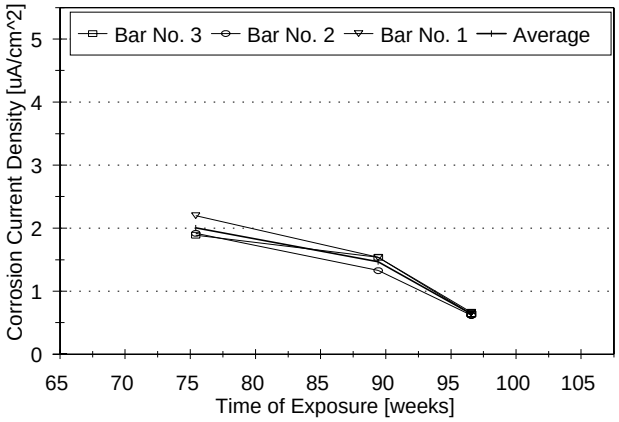

h. SC Specimen - Right Leg (Reinforcing Steel Electrically Disconnected).

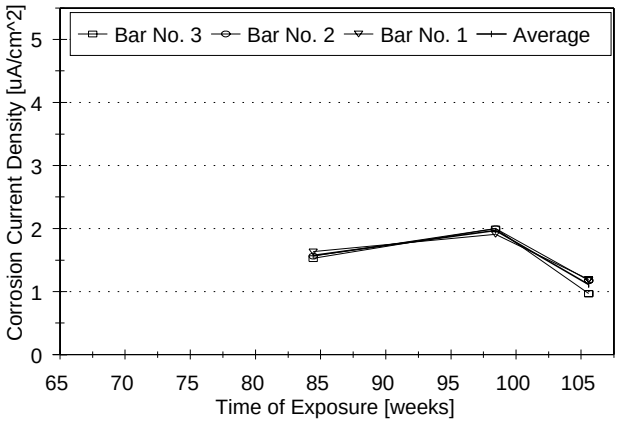

i. SF Specimen - Left Leg (Reinforcing Steel Electrically Connected).

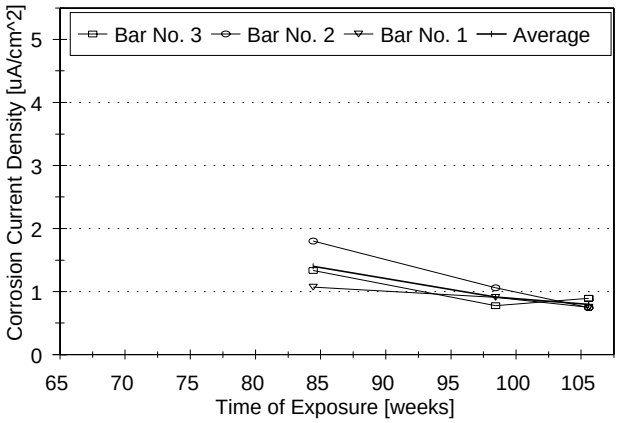

j. SF Specimen - Right Leg (Reinforcing Steel Electrically Disconnected).

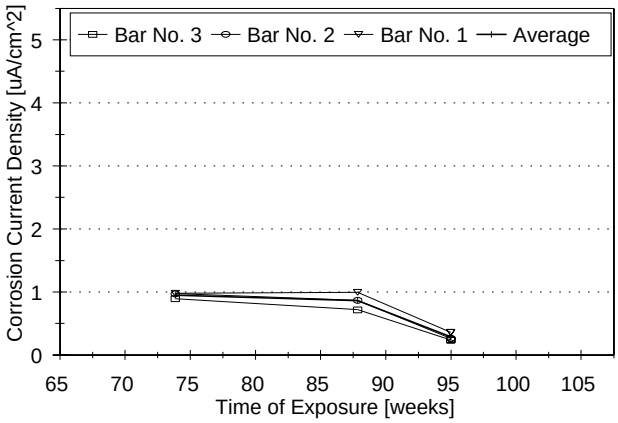

k. SFD Specimen - Left Leg (Reinforcing Steel Electrically Connected).

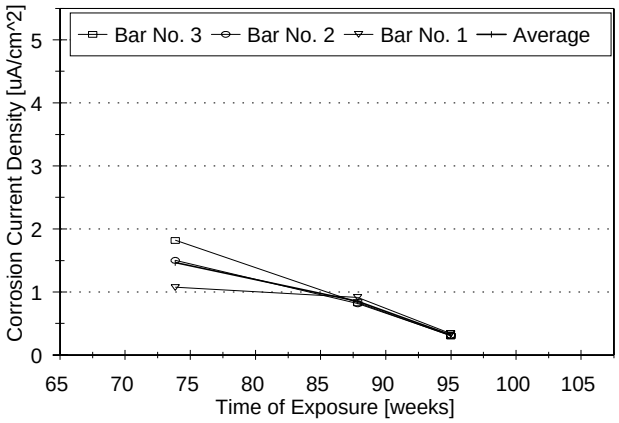

l. SFD Specimen - Right Leg (Reinforcing Steel Electrically Disconnected).

FIGURE 25 g-l. Corrosion Rates in the Immersed Exposure Zone.

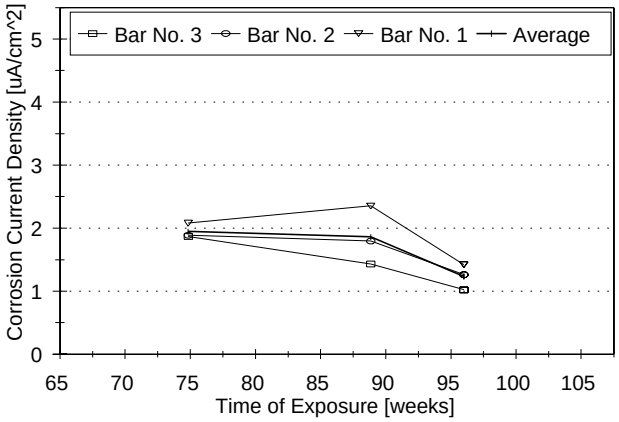

m. DCI Specimen - Left Leg (Reinforcing Steel Electrically Connected).

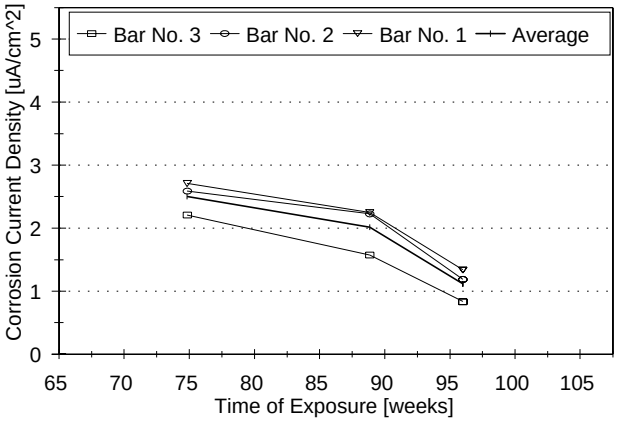

n. DCI Specimen - Right Leg (Reinforcing Steel Electrically Disconnected).

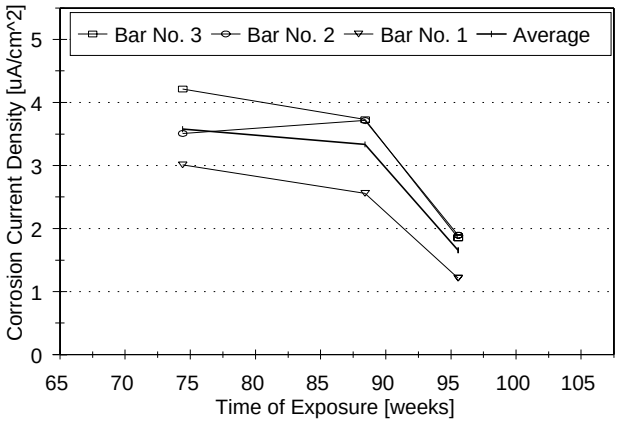

o. R222 Specimen - Left Leg (Reinforcing Steel Electrically Connected).

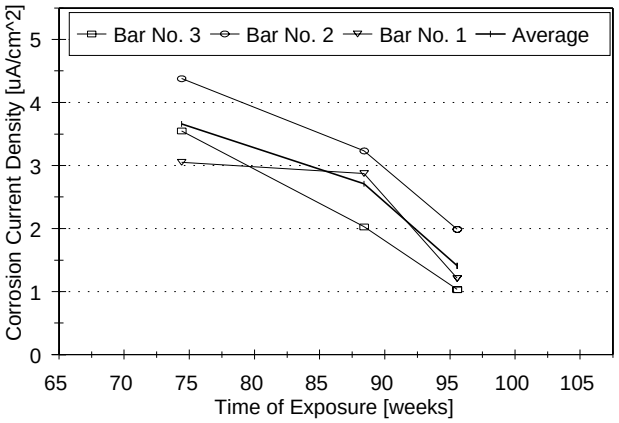

p. R222 Specimen - Right Leg (Reinforcing Steel Electrically Disconnected).

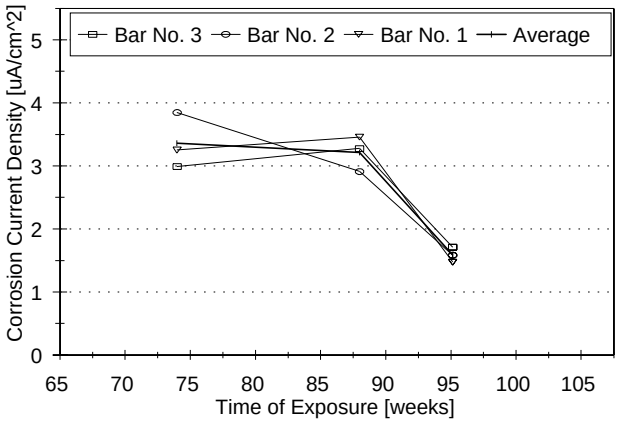

q. A2000 Specimen - Left Leg (Reinforcing Steel Electrically Connected).

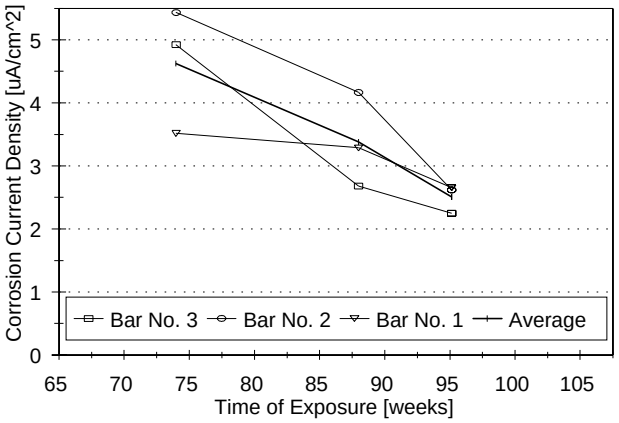

r. A2000 Specimen - Right Leg (Reinforcing Steel Electrically Disconnected).

FIGURE 25 m-r. Corrosion Rates in the Immersed Exposure Zone.

Control Specimens

Corrosion rates in the horizontal zone, Figures 22a and 22b, were similar for both control specimens and were decreasing in time. In the vertical zone, Figures 23a-23d, corrosion rates measured on specimen CTL1 were lower than the ones measured on specimen CTL2. As shown in Figures 23a and 23d two bars had significantly higher corrosion rates than the other bars. Once the specimens were moved outdoors, corrosion rates of these two bars decreased to the level of the two other bars in the same specimen, leg, and exposure zone. Corrosion rates in the tidal zone for the two control specimens decreased once the specimens were moved outdoors, as presented in Figures 24a-24b and 24c-24d for specimens CTL1 and CTL2, respectively. Corrosion rates in the immersed zone for the two control specimens were similar to corrosion rates in the tidal zone and also decreased after moving the specimens outdoors, see Figures 25a-25b and 25c-25d for specimens CTL1 and CTL2, respectively.

The corrosion rate results indicate that the control specimens were in an active region of corrosion when they were kept indoors, since the corrosion rates were higher than 2 mA/cm^2 and the corrosion rates measured outdoors were lower than indoors, see Figures 22a-22b, 23a-23d, 24a-24d, and 25a-25d. The data from the horizontal zone, Figures 22a and 22b, agree with the potential data indicating lesser corrosion activity when the specimens were kept outdoors than indoors. Also, in the vertical zone the highest corrosion rates for the controls were observed in the right leg of CTL2 specimen, the same place where the most negative potentials were found, see Figures 23a-23d. Macrocell action is a probable explanation of differences in corrosion rates in the tidal and immersed zones between the CTL1 specimen, legs reinforcement not connected, and the CTL2 specimen, legs reinforcement connected, see Figures 24a-

24d and 25a-25d.

Specimens with Low Permeable Concretes

Corrosion rates in the horizontal zone, while the specimens were housed indoors, ranged from 1.46 to 2.86 mA/cm^2 for the FA specimen, from 3.01 to 6.32 mA/cm^2 for the SC specimen, from 2.32 mA/cm^2 to 3.32 mA/cm^2 for the SF specimen, and from 0.88 to 2.52 mA/cm^2 for the SFD specimen, see Figures 22c-22f. Some corrosion activity that was observed while the specimens were housed indoors, disappeared after the specimens were moved outdoors. Corrosion rates decreased to 0.83 mA/cm^2 for the FA specimen, 1.51 mA/cm^2 for the SC specimen, 0.64 mA/cm^2 for the SF specimen, and 0.84 mA/cm^2 for the SFD specimen.

Corrosion rate readings in the vertical zone on left leg were similar to the readings on the right leg for the FA, SC, SF, and SFD specimens, see Figures 23e-23l. After the specimens were moved outdoors, the highest corrosion rates were found on the SC specimen, the lowest - on the SFD specimen.

Corrosion rates in the tidal and immersed zones show similar trend as in the vertical zone: corrosion rates for the SC and SF specimens were higher than for the FA and SFD specimens, see Figures 24e-24l and 25e-25l, respectively.

Specimens with Corrosion Inhibitors

Among the CI specimens, corrosion rates in the horizontal zone of the DCI specimen, Figure 22g, were similar to the controls. Also, the R222 and A2000 specimen seem to

be corroding more than the controls since corrosion rates were higher, see Figures 22h and 22i, respectively.

In the vertical, tidal, and immersed zones of the CI specimens, there is no significant difference in corrosion rates between the legs, see Figures 23m-23r, 24m-24r, and 25m-25r, respectively. The values are similar for the R222 and A2000 specimens and the lowest for the DCI specimen. Also, no significant difference between the readings from left leg and the right leg indicates no influence of macrocell action.

The readings agree with potential data and indicate poor performance of both Rheocrete 222 and Armatec 2000 corrosion inhibitors.

4.2.3 Chlorides

Chloride concentrations were determined for all concrete types used for specimen fabrication. After 33 weeks and 1 year of ponding, concrete powder samples were collected from three depths of small concrete blocks that were placed in tidal and immersed zones. After 1.5 years of ponding the samples were collected from all exposure zones of all specimens. Concrete powder samples were collected from three depths for vertical, tidal, and immersed zones, and from four depths from the horizontal zone. Chloride concentrations for tidal, immersed, horizontal, and vertical zones versus depth are presented in Figures 26-29, respectively. The concrete powder samples for chloride concentration determination at 33 weeks and 1 year were collected from the small concrete blocks, that were placed in the Tidal and Immersed Zones when ponding started.

The results of chloride testing indicate that the amount of chlorides present at the bar level is more than sufficient for corrosion to occur, especially for the controls and the CI specimens. Chloride concentration threshold of 0.71 kg/m^3 of concrete [8] was reached at the bar depth, 25 mm, between 33 weeks and 1 year of ponding for the control specimens, DCI, and R222 specimens in all exposure zones, and for A2000 specimen in the horizontal, vertical, and tidal zones. Chloride concentration threshold at the bar depth, 25 mm, was reached by A2000 specimen in the immersed zone before 33 weeks of ponding. However, none of the specimens with low permeable concrete has exceeded the chloride threshold in the first year of ponding. Between 1 and 1.5 years of ponding, the FA and SC specimens have exceeded the chloride threshold, but only in the horizontal zone. After 1.5 years of ponding, chloride concentrations in the remaining exposure zones, as well as for the SF and SFD specimens in all exposure zones, were below the chloride threshold. After 1.5 years of ponding, the highest concentration of chlorides, at the bar depth, were observed in the horizontal and vertical zones, and the lowest in the tidal and immersed zones, see Figures 28a-28b,29a-29b, 26e-26f, and 27e-27f, respectively.

Chloride concentration data agree with the rapid permeability test, see Figure 30. As shown in Figure 30b, after one year of ponding the lowest chloride level and permeability were observed in the LP specimens, higher values were observed in the controls (A4 concrete) and the CI specimens. For corrosion inhibitors, there appears to be no significant difference in a rate of chloride ingress in comparison to the control.

Once the chloride ion concentrations were measured, diffusion coefficients were calculated for all specimen types. The calculations were performed in accordance with the Fick's second law of diffusion, see Equation 4 [102]. The solution to the

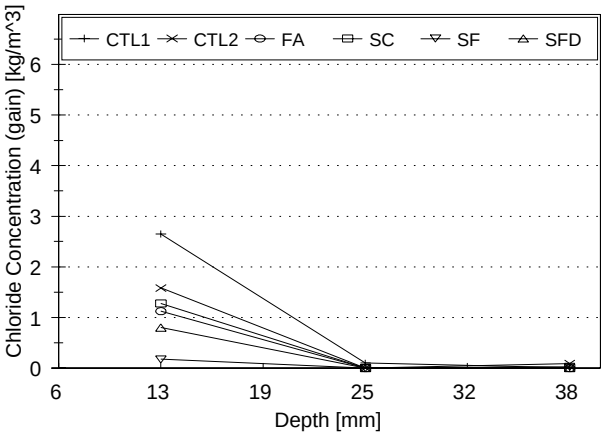

a. LP Concrete after 33 Weeks of Exposure.

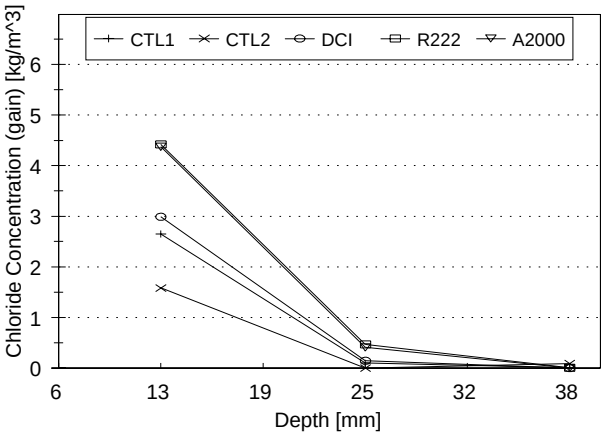

b. CI Concrete after 33 Weeks of Exposure.

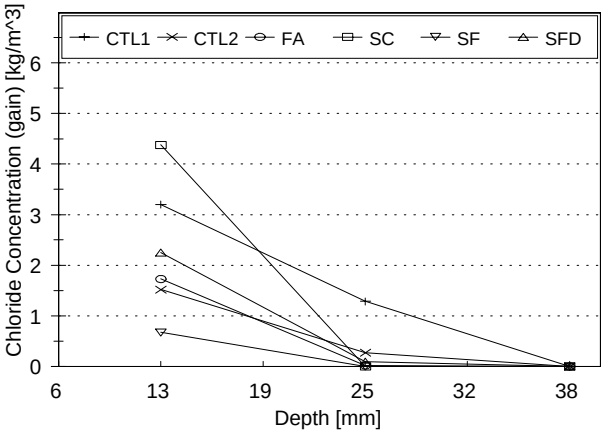

c. LP Concrete after 1 Year of Exposure.

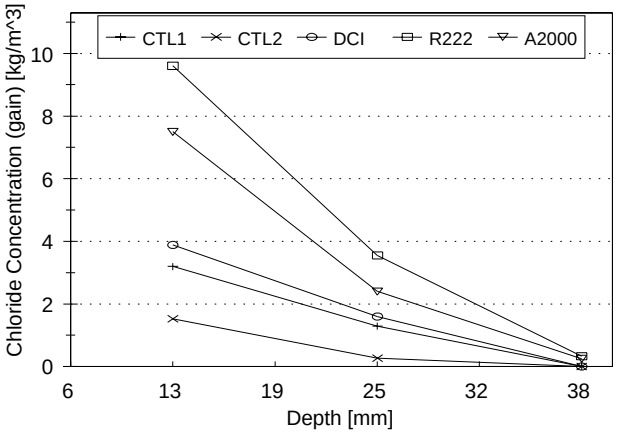

d. CI Concrete after 1 Year of Exposure.

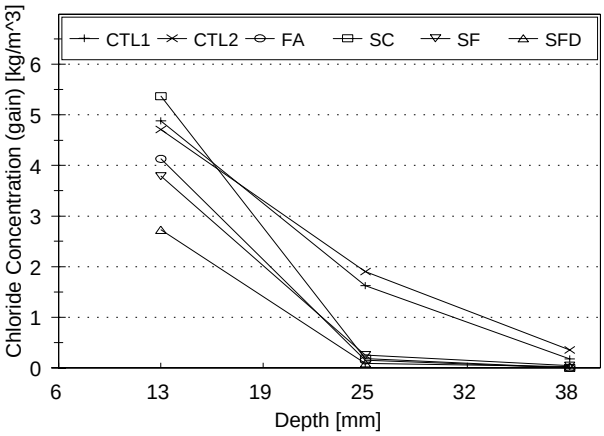

e. LP Concrete after 1.5 Years of Exposure.

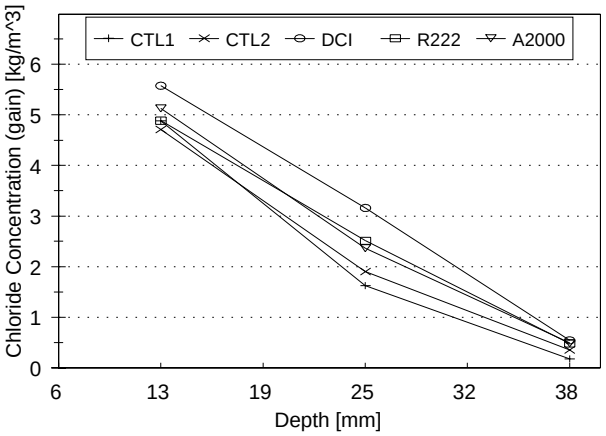

f. CI Concrete after 1.5 Years of Exposure.

FIGURE 26 a-f. Chloride Concentrations for the Tidal Exposure Zone.

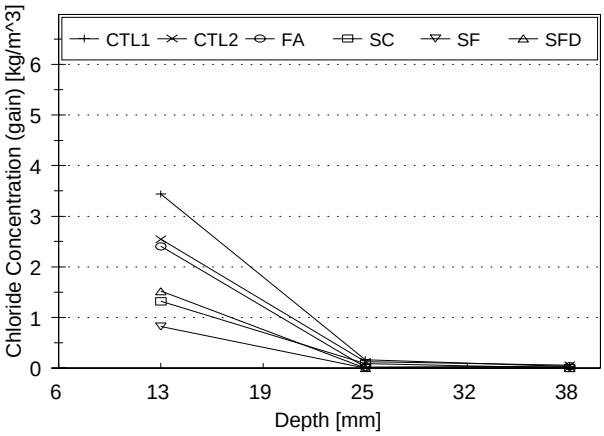

a. LP Concrete after 33 Weeks of Exposure.

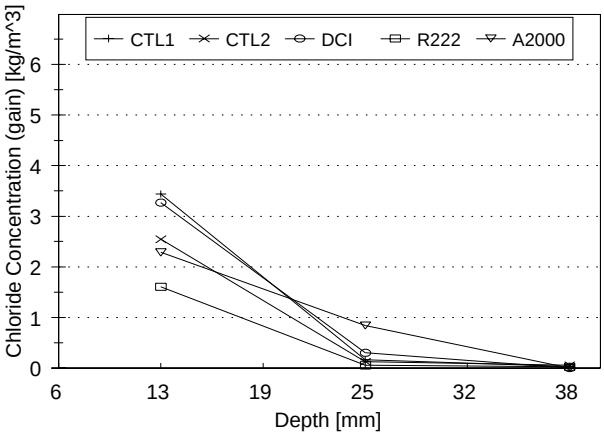

b. CI Concrete after 33 Weeks of Exposure.

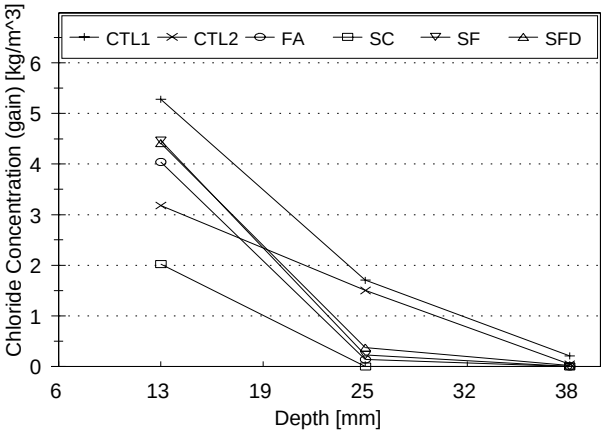

c. LP Concrete after 1 Year of Exposure.

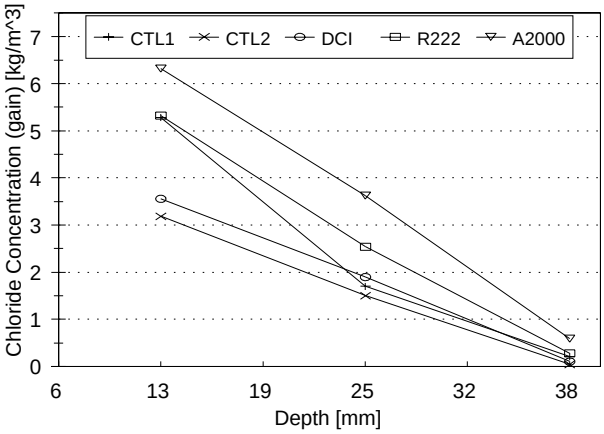

d. CI Concrete after 1 Year of Exposure.

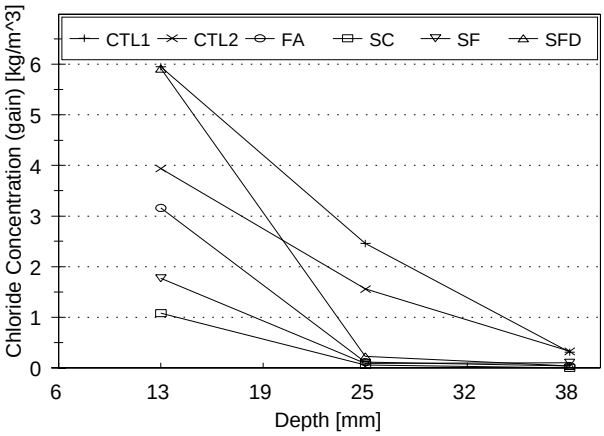

e. LP Concrete after 1.5 Years of Exposure.

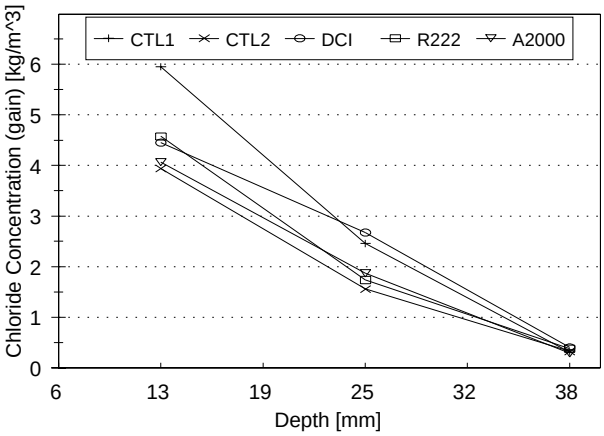

f. CI Concrete after 1.5 Years of Exposure.

FIGURE 27 a-f. Chloride Concentrations for the Immersed Exposure Zone.

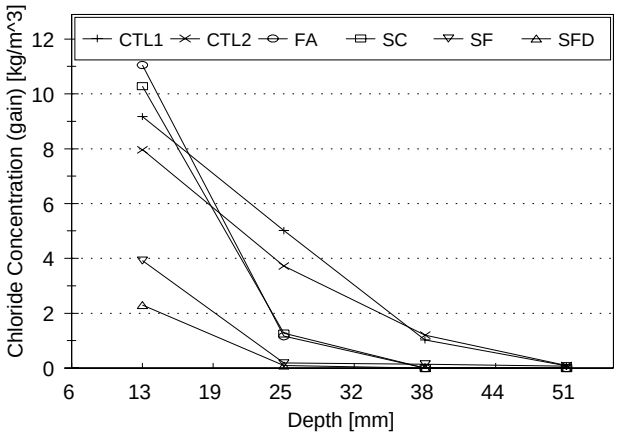

a. LP Concrete after 1.5 Years of Exposure.

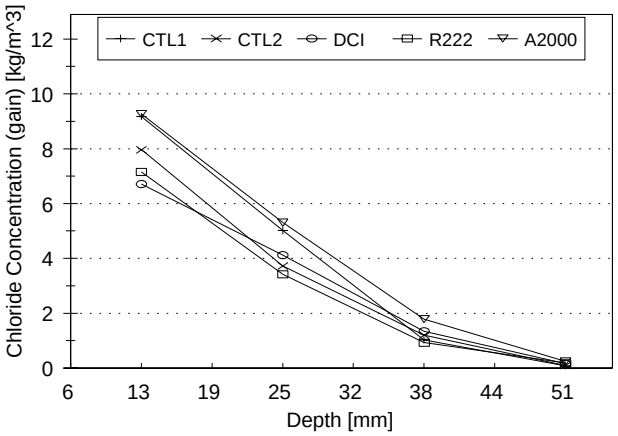

b. CI Concrete after 1.5 Years of Exposure.

FIGURE 28 a-b. Chloride Concentrations for the Horizontal Exposure Zone.

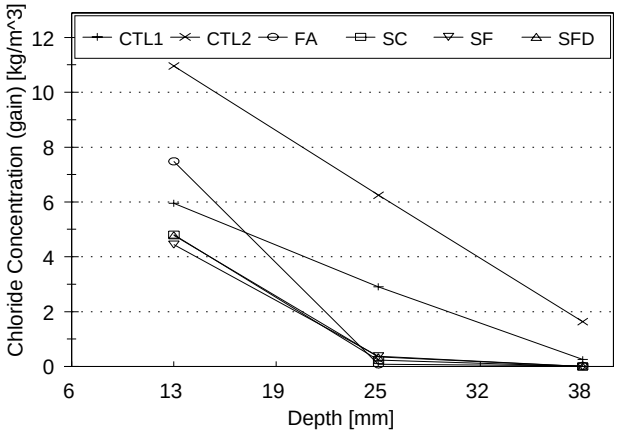

a. LP Concrete after 1.5 Years of Exposure.

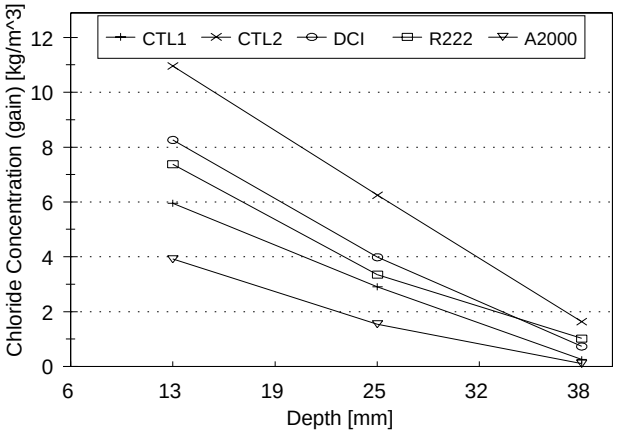

b. CI Concrete after 1.5 Years of Exposure.

FIGURE 29 a-b. Chloride Concentrations for the Vertical Exposure Zone.

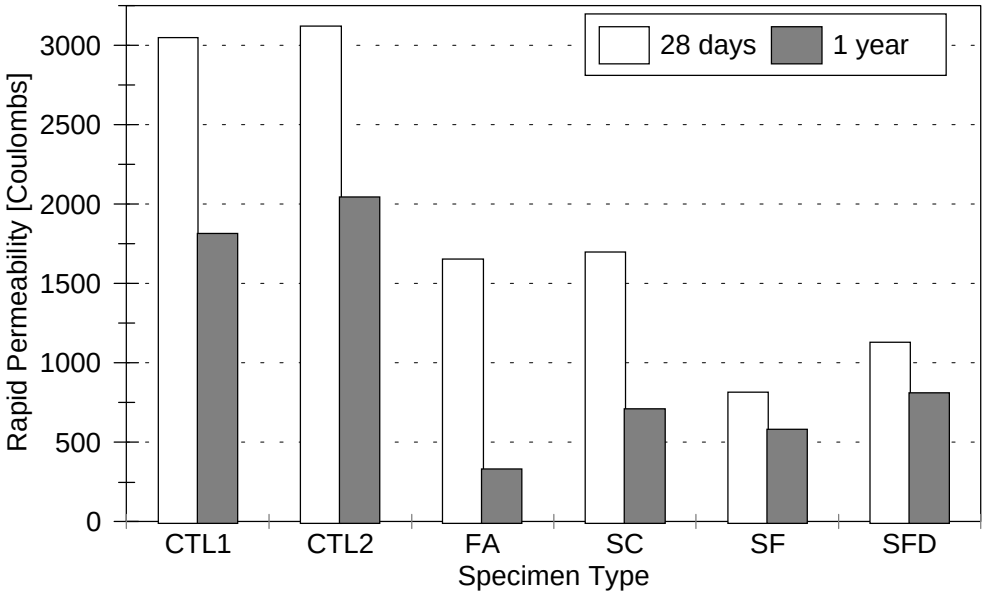

a. LP Concrete Specimens and Controls.

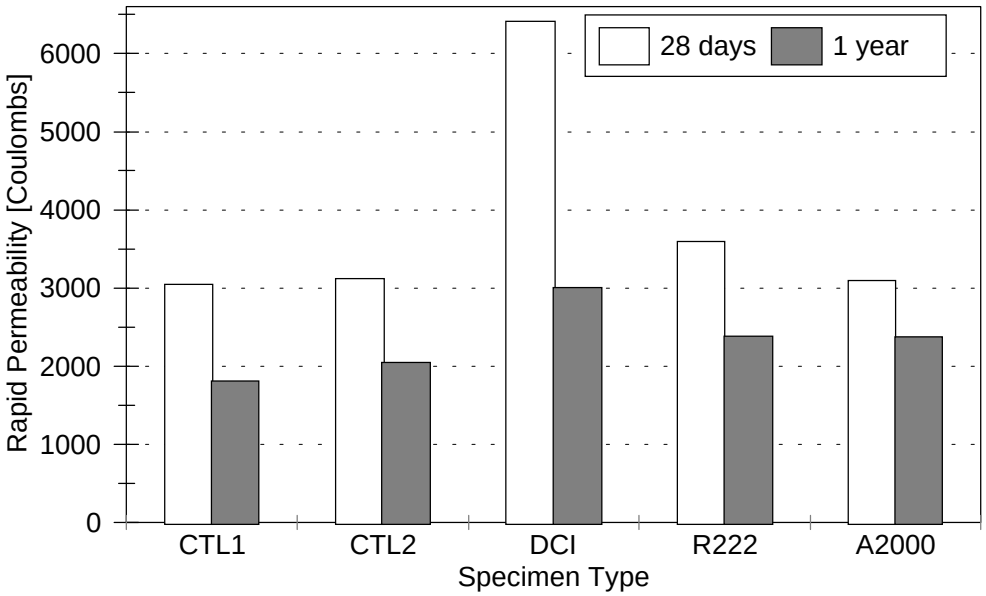

b. CI Concrete Specimens and Controls.

FIGURE 30 a-b. Electrical Indication of Concrete's Ability to Resist Chloride Ion Penetration at 28 Days and 1 Year.

Equation 4 with a boundary condition of surface concentration, C_0, being dependent on square root of time is given by Equation 6 [102].

Since the chloride concentrations were measured at three or four depths (only horizontal zone, 1.5 years of exposure) the "Least Squares Fit Concept", as described by Weyers et al., was employed to obtain the best fit of the diffusion coefficient [103]. Calculated diffusion coefficients corresponding to the minimum of the sum of squared errors, after 1.5 years of indoor exposure, are presented in Table 12.

TABLE 12. Diffusion Coefficients for All Exposure Zones Based on Chloride Data after 1.5 Year of Exposure.

	Diffusion Coefficients [mm^2/year]			
Specimen	Horizontal	Vertical	Tidal	Immersed
BS-1	138	135	85	112
BS-2	135	109	113	113
FA	28	10	16	16
SC	35	20	17	21
SF	18	24	21	18
SFD	19	25	17	18
DCI	199	163	204	217
R222	141	168	179	120
A2000	187	114	158	150

After diffusion coefficients were calculated, a relationship between diffusion coefficients and rapid permeability for corresponding concrete was established. In the regression analysis for each rapid permeability value four diffusion coefficients, corresponding to one of each of the exposure zones, were assigned. Please note that

rapid permeability was measured for each concrete type and not for each exposure zone, as was the case for chloride analysis – diffusion coefficients. The regression analysis used rapid permeability values obtained after one year of curing, while diffusion coefficients were calculated from chloride data after 1.5 year of ponding. Figure 31 presents a linear relationship for all investigated specimens with the correlation coefficient $R^2 = 0.92$. The regression line is described by Equation 16.

$$\text{Perm1y} = 12.76\ (D_c) + 400 \qquad (16)$$

where permeability, Perm1y, is in Coulombs and diffusion coefficient, D_c, is in mm^2/year.

When data from two specimens with high water-to-cement ratios were added a logarithmic relationship was obtained, see Figure 32. This non-linear relationship is in close agreement with the previous study on water-to-cement ratio influence on coefficient of permeability, by Powers [16]. The correlation coefficient R^2, for the logarithmic relationship, was 0.93 and the regression line is given in Equation 17.

$$\text{Perm1y} = 1771 \log (D_c) - 1595 \qquad (17)$$

These high R^2 values show a very good correlation between rapid permeability and diffusion coefficients and indicate that rapid permeability tests can successfully be used for all types of concrete.

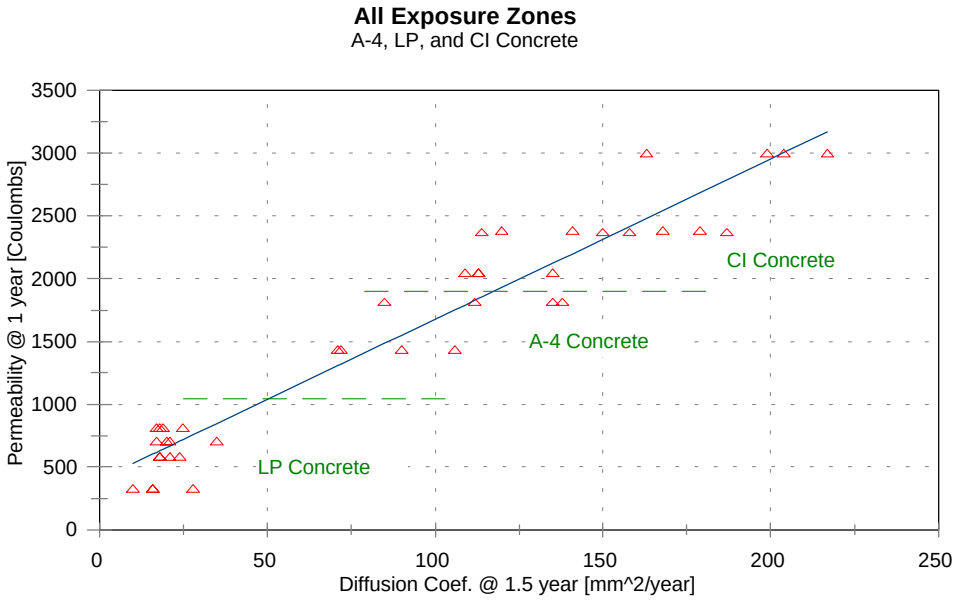

FIGURE 31. Relationship Between Rapid Permeability and Diffusion Coefficient.

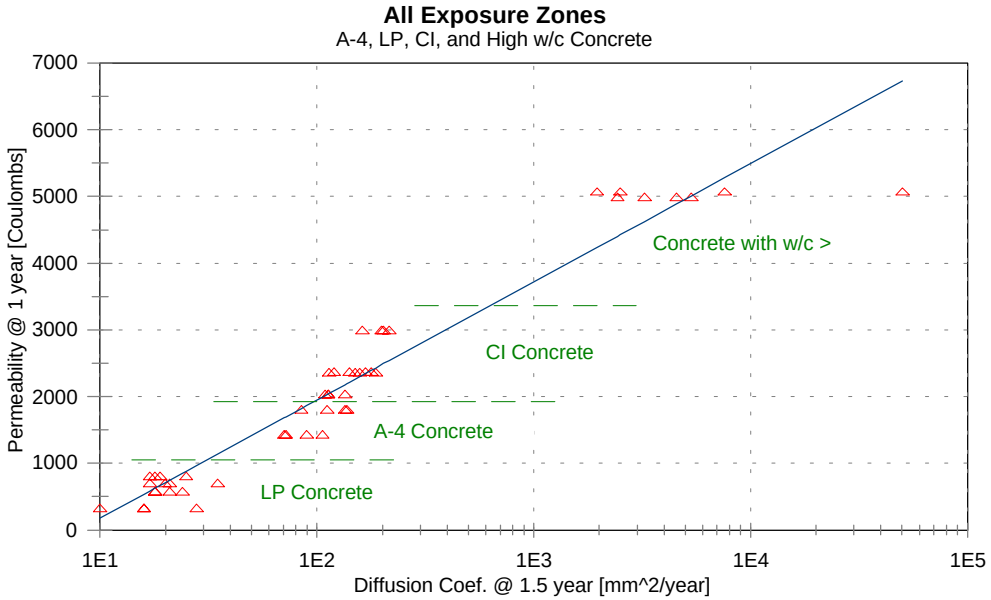

FIGURE 32. Relationship Between Rapid Permeability and Diffusion Coefficient (All Specimens + 2 Specimens with High w/c Ratio).

4.3 Visual Observations

Figures 33a-33i present visually observed cracks and rust stains in the CTL1, CTL2, FA, SC, SF, SFD, DCI, R222, and A2000 specimens after approximately four months of outdoor exposure. As shown, most of cracking had occurred in the horizontal and vertical zones and over the bars that were not included in the corrosion condition assessment.

The structural cracks observed in some specimens appeared to have no influence on the corrosion development on the bars in the vicinity of the these cracks. It was concluded that the silicone rubber and duct tape protection was adequate.

The cracking, other than structural, appeared to be related to the reinforcing steel corrosion. The bars No. 1a and No. 4a in the horizontal zone were expected to corrode first since they were exposed to more severe condition than any other bar. The chlorides diffused from the top, 25 mm of the cover depth in the horizontal zone, and from the side, 25 mm cover depth in the leg. This behavior was especially observed in the control specimens, CTL1 and CTL2. The largest number of cracks and the highest severity were observed in the control specimens and the FA, R222, and A2000 specimens. It is believed that the crack over bar No. 4, at the back side of the FA specimen, was caused by the corrosion of the hook used for lifting the specimen. Nevertheless, the cracks in the vertical zone are clearly related to the corrosion of the underlaying bars. The R222 and A2000 specimens, when compared with the controls, had similar degree of visual damage; however, more cracks were found in the horizontal zone of these specimens than in the controls. It appears that these corrosion inhibitors were not slowing the development of corrosion, but rather

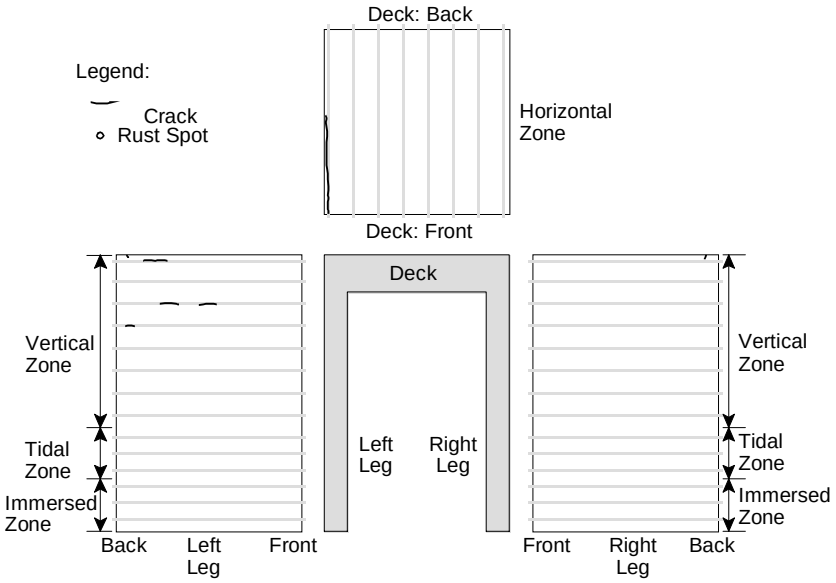

a. CTL1 Specimen.

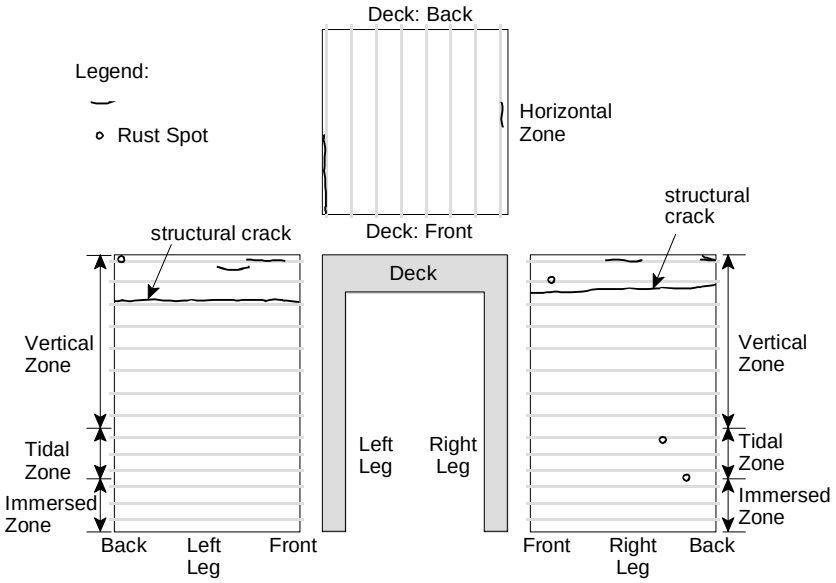

b. CTL2 Specimen.

FIGURE 33 a-b. Visual Observations: Cracking and Rust Spots. October 1996.

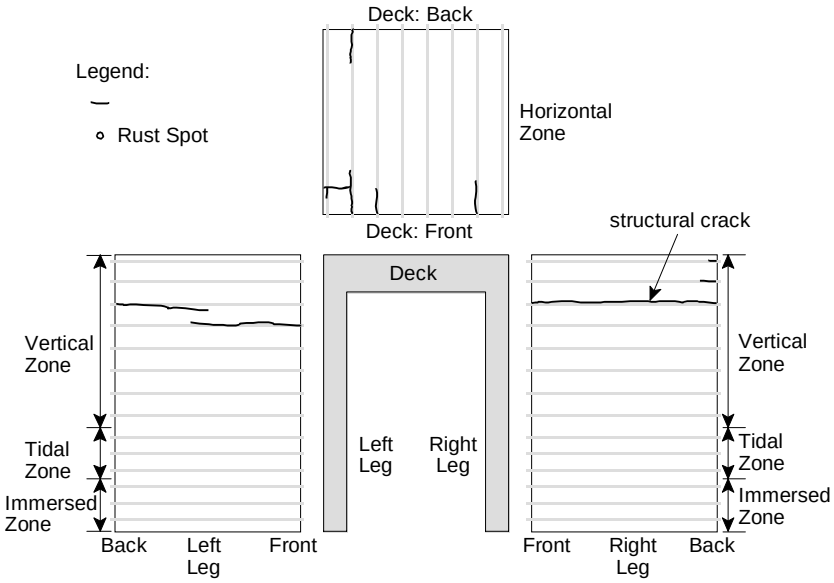

c. FA Specimen.

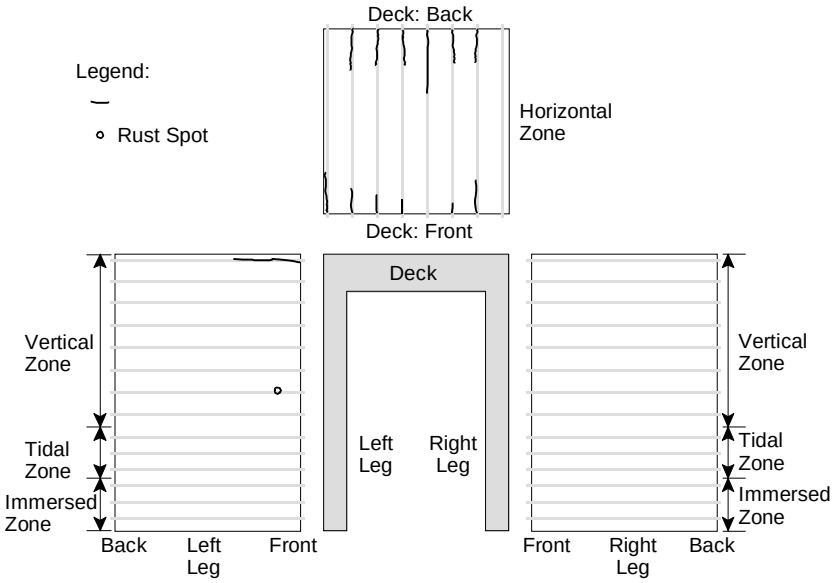

d. SC Specimen.

FIGURE 33 c-d. Visual Observations: Cracking and Rust Spots. October 1996.

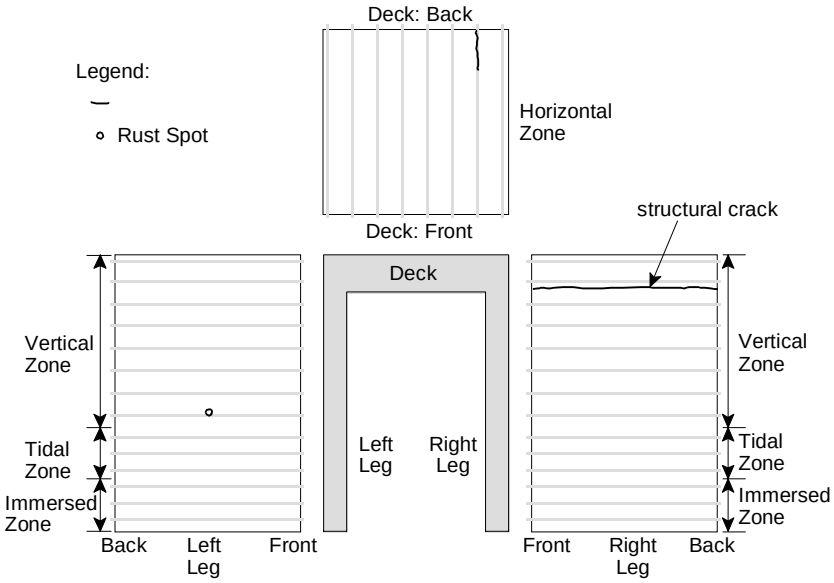

e. SF Specimen.

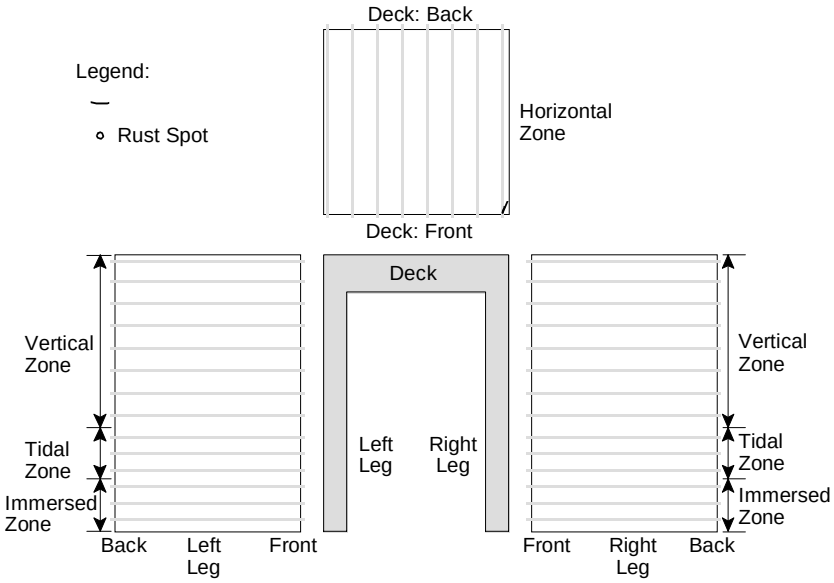

f. SFD Specimen.

FIGURE 33 e-f. Visual Observations: Cracking and Rust Spots. October 1996.

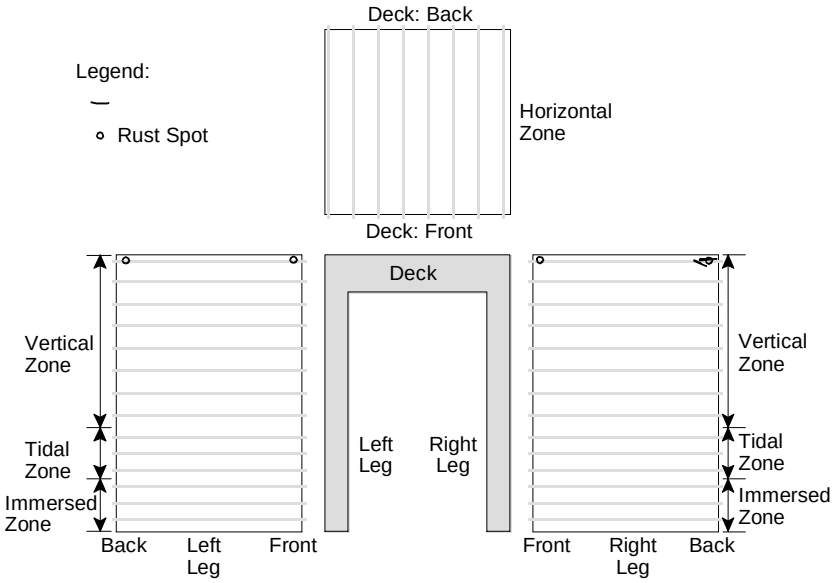

g. DCI Specimen.

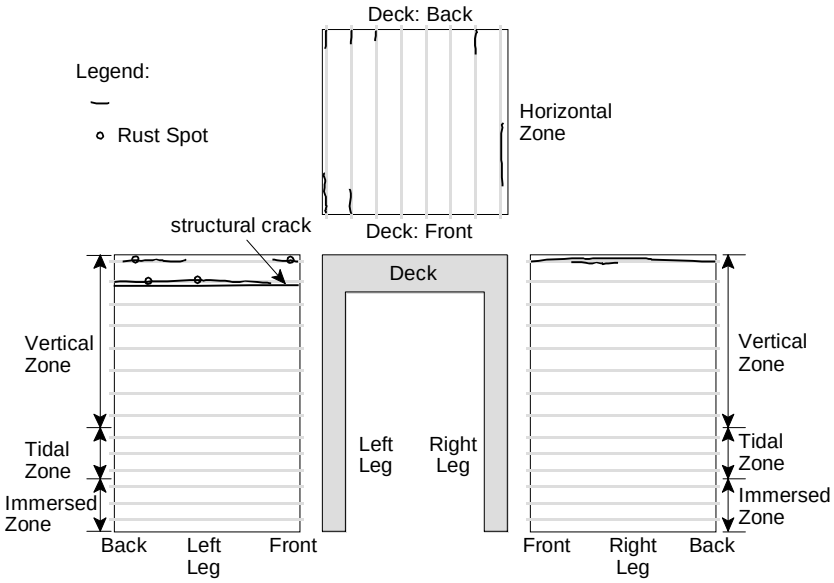

h. R222 Specimen.

FIGURE 33 c-d. Visual Observations: Cracking and Rust Spots. October 1996.

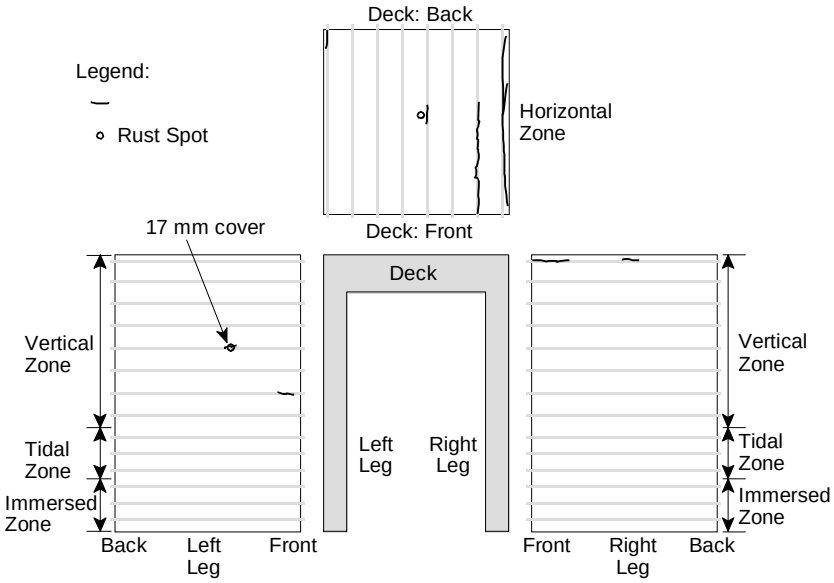

i. A2000 Specimen.

FIGURE 33 i. Visual Observations: Cracking and Rust Spots. October 1996.

accelerating it, especially since the total exposure time of the R222 and A2000 specimens was shorter than the controls. The cracks in the horizontal zone of the SC specimen were found in the early stage of indoor exposure and were probably caused by the subsidence cracking since no corrosion products, typical for cracks caused by corrosion, were visible. Obviously the crack in the upper part of the left leg is corrosion related. The least affected specimens by corrosion were the SF and SFD specimens with one and two cracks, respectively. As for the CI specimens, the DCI specimen looked best since rust spots and cracks appeared only over the bars that had double exposure of chlorides. Also, the cracks were shorter than the ones observed in the R222, A2000, or control specimens.

In one case the rust stain and cracking found on the specimens' surface were caused by the corrosion of the steel ties that must have changed their positions during concrete placement and vibration resulting in a shallower cover depth than the 25 mm for the reinforcing steel. This was confirmed by the cover depth check with a rebar locator device. In the vertical zone of the left leg of the A2000 specimen, a cover depth of 17 mm was found in the location of a crack and a rust spot that occurred over the bar No. 2a.

4.4 Modeling the Time to Corrosion Initiation

Service lives of A4, LP, and CI concretes were determined from the results of the laboratory and field investigations. The laboratory study results were described previously in this chapter. The field investigation consisted of sampling bridge decks for chloride concentration profiles and measuring cover depths. Three 17-year-old structures in the state of Virginia, SN 1026, SN 1029, and SN 8003, were selected for the purpose of the study. Additional 18 bridge decks throughout Virginia were selected for cover depth measurements only.

Cover depths were measured on 21 bridge decks with an average of about 120 readings per deck. A total of 2498 measurements were recorded. Concrete powder samples were collected from twelve locations from each out of three bridge decks. At each location, a sample set consisting of chloride samples from the following depths: 13 mm (6 to 19 mm), 25 mm (19 to 32 mm), 38 mm (32 to 44 mm), and 51 mm (44 to 57 mm), was collected. Sample sets collected at six locations on the SN 8003 bridge deck included two additional samples from depths of 64 mm (57 to 70 mm) and 76 mm (70 to 83 mm). The total number of concrete powder samples collected from the three bridge decks was 156 (48, 48, and 60).

As with the laboratory specimens, powdered concrete samples from the top 6 mm were discarded due to high variability of chloride content close to the surface. Also, chloride concentrations measured at the 13 mm depth are referred to as surface concentration [100].

Field concrete powder samples were analyzed for chloride concentrations in accordance with ASTM C-114 [59]. The average surface chloride concentration was 4.46 kg/m^3 with the standard deviation of 2.36 kg/m^3. The results indicate that surface concentration was distributed according to gamma function with parameters $\alpha = 3.56$ and $\beta = 1.25$. Probability density function (PDF) and cumulative distribution function (CDF) of the surface concentration are presented in Figures 34a and 35a, respectively. The procedure used to calculate field diffusion coefficients was similar to the one used for the laboratory data. The difference was in the solution of the diffusion equation. It has been shown that the for the field data, surface concentration is relatively constant at a depth of 13 mm [103]. Thus, a boundary condition with a surface concentration being constant applies, and Equation 5 was used for D_c determination.

Diffusion coefficients were calculated for each location. For the three bridges and 12 locations from each bridge, the average D_c for 35 values (one outlier was excluded) was 38.4 mm^2/year. It has been observed that the diffusion coefficients were also distributed according to the gamma function. The parameters α and β were 1.42 and 27.05, respectively. The PDF and CDF of the diffusion coefficients is presented in Figures 34b and 35b, respectively.

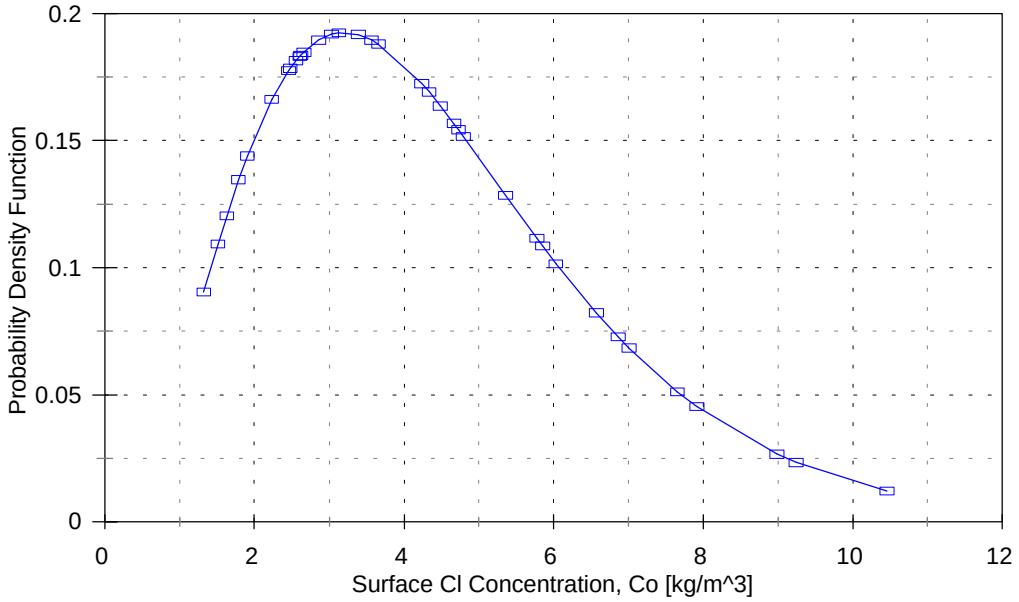

a. Surface Chloride Concentration – Gamma Distribution ($\alpha = 3.56$, $\beta = 1.25$).

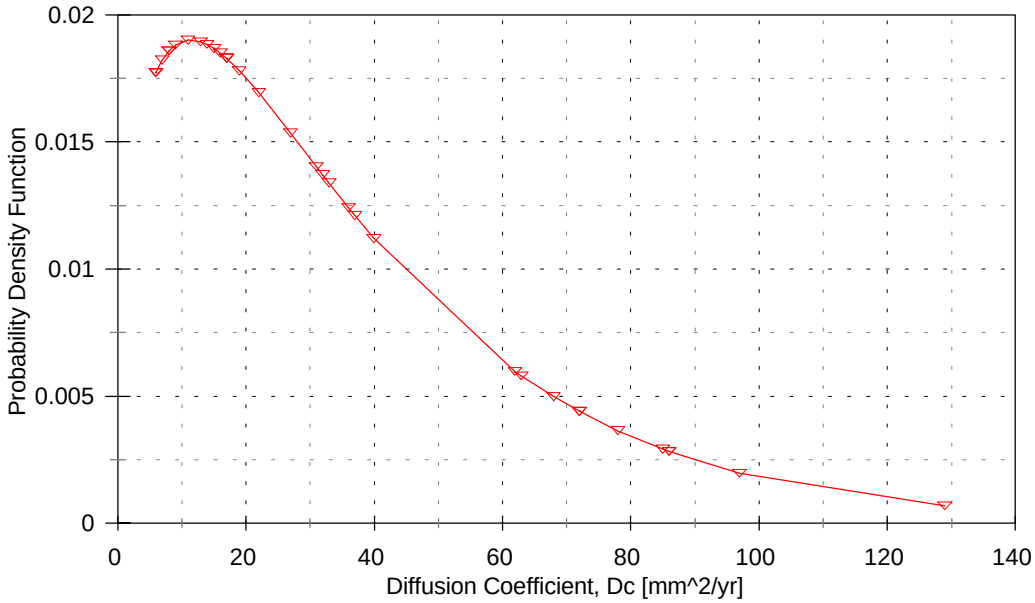

b. Diffusion Coefficient – Gamma Distribution ($\alpha = 3.56$, $\beta = 1.25$).

FIGURE 34 a-b. Probability Distribution Function (PDF) of Surface Chloride Concentration and Diffusion Coefficient.

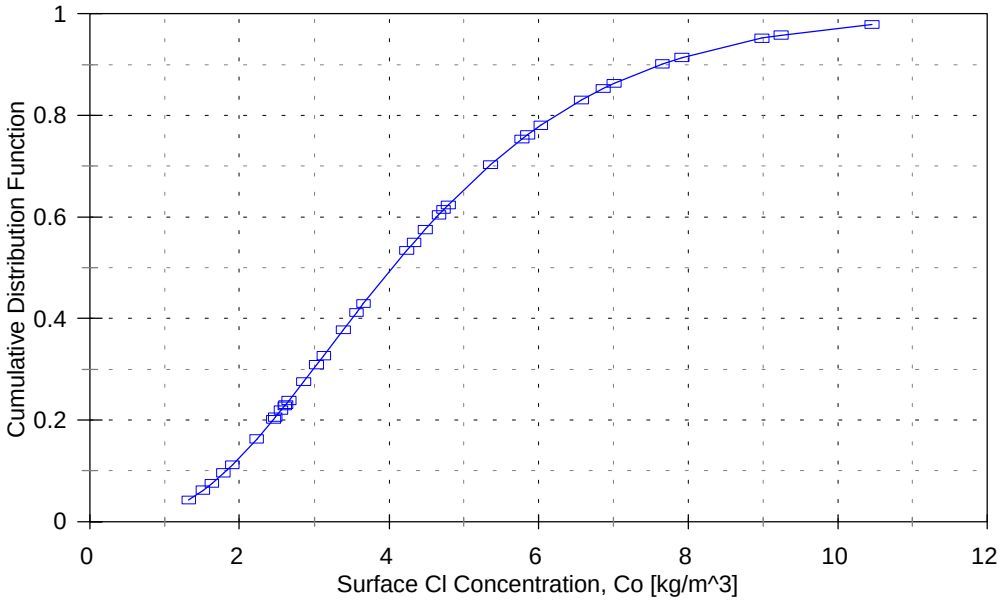

a. Surface Chloride Concentration – Gamma Distribution ($\alpha = 3.56$, $\beta = 1.25$).

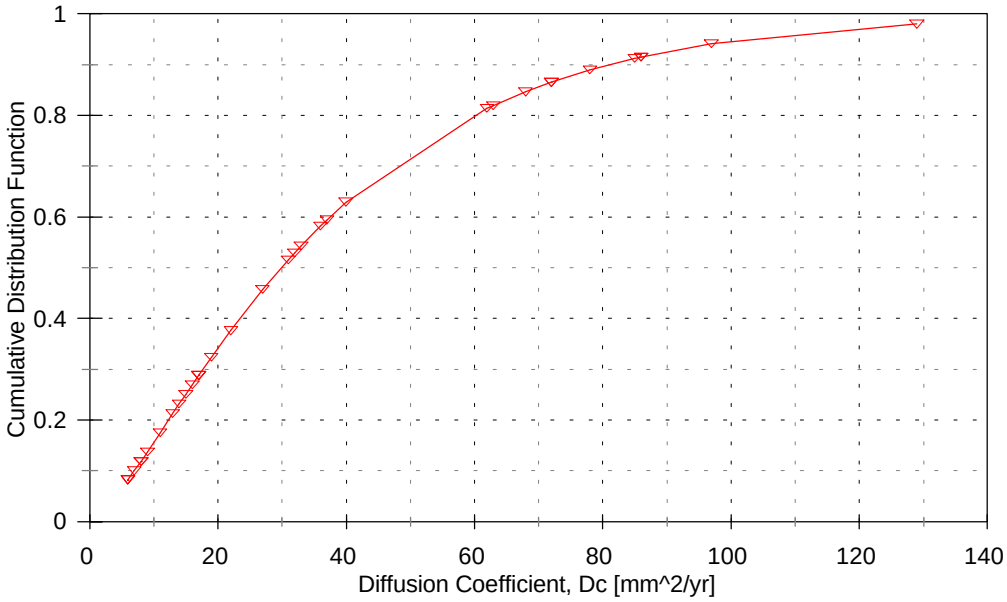

FIGUR E 35 a-b. Cumulative Distribution Function (CDF) of Surface Chloride Concentration and Diffusion Coefficient.

The presented methodology is based on data from the horizontal exposure zone, but the procedure is applicable to other exposure zones as well. Laboratory and field data were used to determine time to corrosion initiation for all concrete types. Calculations were performed by an interactive solution of Equation 5 and solving it for time, t. The following four parameters were used to solve Equation 5: chloride concentration threshold, $C_{(x, t)}$, surface concentration, C_0, reinforcing steel cover depth, x, and diffusion coefficient, D_c.

A value of 0.89 kg/m^3 of concrete was taken for all concrete types, except the SFD concrete, as a chloride concentration threshold. Since the corrosion inhibitor elevates the threshold, a double value of chloride concentration threshold, 1.78 kg/m^3 of concrete, was used for the SFD concrete for illustration purposes only. The manufacturer stated the threshold level for the DCI-S dosage of 20 l/m^3 of concrete used in the laboratory specimen is 5.9 kg chloride/m^3 of concrete.

Surface concentration of 4.05, and 7.63 kg/m^3 of concrete were used in the analysis. These values were taken from the field surface concentration distribution, see Figure 35a, and correspond to 50 and 90% of the CDF, respectively.

It has been shown that about 12% of the reinforcement is capable of causing corrosion damage requiring immediate repair or rehabilitation [74]. Therefore, all calculations use 12% cover depth, a cover depth for 12% of the reinforcing steel, rather than the mean value. Based on 2498 readings from 21 bridge decks in Virginia, cover depths were found to be normally distributed with the mean of 65 mm and standard deviation of 9.1 mm. The average 12% cover depth was equal to 54 mm.

Diffusion coefficients of laboratory specimens could not be used directly in the analysis because laboratory exposure conditions were different from the field conditions. Since no field data is available on LP concretes, a relationship between laboratory and field diffusion coefficients had to be established. To properly simulate field conditions a modified diffusion coefficient, see Equation 18, was used.

$$D_{c\ (modified)} = D_{c\ (field)} \cdot D_{c\ (lab\ specimen)} / D_{c\ (lab\ control)} \qquad (18)$$

where: $D_{c\ (lab\ specimen)}$ = diffusion coefficient of a considered concrete type (laboratory specimen),

$D_{c\ (lab\ control)}$ = diffusion coefficient of a laboratory control specimen (D_c of the CTL 1 specimen was used for calculations), and

$D_{c\ (field)}$ = diffusion coefficient of a field structure.

Equation 18 shows that for the control specimen, $D_{c\ (modified)}$ will always be equal to $D_{c\ (field)}$ simply because $D_{c\ (lab\ specimen)}$ is the same as, or equal to, $D_{c\ (lab\ control)}$. Exact modeling of the field conditions by the control specimen was intentional, especially that concrete bridge decks and laboratory control specimens were made with the same specification concrete, A4 concrete. Note that diffusion coefficients of laboratory specimens are fixed values, while $D_{c\ (field)}$ has a distribution, see Figure 35b. Values of 29.9 and 81.1 mm^2/year corresponding to 50% (mean) and 90% of the field D_c population, respectively, were used in the analysis. For the A4 concrete, $D_{c\ (modified)}$ was equal to the field value, 29.9 mm^2/year. For the FA, SC, SF, and SFD concretes, $D_{c\ (modified)}$ was 6.1, 7.7, 3.9, and 11.3 mm^2/year, respectively.

Figure 36a presents the corrosion initiation times, as a function of cover depth, for the

A4 concrete. The interpretation is that the time to corrosion initiation for 12 % reinforcement and the mean values of D_c and C_0, at 54 mm depth, is 33 years. In other words, 50% of VA bridge decks will reach chloride threshold in less than 33 years. One can also see that for a small percentage of bridge decks, 10% [CDF(C_0) > 90% and CDF(D_c) > 90%,] corrosion initiation will occur in less than 7.5 years. Corrosion initiation times, as a function of cover depth, for the FA, SC, SF, and SFD concretes are presented in Figures 36b-36e, respectively. It is apparent that these concretes would provide much better corrosion protection. Even for both CDF(D_c) and CDF(C_0) of 90%, less than 10% of the bridge decks, at 54 mm depth, initiation times increase from 7.5 years for the A4 concrete to 36, 29, 56, and 93 years for the FA, SC, SF, and SFD concretes, respectively.

The end of functional service life (EFSL) is defined as the condition of a bridge element requiring immediate repair or rehabilitation. In the presented analysis, time till EFSL was taken as the corrosion initiation time plus seven years, which is a reasonable estimate for corrosion development and resultant deterioration. All calculations were performed for the average 12% cover depth of 54 mm. Since the surface concentration and the diffusion coefficient variables have their own distributions, probability considerations could be introduced into the analysis. For example, a time equivalent to 10% probability of EFSL for A4 concrete would be calculated with values of D_c and C_0 corresponding to 90% (100% - 90% = 10%) of the respective CDFs. A relationship between the time till EFSL and its probability for A4 concrete is presented in Figure 37. Another curve, designated as SHRP and also presented in Figure 37, is the curve from the SHRP study on field performance of 120 Virginia bridge decks [103]. The conclusion of the SHRP study was that the time till EFSL for an average bridge deck in Virginia would be 36 years with a standard deviation of 13 years. The modeled time to EFSL for the mean, 50% probability,

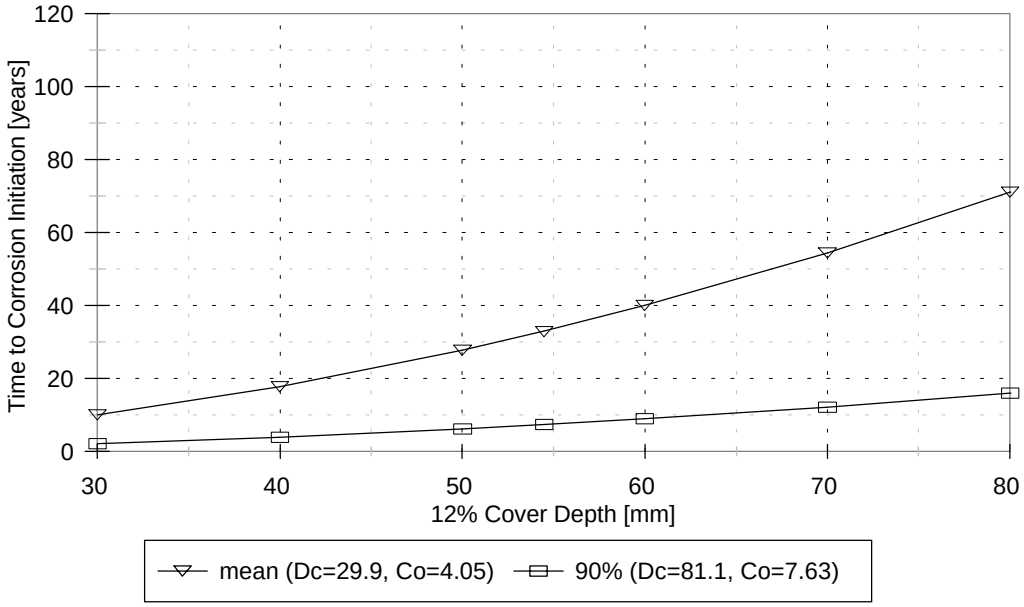

a. A-4 Concrete, Chloride Threshold = 0.89 kg/m^3.

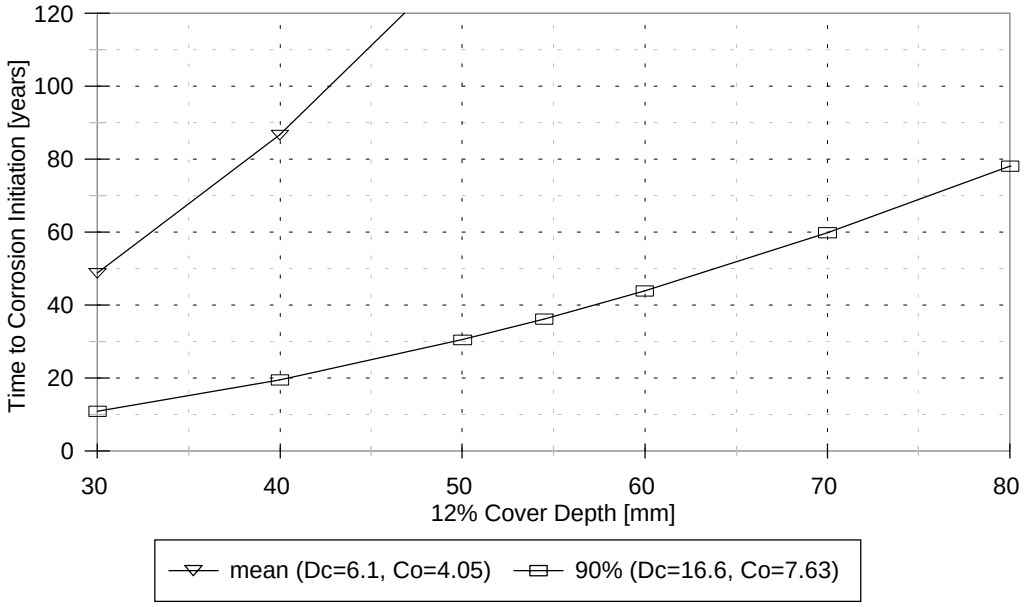

b. FA Concrete, Chloride Threshold = 0.89 kg/m^3.

FIGURE 36 a-b. Predicted Time to Corrosion Initiation, w/c = 0.45.

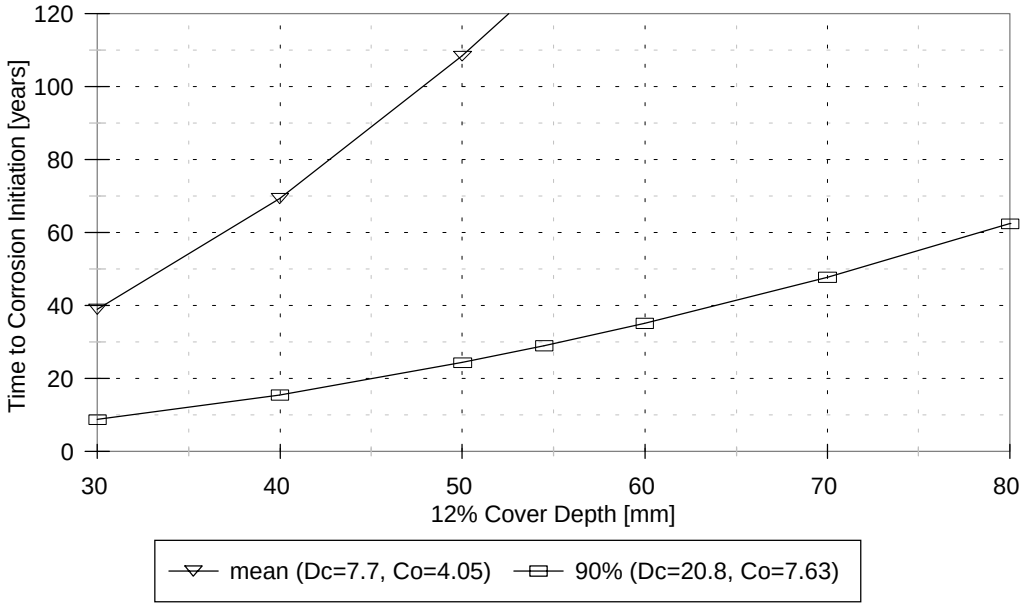

c. SC Concrete, Chloride Threshold = 0.89 kg/m^3.

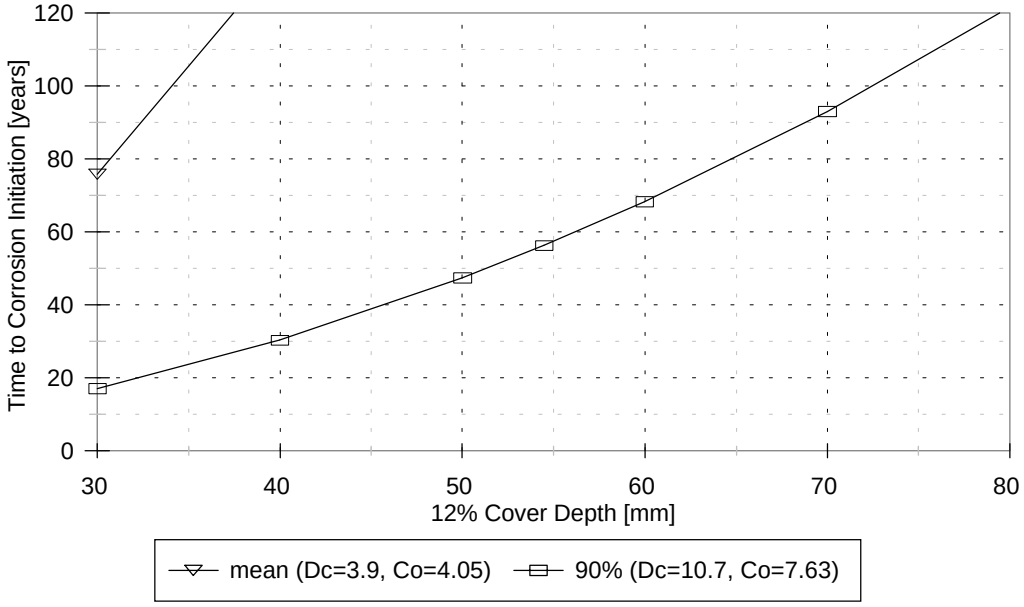

d. SF Concrete, Chloride Threshold = 0.89 kg/m^3.

FIGURE 36 c-d. Predicted Time to Corrosion Initiation, w/c = 0.45.

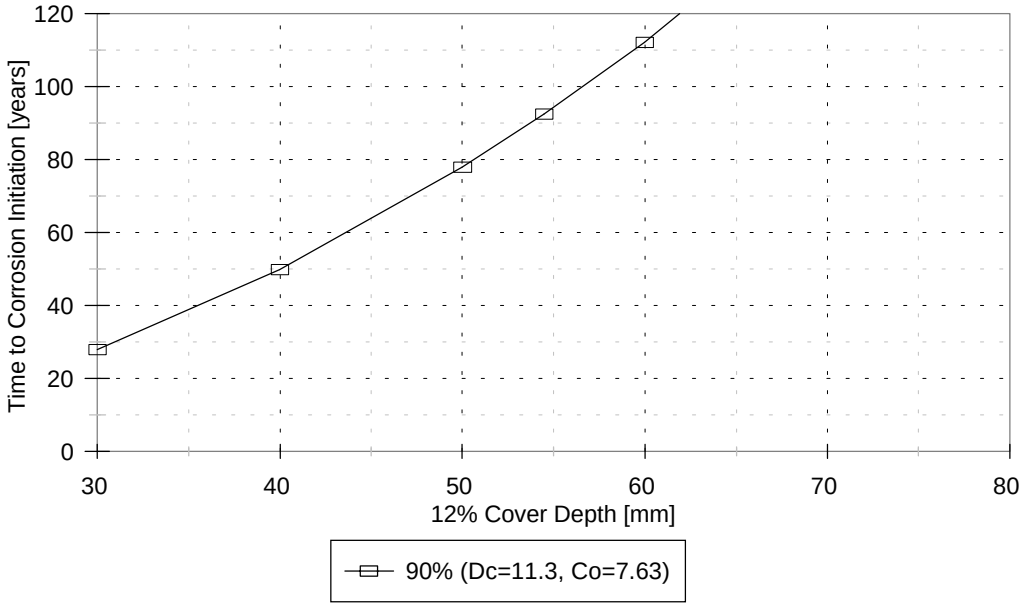

e. SFD Concrete, Chloride Threshold = 1.78 kg/m^3.

FIGURE 36 c-d. Predicted Time to Corrosion Initiation, w/c = 0.45.

bridge deck with A4 concrete is 40 years, see Figure 37. The four years difference, 40 - 36, is very little, especially that the SHRP study was done on bridges that were built when specifications required w/c = 0.46 and 51 mm cover depth. Current Virginia specifications for the A4 concrete require w/c = 0.45 and 64 mm cover. Thus, the model proves to be valid. Similar analysis was performed on all other concretes and the prediction results are presented in Figure 38. The beneficial use of mineral admixtures and SF with DCI-S corrosion inhibitor is evident even at low probabilities of EFSL.

As seen in Figure 38, low permeable concretes require much more time to EFSL than the A4 concrete. This behavior is attributed to pozzolanic reaction of mineral admixtures. Even though the FA and SC concretes yield lower times to EFSL than the

concrete with silica fume, one should not overlook their excellent properties. The particles of fly ash and slag cement are about 100 times larger than the silica fume particles, thus the pozzolanic reaction of these materials is much slower. This can be seen by comparing rapid permeability results at 28 days and 1 year, see Figure 30. Laboratory study, as all laboratory studies, required accelerated tests and chloride ingress was very fast. At early ages the FA and SC concretes were more vulnerable to chloride ingress than the SF concrete simply because the concrete matrix was not developed to the same extent. It is believed that their performance would be better if chlorides were introduced at a later time as would occur in the field conditions.

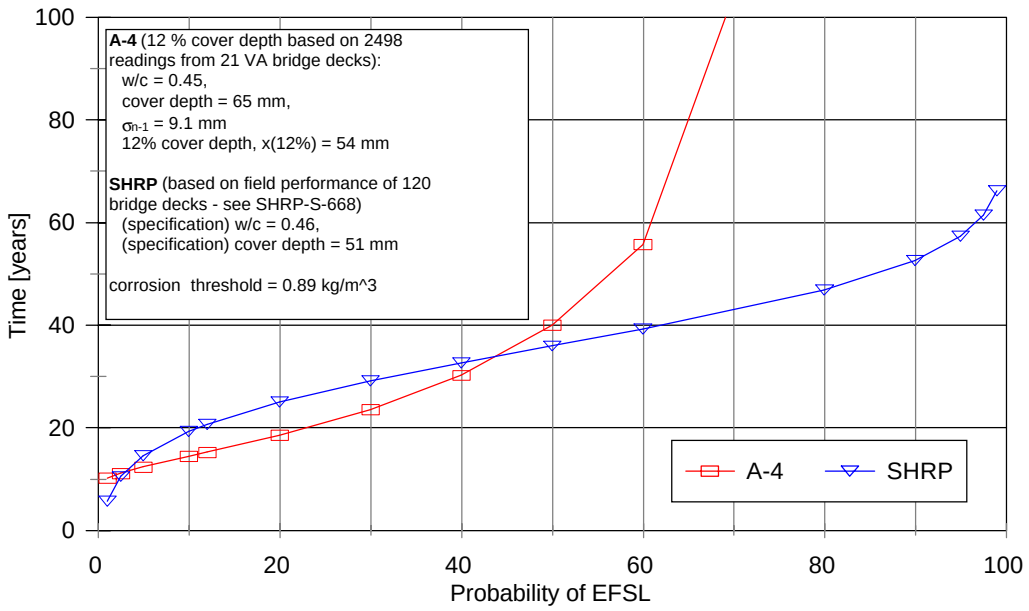

FIGURE 37. Probability of End of Functional Service Life for A-4 Concrete: Comparison between Field Performance (SHRP) and Predictions from Field Data (A-4).

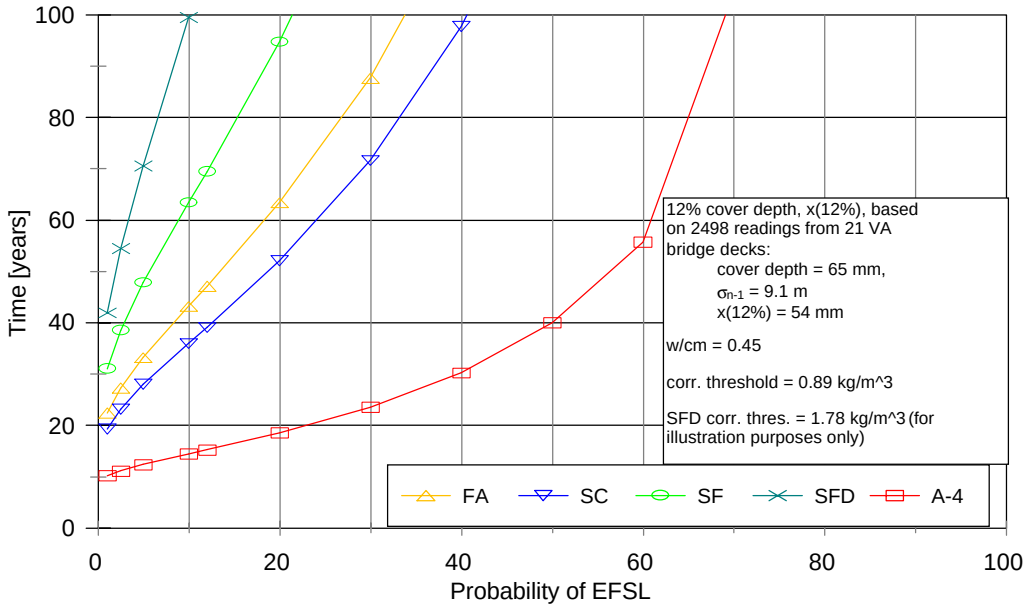

FIGURE 38. Probability of End of Functional Service Life for LP Concrete versus A-4 Concrete: Predictions from Laboratory and Field Data.

5.0 CONCLUSIONS AND RECOMMENDATIONS

The structural cracks observed in some specimens appeared to have no influence on the corrosion development on the bars in the vicinity of these cracks. It was concluded that the silicone rubber and duct tape protection was adequate.

Corrosion potentials observed in the horizontal zone of CTL1 and CTL2 specimens suggest the possibility of an active corrosion process development during indoor exposure. This was confirmed by the corrosion rate results which indicate that the control specimens were in an active region of corrosion when they were kept indoors. Macrocell action is a probable explanation of differences in corrosion rates in the immersed and tidal zones between the CTL1 specimen, legs reinforcement not connected, and the CTL2 specimen, legs reinforcement connected. Based on the potential and corrosion rate data, as well as visual observations, two corrosion inhibitors, Rheocrete 222 and Armatec 2000 (R222 and A2000 specimens), appear to provide little to no corrosion inhibition, while DCI-S corrosion inhibitor (DCI specimen) increases the chloride corrosion threshold limit in concrete. These results confirm the results and conclusions of the companion study on corrosion inhibitors in simulated concrete pore solutions [104]. Potential and corrosion rate data for the LP concretes were inconclusive.

The results of chloride testing indicate that the amount of chlorides present at the bar level is more than sufficient for corrosion to occur for the control specimens; however, it still is very low for the specimens with low permeable concretes. Based on chloride data it appears that the specimens with silica fume are the least prone to chloride ingress. Specimens with fly ash and slag cement will allow for greater intrusion of chlorides, but still much less than the controls. This is confirmed by comparing

diffusion coefficients: they are more than three times lower for the specimens made with concrete with mineral admixtures, as compared to the controls. Chloride concentration data agree with the rapid permeability test results which also show a positive influence of mineral admixtures on concrete chloride ion blocking abilities.

The cracking, other than structural, appeared to be related to the reinforcing steel corrosion. The bars No. 1a and No. 4a in the horizontal zone were expected to corrode first since they were exposed to more severe condition than any other bar. The chlorides diffused from the top, 25 mm of the cover depth in the horizontal zone, and from the side, 25 mm cover depth in the leg. This behavior was especially observed in the control, CTL1 and CTL2, specimens. The largest number of cracks and the highest severity was observed in the control specimens and the FA specimen. It is believed that crack over the bar No. 4, at the back side of the FA specimen, was caused by the corrosion of the hook used for lifting the specimen. Nevertheless, the cracks in the vertical zone are clearly related to the corrosion of the underlaying bars. The cracks in the horizontal zone of the SC specimen were probably caused by the subsidence cracking, since no corrosion products were visible, typical for cracks caused by corrosion. Obviously the crack in the upper part of the left leg is corrosion related. The least affected specimens by corrosion were the SF and SFD specimens with one and two cracks, respectively.

Low permeable concretes provide much better level of protection against moisture and chlorides than the A4 concrete alone. Concretes with fly ash or slag cement may provide the same protection as concrete with silica fume, as long as the concretes are allowed to cure for a longer period of time without salt application. Application of a corrosion inhibitor causes the beneficial elevation of the chloride threshold and results in an increase in time to EFSL.

The rapid permeability test was found to be very reliable for all concrete types. It showed a very good correlation with diffusion coefficients of corresponding concrete types.

The assumption that the distributions of C_0 and D_c are fairly representative of the whole population of Virginia bridges is reasonable because the average service life for Virginia bridge decks with bare steel is 36 years using a specification concrete with w/c of 0.46 and 51 mm cover depth. Using the mean C_0 and D_c values and seven years from the corrosion initiation to spalling, the average service life is about 40 years for a specification concrete with w/c of 0.45 and 64 mm cover. Thus, the presented model is appropriate for service life determinations.

The benefit of having D_c and C_0 distributions is that predictions can be made not only for a particular structure or the average bridge, but for any percentile of bridge decks.

The model provides means for long term planning and better utilization of resources for repair and rehabilitation activities. It may also be included in the bridge management system.

6.0 RECOMMENDATIONS FOR FURTHER RESEARCH

It is recommended that the specimens be further exposed to chloride ions and annual monitoring be continued until more cracking has occurred to better estimate the service life extension provided by mineral admixtures and/or corrosion inhibitors used in the construction of concrete bridge components in Virginia. Also, DCI-S should remain as the only approved inhibiting admixture for use in Virginia at this time.

Even though the presented D_c and C_0 distributions provide good basis for the analysis, more field studies are needed to have a better representation of bridge conditions in Virginia. Also, calculated times to EFSL for concretes with mineral admixtures, as well as the elevated corrosion threshold levels provided by corrosion inhibitors need to be verified.

7.0 REFERENCES

1. Klemm, Waldemar A., *Cementitious Materials: Historical Notes*, Materials Science of Concrete I, edited by Jan P. Skalny, The American Ceramic Society, Inc., 1989.

2. *Our Nation's Highways. Selected Facts and Figures*, Federal Highway Administration, publication No. FHWA-PL-90-024, p. 11, "undated".

3. *A Federal Surface Transportation Program for the Future*, publ. by ARTBA (American Road & Transportation Builders Association), p. 8, "undated".

4. Bennett, J. *Corrosion of Reinforcing Steel in Concrete and its Prevention by Cathodic Protection*, Anti-Corrosion Methods and Materials, v. 33, n. 11, Oct. 1986, pp. 12-15, 17.

5. *Highway Deicing. Comparing Salt and Calcium Magnesium Acetate.* TR News, No. 163, November-December 1992, pp. 17-19.

6. Pfeifer, D. W.; M. J. Scali, *Concrete Sealers for Protection of Bridge Structures*, NCHRP Report 244, Dec. 1981.

7. Weyers, R.E. et. al., *Protocol for In-Service Evaluation of Bridges with Epoxy-Coated Reinforcing Steel*, NCHRP 10-37B, Final Report, November 1995, p.110.

8. Clear, K.C., *Effectiveness of Epoxy-Coated Reinforcing Steel - Final Report*, Canadian Strategic Highway Research Program, Ottawa, Ontario, December 1992, p.128.

9. Sagues, A.A., et al., *Corrosion of Epoxy-Coated Rebar in Florida Bridges*, College of Engineering, University of South Florida, May 1994, p.70.

10. Weyers, R.E., et al., *Field Investigation of the Corrosion Protection Performance of Bridge Decks and Piles Constructed with Epoxy-Coated Reinforcing Steel in Virginia*, Virginia Transportation Research Council, Charlottesville, Virginia, September 1996, p. 34.

11. Krauss, P.D., D.B. McDonald and M. R. Sherman., *Corrosion Investigation of Four Bridges Built Between 1973 and 1978 Containing Epoxy-Coated Reinforcing Steel,* Minnesota Department of Transportation, MN/RC - 96/25, St. Paul, Minnesota, June 1996, p. 163.

12. Fontana, Mars Guy, *Corrosion Engineering*, McGraw-Hill Book Company, 1986.

13. Jones, Denny A., *Principles and Prevention of Corrosion*, Macmillan Publishing Company, New York, NY, 1992.

14. Uhlig, Herbert H.; R. Winston Revie, *Corrosion and Corrosion Control*, John Wiley & Sons, Inc., 1985.

15. Mehta, P. Kumar, "Concrete Structure, Properties, and Materials", Prentice-Hall, Inc., Englewood Cliffs, N.J. 07632, 1993.

16. Powers, T. C., *Structure and Physical Properties of Hardened Portland Cement Paste*, American Ceramic Society Journal, vol. 41, 1958, pp. 1-6.

17. Powers, T. C., *Physical Properties of Cement Paste*, Proceedings, 4 th International Symposium on the Chemistry of Cement, Washington, DC, Vol. 2, 1960, pp. 577-613.

18. Powers, T. C., Copeland, L. E., and Mann, H. M., *Flow of Water in Hardened Portland Cement Pastes,* Special Report 40, Highway Research Board, Washington, DC, 1959, pp. 308-323.

19. Barrer, R. N. *The Solid-Gas Interface*, E. A. Flood (Ed.), Vol II, Dekker, New York,1967, pp. 557-609.

20. Klieger, Paul, Joseph F. Lamond (Eds.), *Significance of Tests and Properties of Concrete and Concrete-Making Materials*, ASTM STP 169C, 1994.

21. Garboczi, Edward J., *Permeability, Diffusivity, and Microstructural Parameters. A Critical Review,* Cement and Concrete Research, v. 20, n. 4, July 1990, pp. 591-601.

22. Klinkenberg, L. J., *The Permeability of Porous Media to Liquids and Gases,* Drilling and Production Practice, American Petroleum Institute, New York,

1941, pp. 200-214.

23. Bamforth, P. B. *The Relationship Between Permeability Coefficients for Concrete Obtained Using Liquid and Gas*, Magazine of Concrete Research, Vol. 39, No. 138, 1987, pp. 3-11.

24. Cady, Philip D.; R.E. Weyers, *Chloride Penetration and the Deterioration of Concrete Bridge Decks*, Cement, Concrete, and Aggregates, vol. 5, no. 2, Winter 1983, pp. 81-87.

25. Dakhil, F. H., Cady, P. D., and Carrier, R. E., *Cracking of Fresh Concrete as Related to Reinforcement*, Journal of the American Concrete Institute, Vol. 72, No. 8, August 1975, pp. 421-428.

26. Weyers, R. E., Conway, J. C., and Cady, P. D., *Photoelastic Analysis of Rigid Inclusions in Fresh Concrete*, Cement and Concrete Research, Vol. 12, No. 4, July 1982, pp. 475- 484.

27. Page, C. L.; Short, N. R.; El Tarras, A., *Diffusion of Chloride Ions in Hardened Cement Pastes,* Cement and Concrete Research, v 11, n 3, May 1981, pp. 395-406.

28. Browne, R. D., *Design Prediction of the Life for Reinforced Concrete in Marine and Other Chloride Environments*, Durability of Building Materials, vol. 1, no. 2, July 1982, pp. 113-125.

29. Kawakami, Hideo, *Study of Chloride Concentration in a Reinforced Concrete Building with Diffusion Theory*, Transactions of the Japanese Concrete Institute, v 7, 1985, pp. 149-156.

30. Nagano, Hiroo; Naito, Takafumi, *Application of Diffusion Theory to Chloride Penetration Into Concrete Located in Splashing Zones*, Transactions of the Japanese Concrete Institute, v 7, 1985, pp. 157-164.

31. Sorensen, Birgit; Ernst Maahn, *Penetration Rate of Chloride in Marine Concrete Structures*, Nordic Concrete Research, n. 1, December 1982, pp. 24.1-24.18.

32. Weyers, Richard E.; Cady, Philip D., *Deterioration of Concrete Bridge Decks from Corrosion of Reinforcing Steel*, Concrete International: Design and Construction, v. 9, n. 1, January 1987, pp. 15-20.

33. Mangat, P. S.; Gurusamy, K., *Chloride Diffusion in Steel Fibre Reinforced Marine Concrete*, Cement and Concrete Research, v 17, n 3, May 1987, pp. 385-396.

34. Uji, K.; Y. Matsuoka; T. Maruya, *Formulation of an Equation for Surface Chloride Content of Concrete due to Permeation of Chloride*, from "Corrosion of Reinforcement in Concrete" edited by C. L. Page, K. W. J. Treadway, and P. B. Bamforth, Society of Chemical Industry, Elsevier Applied Science, 1990, pp. 258-267.

35 Frey, R.; T. Balogh; G. L. Balazs, *Kinetic Method to Analyze Chloride Diffusion in Various Concretes*, Cement and Concrete Research, v. 24, n. 5, 1994, pp. 863-873.

36 Bijen, J. M. J. M., *Maintenance and Repair of Concrete Structures*, Heron, vol. 34, no. 2, Delft University of Technology, Delft, Netherlands, 1989, pp. 1-82.

37 Bhaskara, M. V.; R. K. Maheshwari, *A Review of the Investigation and Evaluation of Corrosion in Concrete Structures*, Indian Highways, Jan. 1987, pp. 22-33.

38 Bazant, Z. P., *Physical Model for Steel Corrosion in Concrete Sea Structures - Theory*, Journal of the Structural division, American Society of Civil Engineers, Vol. 105, No. 6, June 1979, pp. 1137-1153.

39 Bazant, Z. P., *Physical Model for Steel Corrosion in Concrete Sea Structures -Application*, Journal of the Structural Division, American Society of Civil Engineers, Vol. 105, No. 6, June 1979, pp. 1155-1167.

40 Foscante, R. E. ; H. H. Kline, *Coating Concrete - An Overview*, Materials Performance, September 1988, pp. 34-36.

41 Wilson, G. E. B., *The Repair of the Concrete Piles of an Oil Refinery Jetty in New Zealand*, Marine Concrete '86 - International Conference on Concrete in the Marine Environment, London, 22-24 Sep. 1986, The Concrete Society, pp.

349-360.

42 Kilareski, W. P., *Corrosion Induced Deterioration of Reinforced Concrete - an Overview*, Materials Performance, March 1980, p.49.

43 Foley, R. T., *Role of the Chloride Ion in Iron Corrosion*, Corrosion, vol. 26, 1970, p. 58.

44 Cook, H. K., and McCoy, W. J. *Influence of Chloride in Reinforced Concrete*, ASTM STP 629, American Society for Testing and Materials, 1977, pp. 20-29.

45 Fraczek, J., *A Review of Electrochemical Principles as Applied to Corrosion on Steel in a Concrete or Grout Environment*, Corrosion, Concrete, and Chloride, SP-102, American Concrete Institute, Detroit, 1987, pp. 13-24.

46 Slater, J.E., Corrosion of Metals in Association with Concrete", *Corrosion of Metals in Concrete*, ACI SP-49, American Concrete Institute, Detroit, MI, 1975, pp. 21-38.

47 Spellman, D. L., and Stratfull, R. F., *Concrete Variables and Corrosion Testing*, Highway Research Record 424, 1973.

48 Stratfull, D. L., *Half Cell Potentials and the Corrosion of Steel in Concrete*, Highway Research Record, 433, 1973.

49 ASTM C 876. American Society for Testing and Materials. *ASTM Standard Test Method for Half Cell Potentials of Reinforcing Steel in Concrete*. Designation C 876. Philadelphia: American Society for Testing and Materials.

50 Clear, K.C., *Measuring Rate of Corrosion of Steel in Field Concrete Structures*, Transportation Research Record, No. 1211, 1992, pp. 28-38.

51 Hope, B. B., Ip, A. K., and Manning, D., *Corrosion and Electrical Impedance in Concrete*, Cement and Concrete Research, Vol. 15, 1985, pp. 525-534.

52 Feliu, S., Gonzales, J. A., Andrade, C., and Feliu, V., *Determination of Polarization Resistance in Reinforced Concrete Slabs*, Corrosion, Vol. 44, No. 10, 1988, pp. 761-765.

53 Feliu, S., Gonzales, J. A., Feliu, S. Jr., and Andrade, C., *Confinement of Electric Signal for in situ Measurement of Polarization Resistance in Reinforced Concrete*, ACI Materials Journal, Vol. 87, 1990, pp. 457-460.

54 Stern M., A. L. Geary, *Electrochemical Polarization No. 1: Theoretical Analysis of the Shape of Polarization Curve*, Journal of Electrochemical Society, vol. 104, 1957, pp. 56- 63.

55 Clear, K. C., *Test Procedures, Data Analysis, and General Information*, K.C.C. Inc. 3-LP Package, Sterling, VA, 1990.

56 Clear, K.C., *Measuring the Rate of Corrosion of Steel in Field Concrete Structures*, KCC INC 3LP Package, Sterling, VA., pp. 2-20.

57 Newhouse, Charles D., *Corrosion Rates and the Time to Cracking of Chloride Contaminated Reinforced Concrete Bridge Components*, M.S. Thesis, Virginia Polytechnic Institute and State University, Blacksburg, VA, December, 1993.

58 SHRP-S / FR-92-110. *Condition Evaluation of Concrete Bridges Relative to Reinforcement Corrosion*, Volume 8: Procedure Manual, 1992.

59 ASTM C 114. American Society for Testing and Materials. *ASTM Standard Test Method for Chemical Analysis of Hydraulic Cement*. Designation C 114. Philadelphia: American Society for Testing and Materials.

60 ASTM C 1202. American Society for Testing and Materials. *ASTM Standard Test Method for Electrical Indication of Concrete's Ability to resist Chloride Ion Penetration*.. Designation C 1202. Philadelphia: American Society for Testing and Materials.

61 Slater, J.E., Corrosion of Metals in Association with Concrete, *Corrosion of Metals in Concrete*, ACI SP-49, American Concrete Institute, Detroit, MI, 1975, pp. 21-38.

62 ACI 201, *Guide to Durable Concrete,* American Concrete Institute, Detroit.

63 Pritchard, B., "A new era in concrete bridge protection", Highways, Sep. 1986,

pp. 20-21.

64 Clarke, J.L., *Modified Concretes for Use in Bridge Structures*, p. 236-238, from "Concrete Bridge Engineering: Performance and Advances" edited by R. J. Cope, Elsevier Applied Science Publishers Ltd., pp. 346.

65 Bentz, Dale P.; Edward J. Garboczi, *Simulation Studies of the Effects of Mineral Admixtures on the Cement Paste-Aggregate Interfacial Zone*, ACI Materials Journal (American Concrete Institute), v. 88, n. 5, September-October 1991, pp. 518-529.

66 Mehta, P. K., *Mineral Admixtures*, from Concrete Admixtures Handbook, Properties Science and Technology, Ed. V. S. Ramachandran, 1984.

67 Helmuth, R. A., *Fly Ash in Cement and Concrete*, SP040T, Portland Cement Association, Skokie, IL, 1987.

68 ASTM C 618. American Society for Testing and Materials. *ASTM Specification for Fly Ash and Raw or Calcined Natural Pozzolan for use as a Mineral Admixture in Portland Cement Concrete.* Designation C 618. Philadelphia: American Society for Testing and Materials.

69 Lewis, D. W., *Discussion of "Admixtures for Concrete," (ACI 212.1R-81)*, Concrete International: Design and Construction, Vol. 27, No. 5, May 1985, pp. 64-65.

70 Fulton, F. S., *The Properties of Portland Cements Containing Milled Granulated Blast-furnace Slag*, Portland Cement Institute Monograph, The Portland Cement Institute, Johannesburg, South Africa, 1974.

71 Trethewey, K.R., and J. Chamberlain, *Corrosion for Students of Science and Engineering*, Longman Scientific & Technical, 1988, pp.228-230.

72 Prowell, Brian D., "Evaluation of Corrosion Inhibitors for the Repair and the Rehabilitation of Reinforced Concrete Bridge Components", M.S. Thesis, Virginia Polytechnic Institute & State University, Blacksburg, VA, August 1992, 216 pp.

73 Dean, Sheldon W., et al., *Inhibitor Types*, Material Performance, Vol. 20, No. 11, November 1981, pp. 47-51.

74 Funahashi, Miki, *Predicting Corrosion-free Service Life of a Concrete Structure in a Chloride Environment*, ACI Materials Journal (American Concrete Institute), v. 87, n. 6, November-December 1990, pp. 581-587.

75 Miller, R., Krouskop, B., Minkarah, I., Bodocsi, A., "Chloride Penetration and the Effect on Porosity in a Pavement", Paper No. 930327, Transportation Research Board, 72nd Annual Meeting.

76 Tritthart, J., "Pore Composition and Other Factors Influencing the Corrosion Risk of Reinforcement in Concrete", *Progr. Coll. Polym. Sci.*, No. 79, Graz University of Technology, Stremayrgasse, Graz, 1989, pp. 96-106.

77 Verbeck, G.J., "Mechanisms of Corrosion of Steel in Concrete", *Corrosion of Metals in Concrete*, ACI SP-49, American Concrete Institute, USA, 1975, pp. 21-38.

78 Locoge, P.; M. Massat; J. P. Ollivier; C. Richet, *Ion Diffusion in Microcracked Concrete*, Cement and Concrete Research, v. 22, n. 2-3, March-May 1992, pp. 431-438.

79 Jacobsen, Stefan; Jacques Marchand; Luc Boisvert, *Effect of Cracking and Healing on Chloride Transport in OPC Concrete*, Cement and Concrete Research, v. 26, n. 6, June 1996, pp. 869-881.

80 Tumidajski, Peter J., *Application of Danckwert's Solution to Simultaneous Diffusion and Chemical Reaction in Concrete*, Cement and Concrete Research, v. 26, n. 5, May 1996, pp. 697-700.

81 Berke, Neal S.; Maria C. Hicks, *Predicting Chloride Profiles in Concrete*, Corrosion (Houston), v. 50, n. 3, March 1994, pp. 234-239.

82 Tumidajski, P. J.; G. W. Chan; R. F. Feldman; G. Strathdee, *A Boltzmann-Matano Analysis of Chloride Diffusion*, Cement and Concrete Research, v. 25, n. 7, October 1995, pp. 1556-1566.

83 Tumidajski, P. J.; G. W. Chan, *Boltzmann-Matano Analysis of Chloride Diffusion into Blended Cement Concrete*, Journal of Materials in Civil Engineering, v. 8, n. 4, November 1996, pp. 195-200.

84 Mangat, P. S.; B. T. Molloy, *Prediction of Long Term Chloride Concentration in Concrete*, Materials and Structures/Materiaux et Constructions, v. 27, n. 170, July 1994, pp. 338-346.

85 Arora, P.; B. N. Popov; R. E. White, *Fundamental Modeling of Chloride Diffusion in Concrete*, Materials for the New Millennium Proceedings of the Materials Engineering Conference v. 1, 1996, ASCE, New York, NY, USA, pp. 203-212.

86 Zhang, Tiewei; Odd E. Gjorv, *Effect for Accelerated Testing of Chloride Diffusivity in Concrete*, Cement and Concrete Research, v. 25, n. 7, 1995, pp. 1535-1542.

87 Zhang, Tiewei; Odd E. Gjorv, *Diffusion Behavior of Chloride Ions in Concrete*, Cement and Concrete Research, v. 26, n. 6, June 1996, pp. 907-917.

88 Chatterji, S., *On the Applicability of Fick's Second Law to Chloride Ion Migration Through Portland Cement Concrete*, Cement and Concrete Research, v. 25, n. 2, February 1995, pp. 299-303.

89 Zhang, Tiewei; Odd E. Gjorv, *Electrochemical Method for Accelerated Testing of Chloride Diffusivity in Concrete*, Cement and Concrete Research, v. 24, n. 8, 1994, pp. 1534-1548.

90 Feldman, Rolf F.; Gordon W. Chan; Rejean J. Brousseau; Peter J. Tumidajski, *Investigation of the Rapid Chloride Permeability Test*, ACI Materials Journal

(American Concrete Institute), v. 91, n. 3, May-June 1994, pp. 246-255.

91 Arup, Hans; Birgit Sorensen; Jens Frederiksen; Niels Thaulow, *The Rapid Chloride Permeation Test - an Assessment*, Corrosion 93, The NACE Annual Conference and Corrosion Show, paper no. 334, 1993, 11 p.

92 Andrade, C.; M. A. Sanjuan, *Experimental Procedure for the Calculation of Chloride Diffusion Coefficients in Concrete from Migration Tests*, Advances in Cement Research, v. 6, n. 23, July 1994, pp. 127-134.

93 Sennour, M. L.; H. Zhang; H. G. Wheat; R. L. Carrasqoillo, *Corrosion Susceptibility of Concrete Made with Different Chemical and Mineral Admixtures*, Corrosion 93, The NACE Annual Conference and Corrosion Show, paper no. 337, 1993, 11 p.

94 Naik, Tarun R.; Shiw S. Singh; Mohammad M. Hossain, *Permeability of Concrete Containing Large Amounts of Fly Ash*, Cement and Concrete Research, v. 24, n. 5, 1994, pp. 913-922.

95 Zhang, Min-Hong; Odd E. Gjorv, *Effect of Silica Fume on Pore Structure and Chloride Diffusivity of Low Porosity Cement Paste*, Cement and Concrete Research, v. 21, n. 6, November 1991, pp. 1092-1102.

96 Torii, Kazuyuki; Mitsunori Kawamura, *Pore Structure and Chloride Ion Permeability of Mortars Containing Silica Fume*, Cement & Concrete Composites, v. 16, n. 4, 1994, pp. 279-286.

97 Ozyildirim, Celik, *Low-Permeabilty Concretes Containing Slag and Silica Fume*, Virginia Transportation Research Council, VTRC 93-R10, Final Report, January, 1993.

98 Cady, Philip D.; Richard E. Weyers, *Predicting Service Life of Concrete Bridge Decks Subject to Reinforcement Corrosion*, ASTM Special Technical Publication, n. 1137, 1992, pp. 328-338.

99 Cady, P.D. and Weyers, R. E., *Deterioration Rates of Concrete Bridge Decks*, Journal of Transportation Engineering, Vol. 110, No. 1, January 1984, pp.34-44.

100 Weyers, R.E., Fitch, M.G., Larsen, E.P., Al-Qadi, I.L., Chamberlin, W.P., Hoffman, P.C., "Service Life Estimates", *Concrete Bridge Protection and Rehabilitation: Chemical and Physical Techniques*, Strategic Highway Research Program, Contract # C-103, Washington, D.C., November 19, 1992, pp.136.

101 Liu, Y., *Modeling the Time-to-Corrosion Cracking of the Cover Concrete in Chloride Contaminated Reinforced Concrete Structures*, Ph.D. Dissertation, Virginia Polytechnic Institute and State University, Blacksburg, VA, 1996.

102 Crank, J., *Mathematics of Diffusion*, Clarendon Press, Oxford, UK, 1983.

103 SHRP-S-668. *Concrete Bridge Protection and Rehabilitation: Chemical and Physical Techniques*, Service Life Estimates, 1994.

104 Pyc, W. A., *Performance Evaluation of Epoxy- Coated Reinforcing Steel and Corrosion Inhibitors in a Simulated Concrete Pore Water Solution*, M.S. Thesis, Virginia Polytechnic Institute and State University, Blacksburg, VA, 1997.

VITA

Jerzy Żemajtis

Jerzy Z. Żemajtis was born on July 10, 1963 in Olsztyn, Poland. He graduated from Adam Mickiewicz High School in Olsztyn, Poland, in June 1982. In January 1990 he received a B.S./ M.S. degree in Civil Engineering from the Technical University of Gdańsk, Poland. After that she worked for one year as a bridge design engineer in Gdańsk Roads and Bridges Design Office.

In 1991 he received a one year fellowship at Virginia Tech sponsored by the International Road Federation (IRF) from Washington, D.C. After one semester of studies he entered a Ph.D. program in the Materials Division of the Department of Civil Engineering at Virginia Polytechnic Institute and State University. While attending graduate school he worked as a graduate research assistant at the Structures and Materials Laboratory. Upon completion of the course work he was employed as a research associate. He also taught a structural course at Wythville Community College and an advanced material course at Virginia Tech. He defended his dissertation on January 19, 1998.